Analysis of current distribution and circulating currents

in a permanent magnet synchronous machine with parallel coils

Roland van de Wetering

1314742

Supervisors:

Dr. Ir. H. Polinder

Ir. M. van der Geest

Electrical Power Processing

Faculty of EEMCS

ANALYSIS OF CURRENT DISTRIBUTION AND CIRCULATING CURRENTS

IN A PERMANENT MAGNET SYNCHRONOUS MACHINE WITH PARALLEL COILS

Thesis submitted to the faculty of Electrical Engineering, Mathematics and Computer Science (EEMCS) group of Electrical Power Processing (EPP) in partial fulfilment of the requirements for the degree of

Master of Science
in
Electrical Engineering

Supervisors:

Dr. Ir. H. Polinder

Ir. M. van der Geest

Thesis committee:

Prof. Dr. Ir. J.A. Ferreira

Dr. Ir. H. Polinder

Dr. Ir. D. Djairam

Ir. M. van der Geest

August 2013

Delft, The Netherlands

Abstract

In this thesis the current distribution among parallel coils and the presence of circulating currents in an electric machine is investigated. Differences in induced voltage and in impedance between the parallel coils might lead to an uneven current distribution, which may cause the temperature of a single turn to become too high.

To determine the flow of current in the machine it is necessary to model the machine in sufficient detail. For this research the coils in the machine have been modelled as a series connection of a voltage source, and inductance (with mutual coupling to other coils) and a resistance. This was made possible by the machine designer, who provided these parameters for every copper turn in the machine.

The most important result of this research is that the difference in amplitude of the currents through parallel wires is very small, for this specific machine. The phase difference between the currents is larger, but the impact of this is still insignificant. Furthermore, the investigation on circulating currents has shown that the magnitude of these currents mainly depends on the difference in induced voltage between parallel wires and the resistance of the wires. The inductance of the coils was found to have negligible influence on the magnitude due to very good magnetic coupling between the parallel coils.

Contents

Abstract I

1 Introduction 1

1.1 Background 1

1.2 Aim 1

1.3 Approach 1

1.4 Results and significance 2

1.5 Structure of the report 3

2 Literature review 5

2.1 Machine comparison 5

2.2 Modelling of the PMSM 7

2.3 Control of the machine 7

2.4 Circulating currents and current imbalance in parallel windings 8

2.5 System modelling 10

2.6 Summary 11

3 Model description 13

3.1 Load 13

3.2 Inverter 14

3.3 Power source 16

3.4 Torque controller 16

3.4.1 Equations for the machine in the rotor reference frame 16

3.4.2 Controller design 17

3.4.3 Field weakening 20

3.5 Permanent magnet synchronous machine 24

4 Model implementation 29

4.1 Load 29

4.2 Inverter 30

4.3 Power source 31

4.4 Torque controller 32

4.4.1 Current control 32

4.4.2 Reference signal generation 32
4.5 Permanent magnet synchronous machine 34
5 System simulation 37
5.1 Standalone operation of the electric machine 37
5.1.1 Open circuit voltage 37
5.1.2 Short circuit current 38
5.2 Start-up time 41
5.3 Efficiency 41
5.4 Torque, current and voltage trajectories 43
5.4.1 Minimum start-up torque 43
5.4.2 Maximum start-up torque 46
6 System validation 48
6.1 HISPEM overview 48
6.2 Machine properties 49
6.2.1 Measurement setup 49
6.2.2 Phase resistance 51
6.2.3 Induced EMF 52
6.2.4 Phase inductance 55
6.2.5 Rotor moment of inertia 57
6.2.6 Mechanical friction 58
6.3 Current and torque scaling 60
6.4 Machine model 61
6.5 Comparison between measurements and simulation 61
6.5.1 Machine impedance 61
6.5.2 Start-up 62
6.6 Conclusion 66
7 Results 69
7.1 Circulating currents 69
7.2 Current distribution 73
7.2.1 Minimum start-up torque 73
7.2.2 Maximum start-up torque 77

7.3 Single phase to neutral short circuit..... 79
8 Conclusions..... 83
9 Bibliography..... 87
Appendix A Machine parameters and cable impedance. 91

1 Introduction

In this thesis the presence and significance of circulating currents and current sharing between parallel coils in an electric machine will be investigated. The machine will be used as a starter/generator in a helicopter.

1.1 Background

Electric machines used in aerospace applications need to have a high power to weight ratio and high reliability. Permanent magnet synchronous machines (PMSM) can be used to obtain a high power to weight ratio and they can be very efficient as well, but since the excitation flux cannot be turned off they lack the inherent safety of induction and switched reluctance machines.

In order for the PM machines to be useful in the aerospace sector, the lack of inherent safety has to be compensated by smart design of the machine itself and its driving electronics. This problem has partly been solved by using multiphase machines where the coupling between the phases, both electric and magnetic, has been kept low. The magnitude of short-circuit currents can be controlled by properly designing the leakage inductance of the machine [1]. On the controller side, redundancy and fault detection have been implemented [2], [3] and [4].

1.2 Aim

This report will focus on the behaviour of a PMSM without internal faults. The machine will have a winding made up of parallel wires, in order to reduce the negative influence of the skin depth at high electrical frequencies. The parallel wire arrangement might cause circulating currents due to unequal rotor flux linkage and also current imbalance due to differences in impedance between the parallel wires. Furthermore, the case of a short-circuit at the terminals of the machine will be simulated. The goal is to determine whether the impact of circulating currents and current imbalance due to the parallel wires is significant and to determine current profiles in the machine and the inverter in case of a short-circuit at the terminals of the machine. The development of a simulation model (required to reach these goals) of the starter/generator system and its implementation in Synopsis Saber, are also goals themselves.

The focus of this report is thus not directly related to the previously mentioned problems that must be overcome for the use of PMSM in the aerospace sector, or any other sector where failure of the machine is catastrophic. However, the model used to investigate the machine without faults can, with some modifications, also be used to model faults in the windings of the machine. Thus the simulation model is implemented such that it forms a good starting point for further research in fault analysis.

1.3 Approach

The model used for the PMSM originates from the equivalent circuit of a single turn of the conductor in an electric machine. In this circuit there is a series connection of a resistance, an

inductance and a voltage source. In an internal publication of the TU Delft, this model has been applied to every single copper turn in the machine. A very similar publicly available reference can be found in [5]. Since the value of the inductance, resistance and flux linkage of all turns in the machine is available, it is possible to write a matrix equation from which the currents through, and voltages over, every turn can be calculated. For this report the number of equations has been reduced, knowing that in the machine without faults the current is the same within a single coil.

The models for the starter/generator system that have been developed as part of this thesis have their limitations. The switching behaviour of the inverter has for example not been implemented, the only loss mechanism in the machine model is resistive copper loss and the resistance of the copper has also been kept constant (independent of temperature). In reality the resistance would change with temperature. These limitations will have an effect on the results obtained from the models, for example the current ripple due to pulse width modulation will not be visible.

1.4 Results and significance

The main results from the three investigations, about circulating currents, current distribution and a short circuit fault are:

- The magnitude of circulating current in the machine with nothing connected to its terminals is several orders of magnitude less than the currents that flow through it during starting. The cause of the circulating currents is a difference in induced voltage in parallel coils and the main impedance responsible for limiting this current is the copper resistance of the coils, even at high speed.
- The difference in current magnitude between parallel coils in the same phase of the machine is relatively small. The phase shift between the currents is larger in comparison, but the influence of this is still small.
- For the short circuit fault (in which the terminal of phase A is short circuited to the neutral terminal), the influence of the bandwidth of current controllers is important when there is a delay in the inverter. When the bandwidth was chosen to be high there were high frequency, high amplitude oscillations in the inverter output voltages. This in turn leads to high amplitude oscillations in the inverter and machine currents, which can damage these components.

Furthermore:

- A system model has been described and implemented. This model has been a requirement to be able to perform the before mentioned investigations and it contributes to the overarching project which is focused on the actual realisation of the starter/generator system using a PMSM.

- Validation using a real electrical machine setup shows that the system model functions correctly.

The contribution of this thesis is mostly practical and much less theoretical. A simulation model has been developed that can been used to analyse circulating currents and current imbalance between parallel coils in a machine winding. The derivation of the model has been done before in [5] and it is assumed that the resistance, inductance and magnet flux linkage of every individual turn in the machine are already known. With the presented simulation model it should be possible to do similar analysis to different machines relatively fast and the model is flexible enough to simulate fault conditions with minor modifications.

1.5 Structure of the report

This thesis will start with a literature review, in order to get a good idea of what has been done before. The largest part of the research needed to model the system and specifically the machine has been done before and not everything should be reinvented. Next, with the knowledge obtained from the literature study, the models that are needed for the simulations will be developed. After the individual models are defined it is time to build up the system and to run a simulation to see the general behaviour. This gives the opportunity to see if there are major mistakes, like machine torque levels that are far from expected or start up times that are not as calculated. Furthermore simulations of the machine in good condition are needed to compare with fault conditions if they are investigated in further research. Subsequently the simulated motor drive will be compared to an actual motor drive to further enhance the confidence in the modelling. The next part of the thesis is the analysis of circulating currents, current imbalance and a short-circuit at the terminals of the machine. Finally conclusions are drawn from the results and recommendations for further research will be given.

2 Literature review

In this chapter a review of literature that is useful for this research will be given. Many aspects of the research conducted in this thesis have been discussed already by different authors. There is a wide range of information available concerning electrical drives, but in order to use the knowledge documented by other authors efficiently it is necessary keep in mind the goal of the current research so one does not get lost in all the available information.

The first subject to be investigated is the machine choice. For this thesis the machine type was fixed to the permanent magnet synchronous machine, but it still is important to get a good understanding about why this choice was made.

The next subject to be investigated is the modelling of the machine. There are different ways to model the same machine depending on the information that has to be extracted from the model. References [5] and [6] use models which enable the analysis of circulating currents and current imbalance, which is interesting material for this thesis.

The next paragraph is about the control of the machine. A voltage source inverter will be used, while the currents in the machine have to be controlled. This subject has received a lot of attention in literature. This knowledge will be used to implement a controller, but it is not the focus of this research.

The most important aspect of this research will be the analysis of circulating current and current imbalance in the machine. Different authors have contributed to the understanding of the subject and this knowledge is documented in a separate paragraph.

In the final paragraph attention goes to the complete system. The simulation package that will be used to implement the system will be discussed here as well.

2.1 Machine comparison

Choosing the type of machine is not part of this thesis because the decision for a PMSM had already been made. It is, however, still of educational value to find out why the PMSM is a good choice or not. Most sources concerning comparative studies between different machines are related to electric vehicles ([7], [8], [9] and [10]), but there are also publications related specifically to PMSM usage in aerospace applications ([1] , [2], [3] and [4]).

The general machine type comparison is between the DC machine (DCM), the induction machine (IM), the switched reluctance machine (SRM) and the permanent magnet synchronous machine (PMSM). The current solution for the starter engine is a DCM, which according to literature is relatively cheap and easy to control. The downside of this type of machine is that it has a low power density and efficiency. In the starter application there is no controller for the machine, while one would be needed in case one of the other machines were used (although an

induction machine could do without control, by applying alternating voltages with constant amplitude and frequency to its terminals). Because of this the weight disadvantage might be relatively small. The low efficiency might also be acceptable considering the machine is working for a limited amount of time. The PMSM has the advantage of a higher efficiency, good controllability (for torque control, though for field weakening this machine has a disadvantage compared to a synchronous machine with a field winding), less weight and less volume. This machine does however need power electronics to be able to operate which reduces the weight and volume advantage. Permanent magnet machines also have the disadvantage that the field flux cannot be turned off in case of a fault condition. The IM and the SRM do not suffer from this which makes them safer. However these machines need more controlling electronics than the DCM and are not as efficient as a PMSM with the same rating. The following table (taken from [7]) gives an indication of the differences between the machine types.

Table 1 Electric machine comparison from reference [7]

	DCM	IM	PMSM	SRM
Power density	--	o	++	o
Efficiency	-	+	++	+
Costs	+	++	-	+
Reliability	-	++	o	+
Technical maturity	+	+	o	o
Controllability, costs	++	o	+	-

-- very bad, - bad, o neutral, + good, ++ very good

From this table it follows that no machine is definitely the best, the choice depends on the system requirements. When the choice for the PMSM has been made for its high power density and efficiency, then it might be needed to see what can be done about the other aspects. Especially reliability is very important for aerospace applications and reference [1] clearly states why. Firstly there may be no faults that result in a dangerous situation. Secondly the failure rate should be very low. For an average machine the probability of a short-circuit between phases is already too high for the machine to be used in aerospace applications that need high reliability. Thirdly the failure rate due to undetectable faults that, in combination with another fault, might lead to in-flight shutdown should be even lower. It should be noted that this reference is about an electric machine in the fuel control system of an aircraft, which needs to have a higher availability than a starter engine. Solutions to get a very high reliability are given, these include: thermal, magnetic and physical isolation between phases, limiting short-circuit current by properly designing the impedance of the machine and using more phases. Physical isolation by placing concentrated windings on a separate stator tooth are solutions given by both [1] and [4]. Not only the machine itself should be reliable, but also the power electronics controlling it. Reference [2] pays special attention to fault tolerant power converters for aerospace applications. Here a fourth phase leg has been added to a three phase leg inverter in order to control the neutral point of the machine. It has been shown that if a fault is present in one of the phases, a torque pulsation appears which can be effectively reduced with the use of the

fourth phase. Reference [3] is also about fault tolerance and the emphasis is on fault detection. The detection is implemented by comparing the estimated currents from a machine model with the measured currents in the actual machine. Detection of faults is important, because no further actions to reduce the impact of the fault can be taken if the fault has not been detected.

From the literature it follows that the choice for a certain machine type in not always obvious. This holds true for the starter machine as well. The machine currently in use is a DCM and this might be replaced with a PMSM even though the IM and SRM are more reliable. The PMSM has a disadvantage with reliability compared to the latter two, but the reliability might be brought to an acceptable level by designing the PMSM properly and by using fault tolerant drive electronics.

2.2 Modelling of the PMSM

The PMSM can be modelled in different ways and the choice depends on the purpose of the model and on what level of detail is required. In this thesis the temperature of the machine and iron losses are for example not needed, which simplifies the model. On the other hand, currents in parallel wires are of interest, which means that reducing the entire machine to a single phase equivalent with a series connection of a resistance, inductance and a voltage source would not show the needed details.

In references [5] and [6] the turns of the conductor around the teeth in the machine are modelled as a series connection of a resistance, an inductance and a voltage source. Because of this a machine can be modelled in which the impedance of, and induced voltage in, each turn can be different. This allows the analysis of circulating currents and current imbalance in the machine. This is also exactly what has been done in reference [5]. Reference [6] uses the model to analyse machine faults. The circuit parameters of each turn are extracted from a FEM simulation and then put into matrices, which can be used for circuit analysis. The advantage of this approach is that once the FEM simulation has been done, only circuit analysis is needed for further analysis. Not only for analysing the circulating currents and current imbalance, but also machine faults like short circuits in a phase or between phases. Since this way of modelling gives the right amount of detail and also the flexibility to extend the analysis to machine faults it has been found to be very useful for this thesis work.

2.3 Control of the machine

The PMSM is not self-starting, thus some kind of control is definitely needed. The simplest way to get the machine to rotate is to make an electrical equivalent of the brushed commutator in a DCM (though getting a machine to rotate and getting a controlled motion are not the same). For example hall sensors are used to determine the rotor position and this information can be used in so-called six step control. The next step forward is to replace the sensors by a sensorless algorithm, such as back-EMF detection used in reference [11]. Although much research has been done about determining the position of the rotor, it will not be further discussed in this thesis. It is simply assumed that the rotor position is known.

For starter operation the torque should be controlled and for generator operation the power output is important. Generator operation might be considered, but the voltage control that is needed in this case will not be investigated. From [12] it follows that for a non-salient machine the torque is determined solely by the current in the quadrature axis of the rotor reference frame. Thus a current controller can be used to control the torque output of the machine.

In reference [13] information can be found on how the current in a generalized load can be controlled. The load is modelled as a series connection of a resistance, an inductance and a voltage source, which can be used to represent an electrical machine. In this reference both the current source inverter (CSI) and the voltage source inverter (VSI) are mentioned, but only the VSI is used because the CSI is normally only deployed in high power applications. For this thesis also only a VSI will be considered. Furthermore this reference mentions two ways of controlling the current through the load, one is by using hysteresis and the other by using model based control. In order to stay as close as possible to the actual implementation of the controller for the starter/generator the model based control seems to be the most interesting option. It is mentioned however that for this to work it is necessary for the machine parameters to be well known, this would not be the case for the hysteresis controller.

Multiple operating modes of the PMSM can be distinguished and they are well explained in reference [14]. It has previously been mentioned that only quadrature axis current is needed to produce torque. If this is done then the machine is said to be operating in the maximum torque per ampere region. At a certain speed the back-EMF may become so large that it is only just possible to produce the wanted amount of torque with the maximum voltage output of the inverter. If the speed needs to be increased further this can be done by reducing the torque, or by applying field weakening. Because a PMSM does not have a field winding it is not possible to reduce the flux produced by the rotor. It is however possible to produce an opposing flux by injecting a current in the stator. The current has to be in the negative direction of the direct axis in the rotor reference frame. When this is done it is possible to increase the speed without reducing the torque. When the magnitude of the stator flux in the direct axis equals the magnitude of the rotor flux it is not possible to apply further field weakening. When this point has been reached the torque must be decreased to increase the speed, the machine is now said to be operating in maximum torque per flux mode.

References [12], [13] and [14] originate from the same book and overall it can be said that this is very useful literature regarding control of electrical drives.

2.4 Circulating currents and current imbalance in parallel windings

Amongst others references [5], [15], [16] and [17] treat the circulating current and current imbalance that might be present when machine windings are connected in parallel.

Interesting research has been shown in [15], where circulating currents have been investigated in a machine with a fault. The faults that are considered are a short-circuit in the rotor and a

mechanical eccentricity. The currents in the parallel windings are measured and fault detection analysis is done using this information. Although electrical and mechanical faults and the detection might be of interest for further research, such research will not be conducted in this thesis.

Reference [16] assumes that the impedance of the parallel windings in the machine is the same, as well as the flux linked by them. Because of this the conclusion is drawn that there is no current imbalance when there is no fault in the machine. In this reference emphasis is placed on a fault in the machine, while in this thesis faults will not be considered. The assumption that parallel windings are identical will also not be made. There will be differences in resistance, self-inductance and flux linkage between the turns. This also means that there can be circulating currents and one of the goals of this thesis is to find out if these are present.

The previously discussed references are all related to electrical machines, but reference [17] is not. In this reference the current distribution in an inductor with parallel coils is investigated. There is no fault in the inductor, but still the current distribution is not equal amongst the coils due to geometrical differences between the coils. Because of this and because of the way of modelling that is used in this reference the analysis becomes similar to the analysis in this thesis. The reference mentions that the current distribution can be significantly different between the parallel coils. One of the goals is to find out if the same thing happens to the machine under investigation.

Both circulating currents and current imbalance have been investigated in reference [5]. In fact this reference does the analysis that has to be done in this thesis and even more than that. First the problem is stated, which is the uneven current distribution between parallel strands of copper wire wound around the same tooth. This is a problem because at the high frequency machine under consideration the skin and proximity effect play a significant role. These effects influence the impedance of the wires, which then results in uneven current distribution and this in turn leads to higher losses and hot spots in the machine. A FEM analysis has been done on the machine from which the circuit parameters for each and every turn can be extracted. This data is then used to build up a circuit model for the entire machine. The turns around the teeth in a machine can be seen as a resistance, an inductance and a voltage source connected in series. The voltage source represents the induced voltage in the wire due to time varying rotor flux linkage. It was found that the flux linkage is about the same for every coil, the variation being only 0.5%. Because of this the circulating current under no-load condition will be negligible compared to currents under load. The variation in self-inductance between turns was found to be much larger, even more than 50%. Because of this the change in impedance, especially at high speed where the impedance of the inductance becomes higher, there will be a significant current imbalance. The information presented in this reference is very useful and the results can be used for comparison.

2.5 System modelling

The starter/generator itself is part of a system of multiple components. The current distribution inside the machine is of special interest, but other components like the load, the current controllers and the inverter cannot be neglected since they have an influence on the needed and obtained current in the machine. Not every component will be modelled with the same level of detail, the highest level of detail will be found in the machine and its control. The load is modelled at a much higher level. The importance of system level simulation is expressed in reference [18]. This source is mainly concerned with system level optimal design, in which parts of this system can be optimized for the system, instead of being optimized on their own. Optimizing parts on their own might lead to a non-optimal combination of parts and thus a non-optimal system.

In references [19] and [20] a starter/generator has been analysed. In the first reference an induction machine has been used and the analysis is mainly focused on the machine, the inverter and the control of the machine. In the latter reference a switched reluctance machine is used and more of the system is taken into account. Here also attention has been paid to the start-up performance of the machine in combination with its load (the turbine engine). Voltage regulation in generator mode has been taken into account in this source as well. For system simulation reference [20] is appropriate, while for detailed information on control and design of inverters reference [19] is very useful.

In this thesis the modelling and simulation will be done using SaberRD from Synopsys. Many of the advantages of Saber are mentioned in reference [21]. Quotes from this source: “SABER … is a true mixed-signal, mixed technology equations solving simulation tool” and “Unlike other simulators … SABER models these other engineering disciplines in their native domain”. These are major advantages of the Saber software concerning system simulation. For this thesis the electrical and mechanical domain must be used in one simulation and in Saber this is no problem. When accidentally connecting a component modelled in the electrical domain to a component in the mechanical domain, Saber will issue a warning. Other advantages of Saber are that it contains an extensive library of parameterised components and that it is possible to add your own using the MAST model description language. With this language, which was developed as a part of Saber, it is possible to directly write down the equations that have to be solved. Besides being able to literally write down the system equations, another advantage of MAST is that it is non-causal [22]. This means that it is possible to use only one set of equations for e.g. an electric machine, whether the input to the machine is a current, a voltage or a torque applied to its shaft. The appropriate inputs and outputs are determined by the simulator itself. This gives an advantage over causal modelling, in which the inputs and outputs have to be defined up front and where another set of equation is needed when the input changes from e.g. voltage to current. Moreover characterization tools for different components (e.g. an inductor) are integrated and it is possible to use lookup tables and drive cycles.

In reference [23] a power system has been modelled in Saber and this software has also been used in reference [24] for a motor drive system for an electric vehicle. In [23] much attention is paid to Saber. First the possibilities with the software are discussed and later models are developed with increasing complexity. The background information on Saber is useful, but for this thesis the application itself is not. Reference [24], however, is of much more interest for the topic of this thesis. The motor drive system for an electric vehicle shows many similarities with the starter/generator system. Figure 1 shows the system, this figure has been taken from the reference. The flow from reference input to control to machine and load and back is very clear in this figure. The system shown here is actually even more extensive than the one that will be used in this thesis, because the electric source (batteries) and speed control will not be modelled. In this thesis more attention will be paid to the machine itself and less to the entire system.

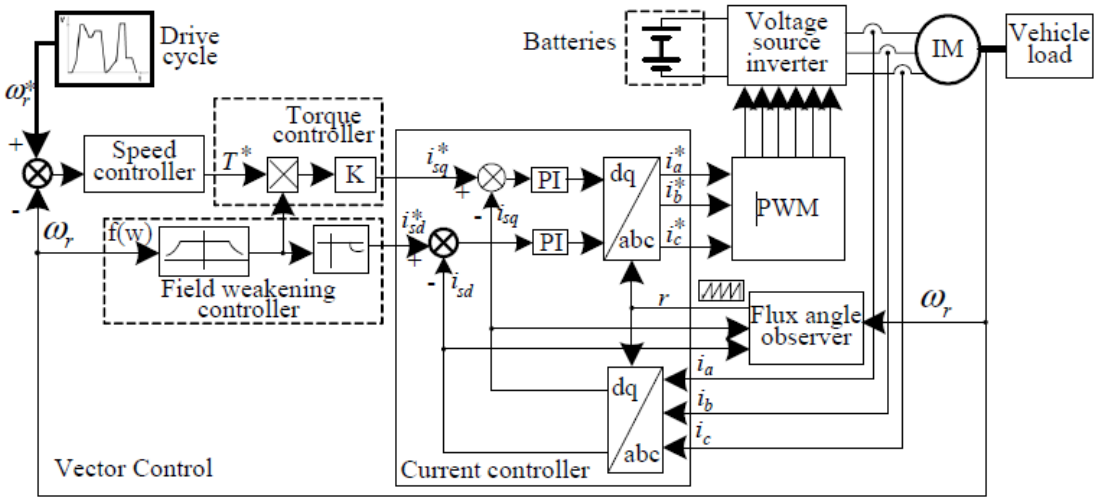

Figure 1 System model of an electric vehicle motor drive, from reference [24]

2.6 Summary

It was mentioned in the introduction to this chapter that the choice for some parts of the system were fixed. Nevertheless a literature review gives a better understanding of why these choices have been made. This holds true especially for the machine type.

For the machine type the emphasis was on the PMSM, as this is the machine that will be used in the simulations later on. Nevertheless, a brief comparison to the DC, induction and switched reluctance machine has been given. Some advantages and disadvantages where mentioned. From this the use of a PMSM can be justified, though the use of the other machines in similar situations can certainly not be ruled out.

There are multiple ways of modelling the same machine, for both the method and the level of detail. Two references have been presented that model individual turns of the machine. This method should enable the analysis of circulating current and current imbalance, which is of interest for this thesis.

A lot has been written about control of electrical machines. All the references specifically related to sensorless control have been omitted, because the rotor position of the machine is assumed to be known. Of interest for this thesis are torque control and the operating modes of a PMSM. A very useful source had been found, that clearly explains when the machine is in which operating mode. This source will be used later on for the design of the controller.

Concerning the current circulation and imbalance in a machine some very interesting sources were found, of which reference [5] was of particular interest. This source analysed this subject for a low voltage machine, but the analysis should be equally applicable to the starter/generator to be analysed in this thesis. However, the results obtained from the analysis might be difference.

In the search for information on system level modelling, references concerning general system modelling, starter/generator modelling and system modelling in Saber have been found. This has given a better insight into why system modelling is necessary and how this can be accomplished with Saber.

3 Model description

In this chapter the various parts of the system model will be described. In the next chapter this description will be used for the actual implementation in Saber.

3.1 Load

The load seen by the electric machine has to be representative for the real load that is present in the helicopter. The best representation would be obtained if every little detail is incorporated, but this is hardly feasible and might also not be necessary, depending on what kind of detail is wanted from the model.

For transient behaviour on a very small timescale (where the order of magnitude is similar to the electrical time constant of the machine) the load might even be neglected completely, assuming that there is enough inertia (large enough mechanical time constant) to keep the angular speed relatively constant in this time interval.

The timescale of interest for this thesis ranges from about the electrical time constant of the machine to the time needed for one starting cycle. In the latter case the angular speed cannot be assumed to be constant and the load has to be taken into account.

The mechanical load consisting of the turbine engine and the mechanical parts connecting the turbine with the starter/generator have been modelled as a moment of inertia and a speed dependent torque. The speed dependent torque can be seen in Figure 2. The non-zero torque at zero speed is due to static friction. Especially at very low temperatures the static friction becomes high, almost halve of the maximum friction. Until about 5 kRPM there is a quadratic increase in torque due to air resistance. After this point the torque decreases because the turbine is started and it helps to overcome the friction forces. Depending on the temperature the net torque due to friction seen by the electric machine becomes zero around 7 to 8 kRPM. At this point the torque generated by the turbine engine is equal to the torque due to friction. At higher speeds the torque developed by the turbine engine increases and the drag-torque seen by the electric machine becomes negative (i.e. the angular speed would increase even if the electric machine would not develop torque itself).

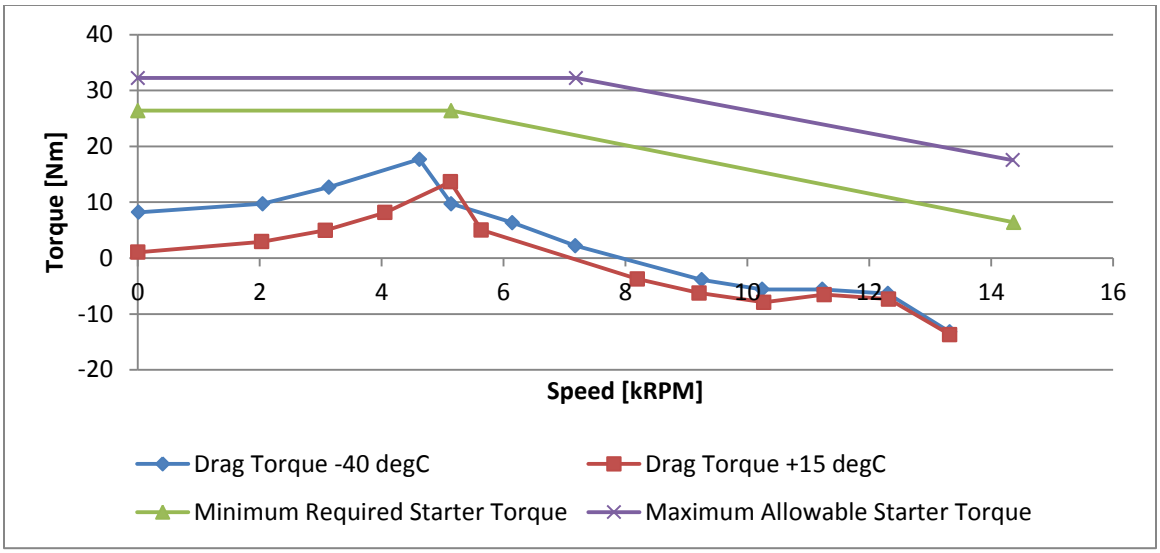

Figure 2 Drag-torque curve and starter torque limits

3.2 Inverter

The electric machine will not produce useful torque unless current is forced through the stator windings. Basically there are two options to force the current through: use a voltage source or a current source connected to the machine. A current source has the advantage that it can be used directly to produce the desired current, while the voltage source has to be controlled in such a way that the desired current is forced through the windings.

In the real situation a voltage source inverter (VSI) is used to turn the DC voltage from the power source into three-phase AC voltage, but this fact alone does not necessarily mean that a voltage source has to be used in the simulation model. In fact it does not even mean that three phase AC is needed. Using transformed coordinated systems (Clark and Park transform) two phase AC or even two DC voltages can be used in the simulation.

When modelling the start-up behaviour of the entire system with a properly functioning and balanced electric machine it might be a good idea to use the Park transformed form of the electric machine equations together with a current source, since this will significantly speed up the simulation. However, in this thesis the circulating currents and current imbalance has to be analysed and because of this the choice has been made not to transform the machine model. The result of this is that a three phase AC source is needed.

Two major assumptions have been made in order to simplify the modelling of the inverter. Firstly pulse width modulation (PWM) has not been implemented and secondly the losses in the inverter have not been taken into account. The first assumption idealizes the output waveform of the inverter. Instead of having a chopped DC voltage, there is a smooth output voltage which is exactly equal to the transformer ratio multiplied by the input voltage. The consequence is that phenomena related to the switching behaviour of a VSI are not taken into account, for example

the current ripple due to switching completely disappears. Because of the second assumption there is no voltage drop over the inverter (other than that caused by the transformer ratio) and no power is dissipated in the inverter. Due to the assumptions that have been made it is possible to model the inverter as three controlled voltage sources. The control input is a value between -1 and 1, which is translated to a virtual duty cycle between 0 and 1. The output is the DC supply voltage multiplied by the duty cycle.

There is one other thing to be mentioned, namely the alternative implementation of space vector modulation. In reference [25] a "pulse centering" method is described which gives identical results as space vector modulation. Where space vector modulation is ideal for digital implementation, the pulse centering method is ideal for the inverter without pulse width modulation. With either method the maximum phase-to-phase voltage output is higher than with sinusoidal modulation by a factor $\frac{2}{\sqrt{3}}$ (about 15% higher). When using sinusoidal modulation and one of the phase reference inputs is +1, than the other two are -0.5 (because of the fixed 120 degrees phase shifts between the phases). The modulation index cannot be increase while maintaining sinusoidal outputs, because a reference input with a magnitude with more than 1 will cause clipping to the limits of the voltage source. With pulse centering this situation, in which one phase is about to clip whilst the others could be increased, is avoided. This is achieved by shifting the reference values such that there is as much space left with respect to the lower boundary as with respect to the upper boundary. With the values mentioned above this would result in shifting al phase reference down with -0.25, resulting in phase references of +0.75 and twice -0.75. The result is that the reference values can be increased further without clipping, until the boundaries of +1 and -1 are reached again (simultaneously). Crossing these boundaries would result in over modulation, which will not be considered. The pulse centering implementation from reference [25] is shown in Figure 3.

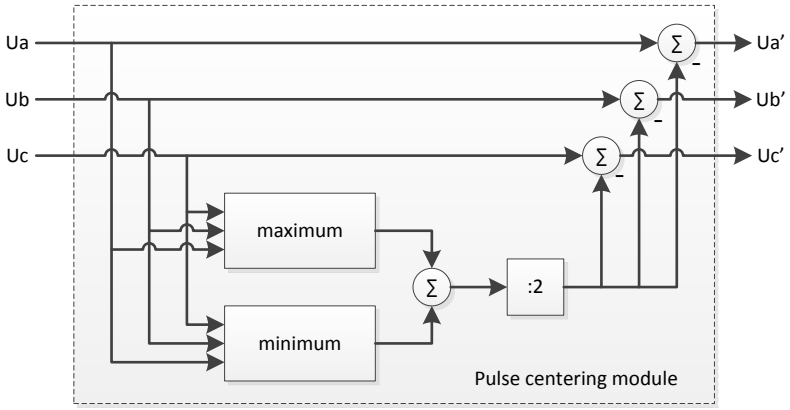

Figure 3 The pulse centering module according to reference [25], figure 2.10

The cables that connect the inverter to the electric machine will be taken into account as well, to make the short circuit analysis more realistic (otherwise there would be zero impedance in

the short circuit path, if the short circuit itself is assumed to be perfect). The parameters used for theses cables can be found in appendix A.

3.3 Power source

The inverter has to be fed by a power source. The implementation of the actual source of power is not known, but the nominal and the lowest value of the voltage have been given. The source is a DC voltage source with a nominal voltage of 270 V and with a guaranteed minimum voltage of 250V. Since there is no detailed information about the source, its effect on starting performance and fault behaviour has not been taken into account. The source used in the simulations will be an ideal voltage source with a voltage of 270 V.

3.4 Torque controller

In this section a torque controller will be developed. This will be done by first looking at the machine equations, in order to determine how torque can be controlled. Secondly a suitable torque controller will be developed. Finally attention will be paid to field weakening to extent the torque capability of the machine at higher speeds for a given supply voltage.

3.4.1 Equations for the machine in the rotor reference frame

The electric machine will be used as a starter and a generator and in both cases a torque controller will be necessary. In neither case speed nor position control will be present, since in starting mode the machine just has deliver torque until it reaches a certain speed and then stop and in generator mode the turbine engine will dictate the speed.

The torque controller has to make sure that the torque produced by the electric machine follows the desired set point and in all cases stays within the minimum and maximum boundaries. The minimum boundary is there to make sure that the maximum start-up time is not exceeded, while the maximum has to make sure that the stress on the mechanical system (shaft, gearbox) stays within safe limits. When the machine is past the speed where it should terminate starter mode, it is not allowed to produce driving torque anymore.

For designing a control system for the synchronous machine, good use can be made of the machine equations in the rotor reference frame. For a balanced three phase machine the fundamental component of the electrical frequency is filtered out of the equations. The steady-state currents and voltages become DC values and it is possible for a PI controller to reduce the error between the reference and the feedback signal to zero.

First we start with the equations of the machine in the rotor, or dq, reference frame according to reference [26], with the field flux linkage replaced by a constant permanent magnet flux linkage:

$$V_d = Ri_d + \frac{d\lambda_d}{dt} - \omega\lambda_q \qquad 3\text{-}1$$

$$V_q = Ri_q + \frac{d\lambda_q}{dt} + \omega\lambda_d \quad 3\text{-}2$$

$$\lambda_d = L_d i_d + \lambda_{pm} \quad 3\text{-}3$$

$$\lambda_q = L_q i_q \quad 3\text{-}4$$

$$T = \frac{3}{2}p\left(\lambda_d i_q - \lambda_q i_d\right) \quad 3\text{-}5$$

Inserting the equations for the flux linkage into the voltage and torque equations, and using the fact that the machine under consideration is non-salient ($L_d = L_q = L$), gives:

$$V_d = Ri_d + L\frac{di_d}{dt} - \omega L i_q \quad 3\text{-}6$$

$$V_q = Ri_q + L\frac{di_q}{dt} + \omega\left(Li_d + \lambda_{pm}\right) \quad 3\text{-}7$$

$$T = \frac{3}{2}p\lambda_{pm} i_q \quad 3\text{-}8$$

Quite a few assumptions have been made to get the equations in this form, the most important being:

- The flux linkage only has the fundamental component, no harmonics.
- The machine behaves linearly, thus no variation of inductance due to saturation.
- No losses except copper losses due to the resistance R.

From the torque equation it follows that the torque is linearly proportional to the current in the quadrature axis. This is very convenient because it allows us to control the torque with a current controller for the quadrature current. The reference for this current controller will be:

$$i_q^* = \frac{2}{3p\lambda_{pm}}T^* \quad 3\text{-}9$$

3.4.2 Controller design

The voltage equations (3-6 and 3-7) are those of a series RL circuit, but unfortunately there is a disturbance term as well, which couples the two equations. The direct axis voltage relation now has a term related to the quadrature axis current and the quadrature axis voltage relations has a term related to the direct axis current and the flux linkage of the permanent magnets. There are at least two options to deal with this coupling between the voltage equations. One option is to neglect these terms in the design of the current controllers and see if the performance is adequate, while the other option is to compensate for this term. The first option has been chosen, since it gives adequate performance.

The controller used to control the current through an RL circuit will now be constructed. The procedure outlined in reference [27] will be followed, in this reference the pole-zero cancellation technique is used to determine the gains of a PI controller. The starting point is the time domain equation of an RL circuit, with a voltage source:

$$v(t) = Ri(t) + L\frac{di(t)}{dt} \tag{3-10}$$

This equation is transformed to the Laplace domain to simplify the mathematics:

$$v(s) = Ri(s) + Lsi(s) = (R + sL)i(s) \tag{3-11}$$

The input to this circuit is the voltage and the output is the current. This gives the following transfer function:

$$H_p(s) = \frac{i(s)}{v(s)} = \frac{1}{R + sL} \tag{3-12}$$

Introducing the time constant $\tau_p = \frac{L}{R}$ gives:

$$H_p(s) = \frac{\frac{1}{R}}{1 + s\tau_p} \tag{3-13}$$

Equation 3-13 has the properties of a low pass filter with a cut-off angular frequency of τ_p and a gain equal to the inverse of the resistance.

The voltage source in the RL circuit is a combination of a controlled source (the equivalent of the inverter) and a controller. The controlled source is modelled as a gain. The value of this gain will be determined later.

$$H_i(s) = G \tag{3-14}$$

The controller itself is a PI controller. The input to the controller is the difference between the reference current and the actual current, this term is the error.

$$e(t) = i^*(t) - i(t) \tag{3-15}$$

The equation for the PI controller is:

$$y(t) = k_p e(t) + k_i \int e(t)\, dt \tag{3-16}$$

In the Laplace domain this becomes:

$$y(s) = k_p e(s) + \frac{k_i}{s} e(s) = \left(k_p + \frac{k_i}{s}\right) e(s) \quad \text{3-17}$$

The resulting transfer function is:

$$H_c(s) = \frac{y(s)}{e(s)} = \left(k_p + \frac{k_i}{s}\right) \quad \text{3-18}$$

Though it will soon be evident that it is more convenient to write the transfer function in the following form (compare the term between brackets with the denominator of equation 3-13):

$$H_c(s) = \frac{y(s)}{e(s)} = \frac{k_i}{s}\left(1 + s\frac{k_p}{k_i}\right) \quad \text{3-19}$$

The open loop system transfer function is:

$$H_{ol}(s) = H_c(s) H_i(s) H_p(s) \quad \text{3-20}$$

This results in:

$$H_{ol}(s) = \frac{k_i}{s}\left(1 + s\frac{k_p}{k_i}\right) G \frac{\frac{1}{R}}{1 + s\tau_p} \quad \text{3-21}$$

Here it can be seen why the PI controller term was rewritten, when choosing:

$$\frac{k_p}{k_i} = \tau_p \quad \text{3-22}$$

Then the zero (the term between brackets) can be used to cancel the pole (the term in the denominator of the RL transfer function) in equation 3-21. Doing this results in:

$$H_{ol}(s) = \frac{k_i G}{sR} \quad \text{3-23}$$

This is the equation of an integrator with a gain of $\frac{k_i G}{R}$. The bandwidth of the closed loop system can be determined by finding the unity gain angular frequency of the open loop system:

$$\omega = \frac{k_i G}{R} \quad \text{3-24}$$

From this it follows that the bandwidth can be chosen infinitely large. In practice this is not true due to, for example the pulse width modulating inverter. Reference [27] mentions that the bandwidth of the controller can be taken one to two orders of magnitude lower than the switching frequency, to avoid interference with the switching frequency noise.

The two design equations of the PI controller are:

$$k_i = \frac{\omega R}{G} \qquad 3\text{-}25$$

$$k_p = K_i \tau_p \qquad 3\text{-}26$$

The gain *G* can be determined with the help of Figure 4. From the controller's point of view everything is in the rotor reference frame, but since the actual inverter is not, the park and inverse park-transform have been shown as well. On the left side is the input from the controller and this input is transformed back to the three phase stator reference frame. Then the pulse centering module centres the waveforms and also a gain has been added to this module because the pulse centering module gives the ability to increase the phase-to-phase voltage without clipping. The signals are then shifted up because the inverter can only generate positive voltages with respect to the ground level of the power supply. The gain of the inverter itself is half the supply voltage. The total gain of this system is:

$$G = \frac{U_{dc}}{\sqrt{3}} \qquad 3\text{-}27$$

On the right the signals are transformed to the rotor reference frame again, since this allows us to use them in the controller design again.

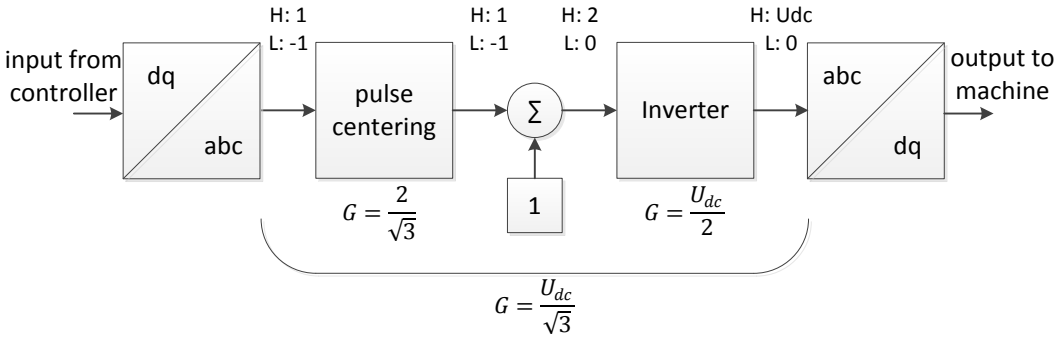

Figure 4 Determination of the gain between controller and machine

3.4.3 Field weakening

The reference input for the torque (i_q) controller is stated in equation 3-9. The input for the field weakening controller (i_d) has not been discussed yet. Furthermore the (related) situation in which the controller demands a higher voltage than is physically possible with the supply voltage needs to be discussed.

To be able to control the machine the condition in equation 3-28 must be met at all times. This means that the magnitude of the voltage on the terminals of the machine should never be larger than the maximum inverter output.

$$v_d^2 + v_q^2 \leq v_{dq,max}^2 \qquad 3\text{-}28$$

For the non-salient machine under consideration the torque only depends on i_q, thus i_d can simply be set to zero. Operating under these conditions is called maximum torque per ampere (MTPA). This operating condition is possible until base speed is reached, the highest speed where nominal torque can be delivered with nominal voltage. It is possible to increase the speed until the induced voltage equals the maximum inverter voltage, but then no torque can be developed anymore (if there is an opposing load torque this speed cannot actually be reached). The equations below are used to calculate the maximum speed capability for a machine with zero resistance and in steady state.

$$i_d = 0 \tag{3-29}$$

$$v_d = -\omega\lambda_q \tag{3-30}$$

$$v_q = \omega\lambda_d = \omega\left(Li_d + \lambda_{pm}\right) = \omega\lambda_{pm} \tag{3-31}$$

$$v_{dq} = \sqrt{v_d^2 + v_q^2} = \omega\sqrt{\lambda_q^2 + \lambda_{pm}^2} \tag{3-32}$$

$$\omega = \frac{v_{dq}}{\sqrt{\lambda_q^2 + \lambda_{pm}^2}} \tag{3-33}$$

$$\omega_{max}\left(\lambda_q \to 0\right) \to \frac{v_{dq,max}}{\lambda_{pm}} \tag{3-34}$$

When i_d is allowed to become negative it is possible to operate at speeds where the induced voltage in the machine is higher than the maximum output voltage of the inverter. The reason that this is possible is that the speed dependent term in equation 3-7 can be reduced. It is even possible to cancel this term by using the condition in equation 3-35. For a perfect machine, i.e. one without losses, the value of i_d under this condition would be equal to the machine current when the phases were all short-circuited to each other.

$$i_d = -\frac{\lambda_{pm}}{L} \tag{3-35}$$

According to reference [14] the operating mode is basic field weakening when the direct axis current is between zero and $-\frac{\lambda_{pm}}{L}$ and maximum torque per flux (MTPF) when it is at $-\frac{\lambda_{pm}}{L}$. The maximum speed for a machine without resistance and under steady state condition has been computed again to give insight into the effect of field weakening on this parameter.

$$i_d = -\frac{\lambda_{pm}}{L} \tag{3-36}$$

$$v_d = -\omega\lambda_q \tag{3-37}$$

$$v_q = \omega\lambda_d = \omega\left(Li_d + \lambda_{pm}\right) = 0 \quad \text{3-38}$$

$$v_{dq} = \sqrt{v_d^2 + v_q^2} = \sqrt{\left(-\omega\lambda_q\right)^2} = \omega\lambda_q \quad \text{3-39}$$

$$\omega = \frac{v_{dq}}{\lambda_q} \quad \text{3-40}$$

$$\omega_{max}\left(\lambda_q \to 0\right) \to \infty \quad \text{3-41}$$

In practice machines are not ideal and there is always load torque due to friction, which means that even at constant speed a torque (and thus a flux in the quadrature axis) has to be applied. This means that the flux cannot be reduced to zero without deceleration, hence it is not possible to approach infinite speed (also the machine might not be able to reach very high speeds without failing mechanically). The equations do however show that the maximum speed can be increased, but at the cost of torque reduction.

The input to the direct axis current controller needs to be known in order to perform field weakening. Another PI controller could be used which controls the current such that the output of the inverter stays below its maximum, while still being able to produce torque. This approach has been taken by reference [28]. This approach requires detailed stability analysis of the controller itself, which is outside the scope of this thesis. It has been chosen instead to use the steady state equations of a non-salient machine without resistance to calculate the required value of the direct axis current. The required equations are listed below.

$$v_d = -\omega L i_q \quad \text{3-42}$$

$$v_q = \omega\left(Li_d + \lambda_{pm}\right) \quad \text{3-43}$$

$$v_{dq,max} \geq \sqrt{v_d^2 + v_q^2} = \sqrt{\left(-\omega L i_q\right)^2 + \left(\omega\left(Li_d + \lambda_{pm}\right)\right)^2} \quad \text{3-44}$$

$$i_d = -\frac{\lambda_{pm}}{L} + \sqrt{\left(\frac{v_{dq,max}}{\omega L}\right)^2 - i_q^2} \quad \text{3-45}$$

Equation 3-45 gives the final result. The upper limit of i_d is chosen to be zero, because a positive current would only introduce more losses. The lower limit is $-\frac{\lambda_{pm}}{L}$. While it would be possible to have a more negative current, this would cause an adverse effect. Because of this the part underneath the square root can be given a lower limit of zero, such that the situation in which the square root of a negative number is taken does not occur. Going beyond either limit would reduce to amount of torque that can be produced for a certain maximum voltage vector.

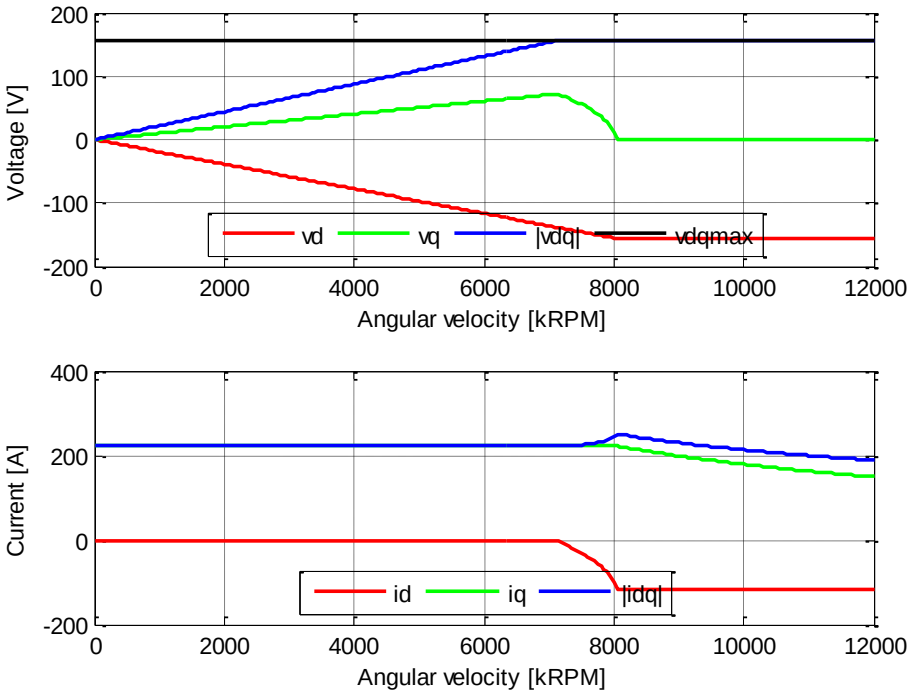

Figure 5 Voltage and current as a function of speed, with field weakening

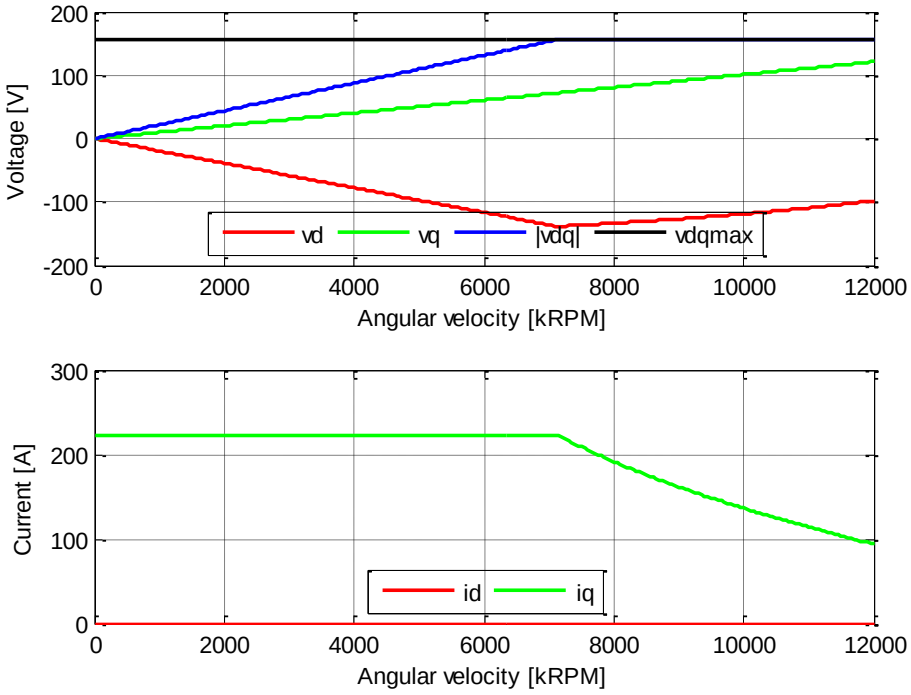

Figure 6 Voltage and current as a function of speed, without field weakening

Figure 5 and Figure 6 show the trajectory followed by the voltage and current during the start-up of the starter/generator. The values follow from a simple analytical calculation for which the assumptions of steady state and zero copper resistance have been made. This has been done to clarify why field weakening can be used, not to give an accurate representation of the voltage and current during start-up.

In the graphs showing the voltages the two orthogonal voltage components are shown, together with the magnitude of these components and the maximum possible value (limited by the DC supply voltage). In the graphs showing the currents again the two orthogonal components are shown and in the case of start-up with field weakening also the magnitude of these components is shown (the magnitude of the current in the case without field weakening is equal to i_q, since i_d equals zero). The voltage magnitude runs into the maximum possible value at around 7 kRPM in both cases (with and without field weakening). When no field weakening is applied this means that the current in the quadrature axis (and thus the torque) has to be decreased. When field weakening is applied it is possible to continue generating the same amount of quadrature axis current for another 1 kRPM. It can be seen that by using field weakening the quadrature axis current can be kept considerably larger from 7 kRPM onwards. When the speed of 12 kRPM is reached the start-up will end and just before the end the quadrature axis currents are 149 A and 94 A for the case of field weakening and no field weakening, respectively. This means that at the end it is possible to generate almost 60% more torque by applying field weakening (however, it must be noted that this difference becomes smaller when copper resistance is included).

In both cases the quadrature axis current reference value has been set to 223 A, the current which would give the maximum allowed torque output of the starter/generator. The parameters that have been used for the maximum voltage and the machine impedance are representative for the actual starter/generator system.

3.5 Permanent magnet synchronous machine

The electric machine that has to be modelled consists of a rotor with surface mount permanent magnets and a stator with a three phase concentrated winding. The machine has four teeth per phase and around each tooth there are three parallel strands made up of 49 turns each. The windings around the four teeth of a single phase are connected in parallel.

The equivalent model of a PMSM has been used to model the machine. The model consists of a resistor, an inductor and a voltage source in series. The machine has been analysed by the machine developer using FEM. From this analysis the inductance (self and mutual), flux linkage and resistance of every copper turn is known.

Figure 7 shows the circuit representation of a single turn. The voltage source in this equation represents the voltage induced in the coil due to the change of flux linkage with the permanent magnets on the rotor, according to equation 3-46.

$$e = \frac{d\lambda_{pm}}{dt} \tag{3-46}$$

The voltage over this circuit is expressed by equation 3-47.

$$u = Ri + L\frac{di}{dt} + e \tag{3-47}$$

It has to be noted that in this formula the coupling with other coils has not been taken into account. The mutual coupling will be introduced later on.

Figure 7 A single turn equivalent circuit

How are these equations useful? The current in the coil can be calculated and most of the analyses that will be done is based on the currents through individual coils. In the final application, however, the machine should generate torque to either start the turbine engine in starter mode or deliver power to the electrical circuit in generator mode. Thus an equation for the torque is necessary and a brief derivation will be given next.

From the FEM analysis followed that the flux from the permanent magnets linked with the coils is mostly sinusoidal. For the derivations of the power and torque, the voltage source in Figure 7 is assumed to be completely sinusoidal. This assumption is reasonable since the harmonics in the back-EMF are very small compared to the fundamental component. With this assumption the flux linkage can be written as:

$$\lambda_{pm}(t) = \hat{\lambda}_{pm}\cos(\omega_e t + \varphi) \tag{3-48}$$

Now it is possible to calculate the induced voltage according to equation 3-46:

$$e(t) = \frac{d\lambda_{pm}}{dt} = -\omega_e\hat{\lambda}_{pm}\sin(\omega_e t + \varphi) \tag{3-49}$$

And using this result the power going into this voltage source is found to be:

$$P_e(t) = e(t)i(t) = -\omega_e\hat{\lambda}_{pm}\sin(\omega_e t + \varphi)i(t) \tag{3-50}$$

The rotor flux that links with the stator coils is used to produce torque. The instantaneous torque is:

$$T_m(t) = \frac{P_e}{\omega_m} = p\frac{P_e}{\omega_e} = -p\hat{\lambda}_{pm}\sin(\omega_e t + \varphi)i(t) \qquad 3\text{-}51$$

The current is a function of time, which is important to mention. If it were constant then the average torque would be zero. In practice a sinusoidal current is driven through the coil and this causes a pulsating torque for a single phase. For a three phase system the three pulsating torques add and, ideally, give a steady (i.e. non-pulsating) torque.

As mentioned previously there are three parallel strands of 49 turns each around a single tooth. This configuration is shown in Figure 8. It can be seen that the tooth winding is represented by $3 \cdot 49 = 147$ individual turns. Now that there are multiple turns the mutual coupling between them has to be taken into account as well. With this amount of turns, and an equation for each one of them, it is convenient to start using matrix equations. It is also possible to reduce the amount of equations to 3, since we know that the current in a series circuit is the same everywhere in that circuit. The resulting equation, in which the self and mutual inductance of individual turns have already been grouped into self and mutual inductance of a single strand, is equation 3-52.

$$\begin{bmatrix} u_1 \\ u_2 \\ u_3 \end{bmatrix} = \begin{bmatrix} R_1 & 0 & 0 \\ 0 & R_2 & 0 \\ 0 & 0 & R_3 \end{bmatrix} \begin{bmatrix} i_1 \\ i_2 \\ i_3 \end{bmatrix} + \begin{bmatrix} L_1 & M_{12} & M_{13} \\ M_{21} & L_2 & M_{23} \\ M_{31} & M_{32} & L_3 \end{bmatrix} \frac{d}{dt} \begin{bmatrix} i_1 \\ i_2 \\ i_3 \end{bmatrix} + \begin{bmatrix} e_1 \\ e_2 \\ e_3 \end{bmatrix} \qquad 3\text{-}52$$

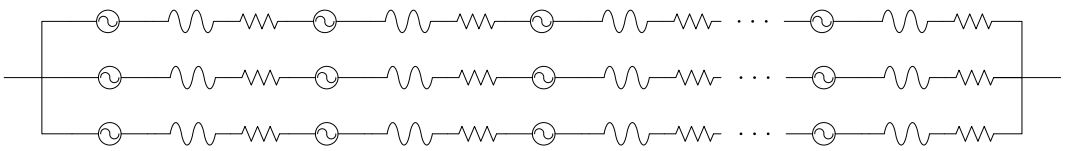

Figure 8 The tooth winding made up out of three parallel strands

This is a good moment to come back to the possibility to use the models that are developed here in case of internal short-circuit analysis. It had been said that this was possible with minor modifications. In case one or more turns of a strand are short circuited, the current is not the same anymore in every point in the strands (because there is now a parallel path). The modification that has to be done is to add an extra equation for every parallel path that is added.

The next step towards a machine model, after the single turn and the tooth winding, is the model for a complete phase. There are four teeth, with identical winding, connected in parallel and this can be seen in Figure 9. In this figure the strands have been modelled as turns, which is possible due to the fact that the current is the same everywhere in a strand as mentioned previously.

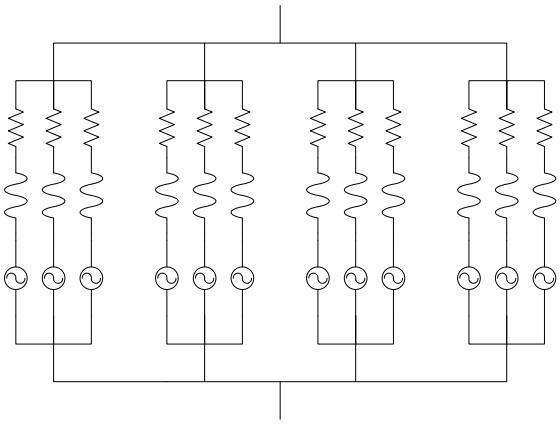

Figure 9 The phase winding consisting of four parallel tooth windings

Since all teeth are wound identically and internal machine faults will not be treated in this thesis, it is possible to represent the phase winding by an equivalent winding of 3 strands instead of the 12 shown in the figure. When doing this the entire three phase machine can be modelled as is shown in Figure 10. A further assumption (one that causes only a very small error) is that there is no mutual coupling between the tooth windings in the same phase. The reason that the error introduced by this is very small is because there are two teeth from other phases between teeth from the same phase, thus the flux of one tooth linked with another tooth in the same phase will be negligible.

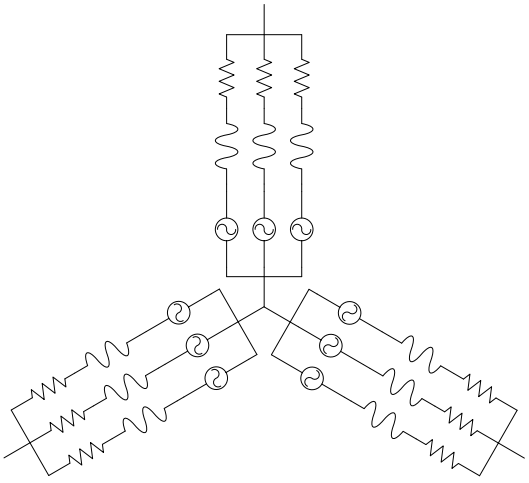

Figure 10 The complete machine

In this model there are 9 unknowns[1]: the currents through the strands. Thus there are only 9 equations that have to be solved. If there would be a short circuit in the machine it is not possible to combine the teeth from the same phase, resulting in 4 times the amount of equations, plus extra equations to solve for the currents in the shorted turns.

[1] Actually there are 8 unknowns: one current is not needed to solve the equations, it follows directly from the others. This fact has not been used in the actual machine implementation.

4 Model implementation

In this chapter the implementation of the models, as described in the previous chapter, will be discussed. The models are implemented in the SaberRD simulation package in different ways. Look-up tables, standard components and the MAST modelling language have been used. The structure of this chapter is very similar to that of the previous one, thus first the mechanical load will be discussed, then the inverter and power source followed by the torque controller and the electrical machine.

4.1 Load

The load that has to be implemented consists of a speed dependent torque and of inertia. In Figure 2 the speed dependency of the torque was shown. Since the torque is defined for several values of the speed, it seems logical to implement this part of the load as a look-up table. Figure 11 shows the model of the complete load in which the look-up table can be found. The input to this model (on the left) is the shaft speed and the output (on the right) is the torque applied to the same shaft. The shaft is connected to the electrical machine. The tool which was used to enter the data for this table is shown in Figure 12.

In Saber a line in the diagram does not always represent just a single number. The lines shown in the figure below for example represent the angular speed and a torque can be applied to them as well. The lines can thus be seen as shafts and we can also put sensors on it to determine the speed and position angle of the shaft. The speed does not have to be fed back to the electrical machine, because this information is present on the shaft to which the machine is applying torque. This also explains why the input and the output of the look-up table are connected to each other. The input simply senses the speed, while on the output a torque is applied to the same line.

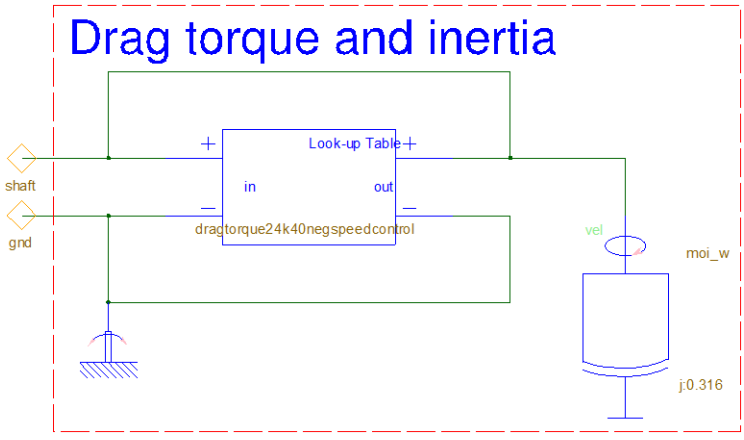

Figure 11 The complete load implemented in Saber

In the lower left corner of Figure 11 is a standard component of Saber which is the implementation of an inertia. This component simply gives a torque proportional to the angular acceleration.

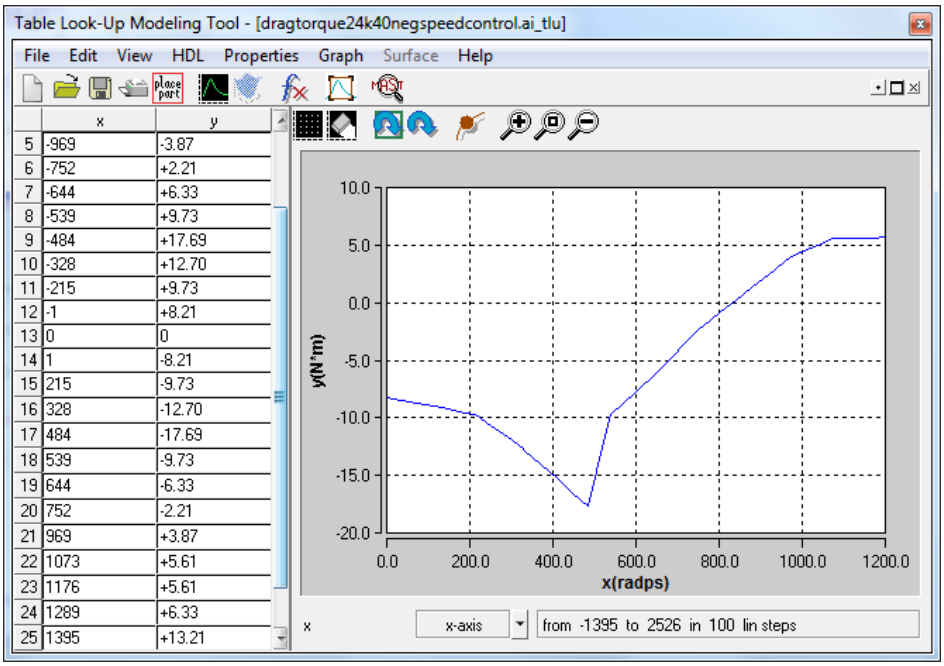

Figure 12 The table look-up tool used to implement the speed dependent torque

4.2 Inverter

The inverter has been modelled using schematic blocks and MAST models. Figure 13 shows the implementation. On the left in this figure is the inverse Park transform, which transforms the voltages requested by the current controllers in the rotor reference frame to 3 phase voltages with a value between -1 and 1. These voltages are then multiplied with a gain of $\frac{2}{\sqrt{3}}$, which is possible due to the pulse centering method that is applied next. After the pulse centering the signals are again between -1 and 1, and this is then scaled such that the signals are between 0 and 1. The signals are then fed to the ideal inverter, which are simply three voltage sources. The voltage sources are implemented in MAST as ideal transformers using equations 4-1 and 4-2. The MAST language allows the equations to be written down literally like this.

$$i_{in} = -n \cdot i_{out} \qquad 4\text{-}1$$

$$v_{out} = n \cdot v_{in} \qquad 4\text{-}2$$

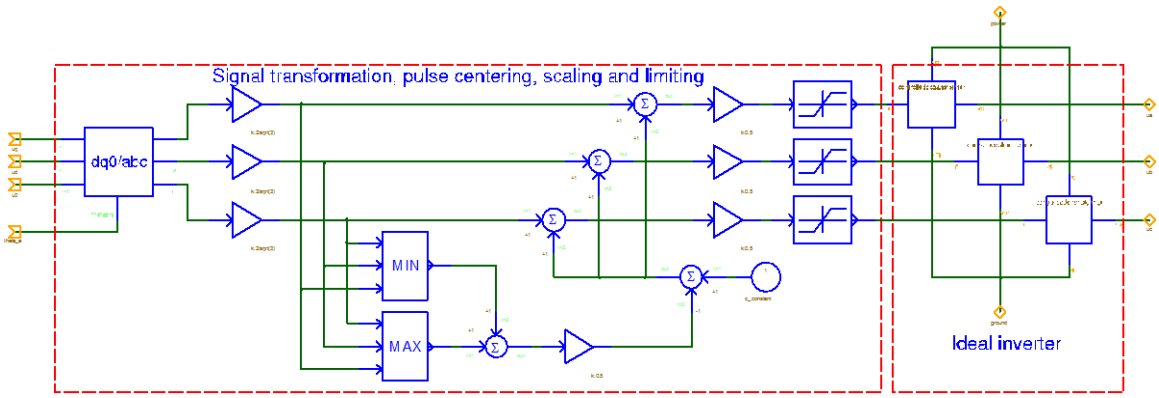

Figure 13 Inverter model

As mentioned in the previous chapter the cables connecting the inverter and the electric machine have been implemented as well. The actual implementation is a series connection of a resistance and an inductor for each phase. Mutual coupling between these cables has not been taken into account.

4.3 Power source

For the voltage source a standard Saber component representing an ideal voltage source is used, as can be seen on the left in Figure 14. On the right is the inverter from the previous paragraph, which is here shown as a module. On the left side of the inverter are the inputs from the current controllers and the speed of the electrical machine and on the right there are the phase outputs.

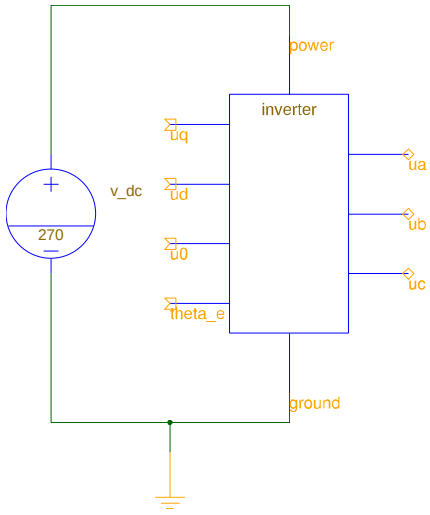

Figure 14 Voltage source connected to the inverter

4.4 Torque controller

The torque controller consists of two current controllers (for the currents in the direct and quadrature axis) and a reference signal generator. The latter determines the input signals for the current controllers.

4.4.1 Current control

Current control is implemented using equations 3-25, 3-26 and 3-27. Figure 15 shows the direct axis current controller. The gain block on the left and the division together implement equations 3-25 and 3-27. The gain in the integrator block itself is set to 1. The other gain block implements equation 3-26, which is a multiplication by the time constant of the machine. Finally the output voltage reference is limited by the saturation block to avoid output values that would cause clipping of the inverter. The current controller for the quadrature axis is similar, only the saturation block has variable inputs for the limits in this case (such that the combined values for the reference voltages do not cause clipping either).

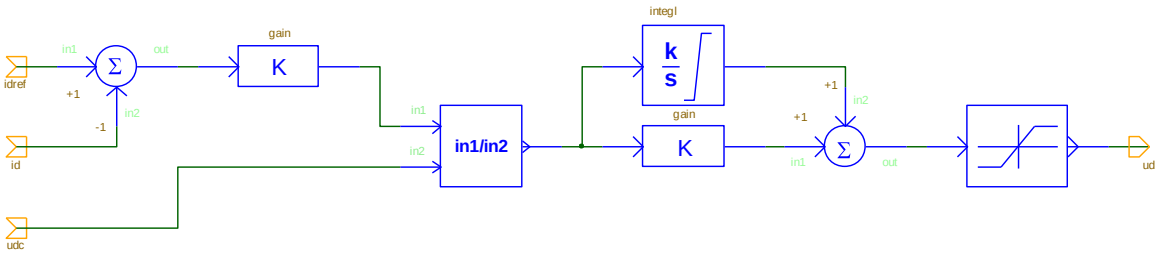

Figure 15 Controller for the direct axis current

4.4.2 Reference signal generation

Figure 16 shows the generation of the quadrature axis current reference. The look-up table on the left is used to generate a reference torque that is between the allowed limits as shown in Figure 2. The clock and the switch in the figure are used to set the reference torque to zero at the beginning of the simulation in order to start the simulation with zero initial conditions. Saber does an initial point calculation before starting a simulation. When the torque reference is non-zero at time zero, then Saber will calculate the initial currents needed to produce this torque at time zero during what is called the DC analysis. Problems were encountered using this approach and because of this the torque reference is set to zero during the first millisecond of the simulation. The gain block at the right does the actual calculation needed to obtain the reference current, according to equation 3-9.

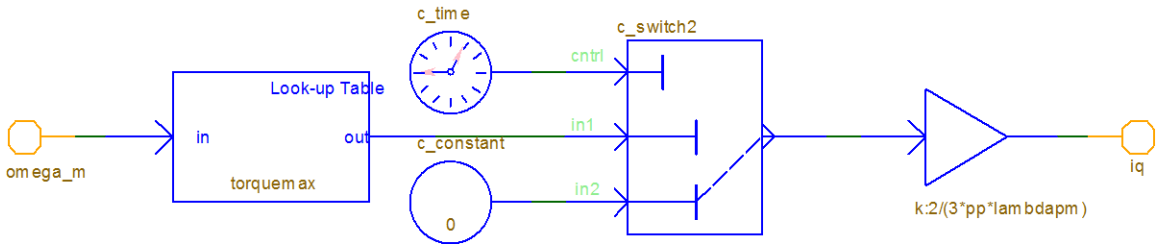

Figure 16 Generating the quadrature axis current reference from the requested torque

Because the magnitude of the DC voltage source is limited, it may not always be possible for the current controllers and the inverter to generate a current equal to the reference current. Field weakening may be applied, but even then the limits of the inverter output may be reached. The current in both direct and quadrature axis current are calculated such that there is a margin between the actual inverter output and the maximum output. These calculations have been done using the same steady state calculations used in section 3.4, thus also neglecting the stator resistance. The resulting equations are 4-3, 4-4 and 4-5. The implementation of these formulas has been done using the standard mathematics blocks from the Saber library.

$$u_{dq,max} = k\frac{u_{dc}}{\sqrt{3}} \tag{4-3}$$

$$i_{d,ref} = -\frac{\lambda_{pm}}{L} + \sqrt{\left(\frac{u_{dq,max}}{\omega L}\right)^2 - i_{q,torqueref}^2} \tag{4-4}$$

$$-\frac{\lambda_{pm}}{L} \leq i_{d,ref} \leq 0$$

$$i_{q,ref} = sign(i_{q,torqueref})\sqrt{\left(\frac{u_{dq,max}}{\omega L}\right)^2 - \left(i_{d,ref} + \frac{\lambda_{pm}}{L}\right)^2} \tag{4-5}$$

$$|i_{q,ref}| \leq |i_{q,torqueref}|$$

In equation 4-3 the maximum voltage magnitude in the rotor reference frame is calculated. The factor k is there to implement the previously mentioned margin on the inverter output. This margin is needed to cope with the errors induced by the assumptions of steady state and zero stator resistance. The variable $i_{q,torqueref}$ in equations 4-4 and 4-5 is the output from Figure 16 and $i_{q,ref}$ is the reference current that actually goes to the current controllers ($i_{q,ref}$ always has a magnitude smaller than or equal to $i_{q,torqueref}$). The outcome of the parts of the equations underneath the square root has been given a lower limit of zero. This is possible due to the limits that have been put on the current-reference signals.

4.5 Permanent magnet synchronous machine

The electric machine to be implemented has been described in section 3.5. Here it was shown that 9 equations have to be solved. This would be a good opportunity to use matrix notation, but unfortunately no support for matrix operations in Saber has been found. Because of this the 9 equations have been fully written out. One of these equations is shown below.

$$u_a = R_1 \cdot i_1$$

$$+\frac{d}{dt}(L_{11} \cdot i_1 + L_{12} \cdot i_2 + L_{13} \cdot i_3 + L_{14} \cdot i_4 + L_{15} \cdot i_5 + L_{16} \cdot i_6 + L_{17} \cdot i_7 + L_{18} \cdot i_8 + L_{19} \cdot i_9) \qquad 4\text{-}6$$

$$-\lambda_{pm1} \cdot pp \cdot \omega_m \cdot sin(pp \cdot \theta_m + \varphi_1)$$

This equation has been copied from the MAST file of the machine model (subscripts have been added and symbol names have been replaced by the symbols themselves for clarity). It is not common practice to use differentiation in numerical simulations because of noise amplification. Nevertheless the term $\frac{d}{dt}$ can be found in the above equation. This has been done intentionally, as Saber does not have a keyword for integration. This means that equations that use integration should be rewritten to use differentiation. This is only a matter of notation and the simulator that solves the equations can actually use integration techniques to solve the equation.

When the currents are known it is possible to calculate the torque. The equation below shows a part of the torque equation.

$$T_m = -i_1 \cdot \lambda_{pm1} \cdot sin(pp \cdot \theta_m + \varphi_1)$$

$$-i_2 \cdot \lambda_{pm2} \cdot sin(pp \cdot \theta_m + \varphi_2) \qquad 4\text{-}7$$

$$- \ldots$$

There is also a negative contribution to the torque due to the inertia of the rotor, this has been implemented using this equation:

$$T_l = -J_r \cdot \alpha_m \qquad 4\text{-}8$$

The torque applied to the output shaft now becomes:

$$T = T_m + T_l \qquad 4\text{-}9$$

In the previous equation the rotor angle, speed and acceleration have been used. This means that equations are needed to determine the value of these quantities as well. These equations are quoted below.

$$\theta_m: \omega_m = \frac{d\theta_m}{dt} \qquad 4\text{-}10$$

$$\omega_m: \alpha_m = \frac{d\omega_m}{dt} \qquad 4\text{-}11$$

In the first equation is written "θ_m:" which means that the equation should be used to solve for θ_m (the mechanical angle of the rotor).

Figure 17 shows the symbol that is used for the electric machine. This symbol is used in the complete system and it hides all of the equations. On the left side there are 4 electrical connections for the phase terminals and the neutral point of the star connection. On the right side there are two mechanical connections, one for the stator and one for the rotor. The stator will be connected to a reference (mechanical ground) and the motion of the rotor will be with respect to this reference.

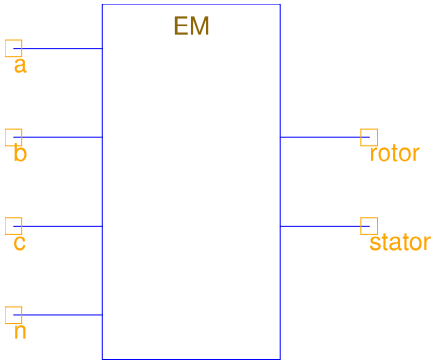

Figure 17 The symbol for the electric machine

It has already been mentioned before that the lines and connections in Saber do not represent just a number, but the real characteristics of in this case electrical and mechanical connections. This means that the voltage levels that are applied to the machine need a reference. For the mechanical connection this reference was already determined to be the stator which is connected to mechanical ground. The *branch* keyword in Saber can be used to tell the simulator the relations between terminals. For example the voltage between terminal *a* and the neutral point *n* can be written like this:

$$branch\ u_a = v(a, n) \qquad 4\text{-}12$$

This means that voltage *ua* is the voltage difference between the points *a* and *n*. While voltage is over a component, the current goes through. In MAST this can be written like this:

$$branch\ i_1 = i(a \rightarrow n) \qquad 4\text{-}13$$

Thus the current going from a to n is i_1 in this case. The same thing can be done for mechanical connections. Here speed is the speed difference between to connections and the torque is from

one connection to the other. The *branch* equations for the mechanical connection are shown below.

$$branch\ \omega_m = \omega_{radps}(rotor, stator) \quad \text{4-14}$$

$$branch\ T = T_{Nm}(rotor \rightarrow stator) \quad \text{4-15}$$

Notice the similarity between voltage and speed and between current and torque.

Now that the models are implemented, it is time to move on to the system simulations. These will be presented in the following chapter.

5 System simulation

In this chapter the start-up phase will be investigated. Voltage regulation in generator mode has not been implemented and because of this the generator phase will not be given much attention. Before investigating the entire system, first the validity of the electric machine model will be tested.

5.1 Standalone operation of the electric machine

In first instance the machine itself is investigated, to determine if the model is functioning correctly. For this the open circuit voltage and the short circuit current will be determined using simulations.

5.1.1 Open circuit voltage

According to the machine parameters the flux magnitude should be about 24.09 mWb. At a speed of 24 kRPM (the nominal speed in generator mode), this should give an induced EMF of:

$$E = \omega_e \lambda_{pm} = \frac{24 \cdot 10^3}{60} \cdot 4 \cdot 2\pi \cdot \frac{24.09 \cdot 10^{-3}}{\sqrt{2}} = 171.25\ V \qquad 5\text{-}1$$

Figure 18 shows the sinusoidal waveforms of the induced EMF at 24 kRPM. These waveforms are obtained by measuring directly at the terminals of the machine, when nothing else is connected to the terminals. The RMS values of these waveforms are shown in Table 2. The measured values are very close to the calculated value, thus the model gives the correct results.

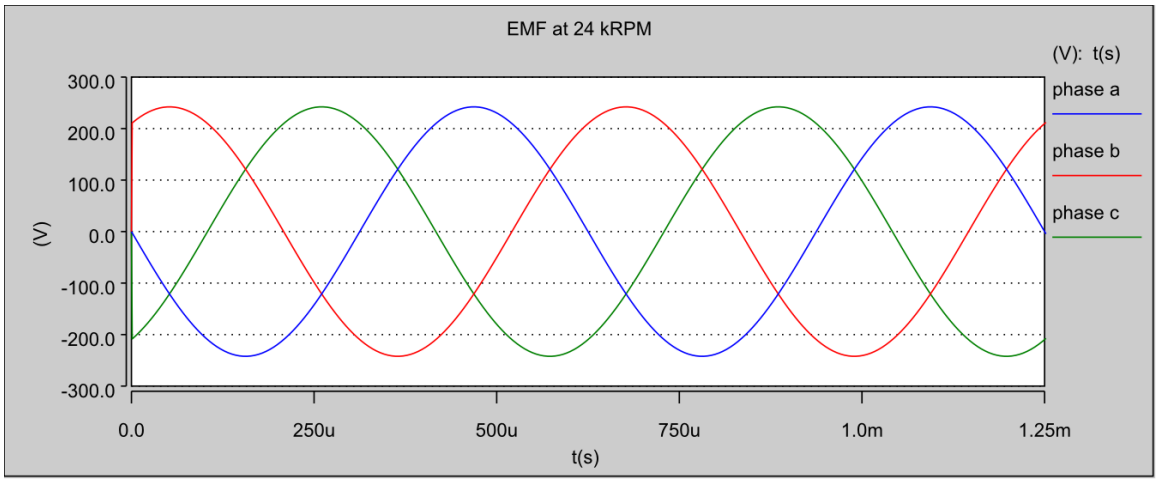

Figure 18 Induced phase voltages at 24 kRPM

Table 2 Phase voltages

Phase	RMS voltage [V]
A	171.26
B	171.22
C	171.24

5.1.2 Short circuit current

The machine has been short circuited at its terminals to determine the short circuit current. Figure 19 shows the RMS short circuit current of the three phases from zero speed to nominal speed in generator mode.

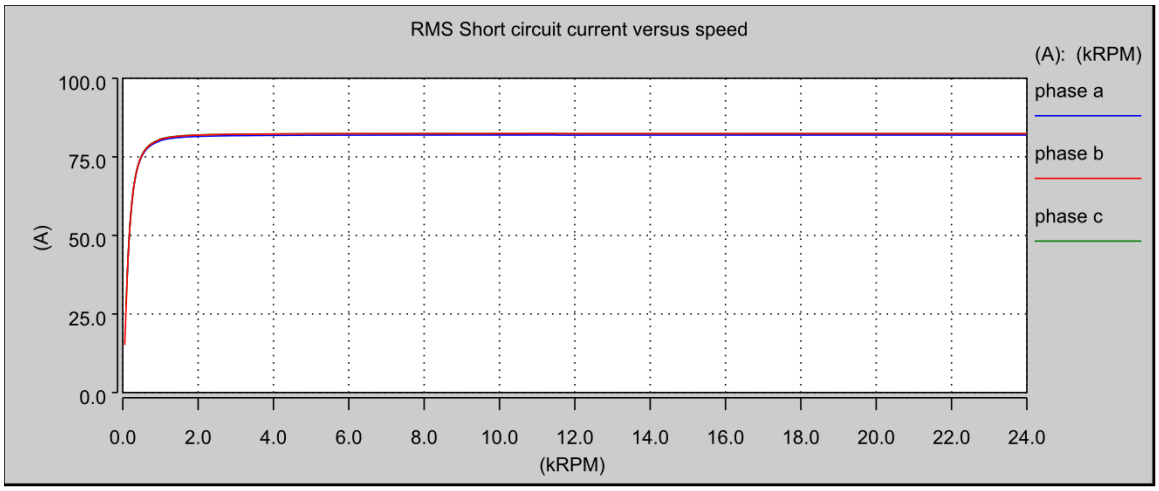

Figure 19 Short circuit current versus speed

Above approximately 2 kRPM the short circuit current becomes constant, seemingly independent of speed. This can be explained by looking at the impedance of the machine. This impedance has a constant, resistive, part and a speed dependent, inductive, part.

The short circuit current is determined by equation 5-2.

$$|I(\omega)| = \frac{|U(\omega)|}{|Z(\omega)|} = \frac{\omega_e \lambda_{pm}}{\sqrt{R^2 + (\omega_e L)^2}} \qquad 5\text{-}2$$

From the denominator of this equation can be concluded that at low speeds the resistive part is dominant, while at higher speeds the inductive part becomes dominant. The impedance of the restive and the inductive part are equal at a frequency of:

$$R = \omega_e L \rightarrow \omega_e = \frac{R}{L} \qquad 5\text{-}3$$

At very low frequencies the short circuit current can be determined using equation 5-4, while at higher frequencies it can be determined by equation 5-5.

$$|I(\omega)| = \frac{\omega_e \lambda_{pm}}{R} \quad \text{5-4}$$

$$|I(\omega)| = \frac{|U(\omega)|}{|Z(\omega)|} = \frac{\omega_e \lambda_{pm}}{\omega_e L} \rightarrow |I| = \frac{\lambda_{pm}}{L} \quad \text{5-5}$$

Table 3 shows the value of the asymptotes of the phase currents. These can be used to calculate the value of the combined self and mutual inductance of the phases. In equation 5-6 this has been calculated for phase A.

$$I = \frac{\lambda_{pm}}{L} \rightarrow L = \frac{\lambda_{pm}}{I} = \frac{\left(\frac{24.09 \cdot 10^{-3}}{\sqrt{2}}\right)}{81.93} = 207.9\ \mu H \quad \text{5-6}$$

Table 3 RMS short circuit phase currents at high speed

Phase	RMS current [A]
A	81.93
B	82.38
C	82.41

It has to be noted that while the short-circuit current of phases B and C are almost equal, there is a marginally larger difference with phase A. The difference is only 0.6% and this difference is due to the inductance matrix that has been obtained using FEM. For phase A the self-inductances are somewhat higher. The differences are so small that no further attention will be paid to this discrepancy.

Figure 20 shows a close-up of the low speed region. The point where the phase currents are approximately $\frac{1}{\sqrt{2}}$ of their asymptotic value has been marked. The speed at this point is the speed at which the impedance due to resistance and inductance is equal.

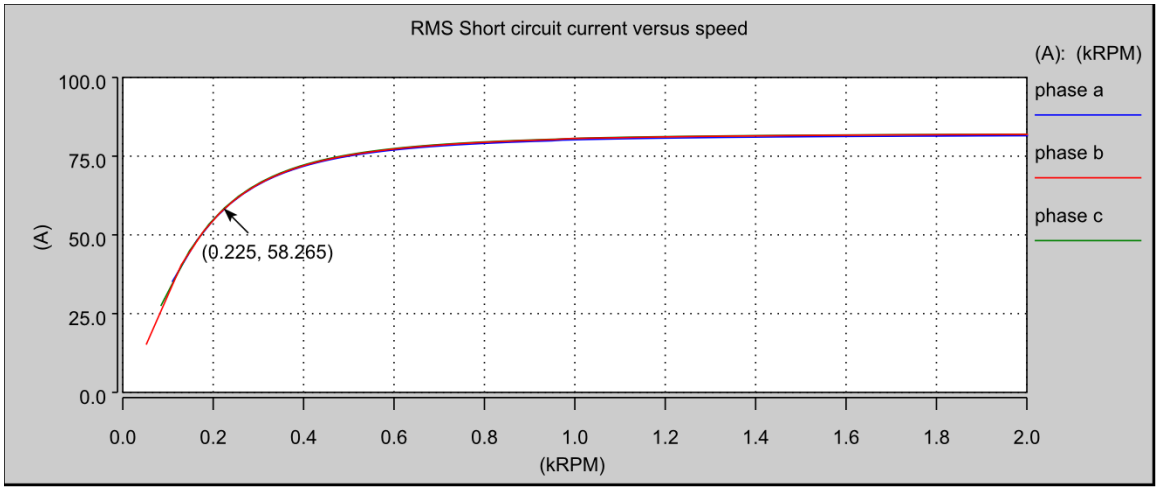

Figure 20 Close-up of low speed region

The total impedance at this speed is:

$$|Z| = \frac{U}{I} = \frac{\omega_e \lambda_{pm}}{I} = \frac{\left(\frac{0.225 \cdot 10^3}{60} \cdot 4 \cdot 2\pi \cdot \frac{24.09 \cdot 10^{-3}}{\sqrt{2}}\right)}{58.27} = 27.55\ m\Omega \quad (5\text{-}7)$$

The impedance of the resistive part must be:

$$|Z| = \sqrt{R^2 + (\omega L)^2} = \sqrt{2R^2} = \sqrt{2}R \rightarrow R = \frac{|Z|}{\sqrt{2}} = 19.48\ m\Omega \quad (5\text{-}8)$$

This result can be checked by comparing it to the impedance of the inductance at this frequency, because the result should be equal. The impedance due to the inductance is:

$$|Z_L| = \omega_e L = \frac{0.225 \cdot 10^3}{60} \cdot 4 \cdot 2\pi \cdot 207.9 = 19.59\ m\Omega \quad (5\text{-}9)$$

It can be seen that there is a small error, since the impedances are not completely equal. The value for the resistance should of course be very close to the one that we expect from the machine parameters. The parameters show that four parallel coils in a phase have a resistance of $58.14\ m\Omega$. This gives a phase inductance of $19.38\ m\Omega$ (since the coils around three teeth are again connected in parallel), which is close to the value calculated using the measurement data.

The graphs, the data extracted from them and the calculation show that the model functions correctly.

5.2 Start-up time

For the start-up sequence to complete, the electric machine must reach a speed of 12 kRPM. Two reference torque curves have been used, these are the minimum and the maximum torque as defined in Figure 2. With the supply voltage of 270 V it is not always possible to actually obtain a torque equal to the reference torque, but this will be discussed in paragraph 5.4.

Table 4 shows the time needed to reach 12 kRPM. With the maximum torque as a reference it takes 5.8 seconds less to reach this speed, which is almost 26% faster. This makes the time saving by using maximum torque quite significant.

Table 4 Start-up time

Torque	Time [s]
Minimum	22.6
Maximum	16.8

In Figure 21 the speed has been plotted as a function of time. In the period between 8 and 14 seconds much time is lost with the minimum torque reference. This can be explained by looking at Figure 2 again. The peak in the load torque causes the effective torque that is left to speed up the inertia to be quite low. When using a low starter torque the impact is largest, since the relative decrease in torque is much larger.

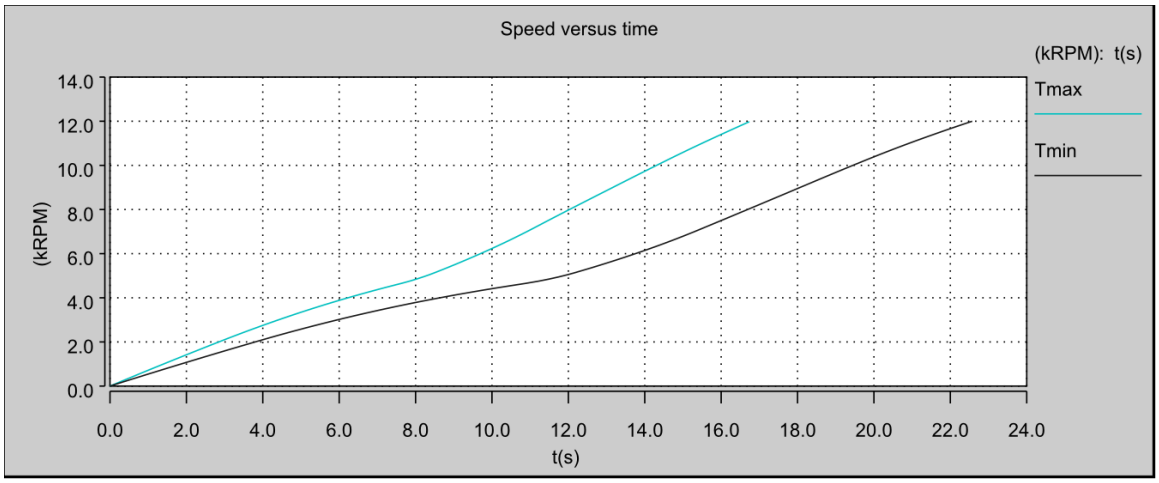

Figure 21 Speed versus time for minimum and maximum starter torque

5.3 Efficiency

Even though it is not the focus of this thesis, it is still interesting to know some reasons why the minimum or maximum starter torque should be used (or some value in between). The first reason is of course the time needed to perform the start-up. It has been shown in the previous paragraph that there is a significant difference in start-up with different torque references. Another reason might be the energy consumption and the rate at which it is consumed, i.e. the power. This will be treated briefly in this paragraph.

A comment should be made first. The machine model created for this thesis was not made with efficiency measurements in mind. Because of this only copper losses have been taken into account, whilst hysteresis and eddy current losses are not. This makes the model less suitable, though not completely useless, for determining the efficiency.

Figure 22 and Figure 23 show the electrical and mechanical power and energy as a function of time, for respectively minimum and maximum starter torque. The difference between the electrical and mechanical energy has been given as well. This energy is turned into heat in the conductors of the machine and the cables from the inverter to the machine. It can clearly be seen that the power levels are higher when using maximum torque. Due to the higher currents associated with the higher torque there is also a larger difference between the electrical input power and the mechanical output power.

In Table 5 and Table 6 the total electrical and mechanical energy, and the difference between them, has been tabulated. From this data follows that the total amount of energy needed to perform the start-up is higher with minimum torque than with maximum torque. This is due to friction, because a load without loss mechanism would have required the same amount of mechanical energy independent of the torque magnitude and time. The interesting result is that while it takes more energy to start-up using minimum torque, the amount of electrical energy turned into heat in the machine is actually less. If the machine were powered from batteries and the total energy consumption is most important, than it is better to use maximum torque. When the machine temperature is very high before the start, then it is better to use minimum torque. In that case less energy is turned into heat in the machine itself (more if the load is also included).

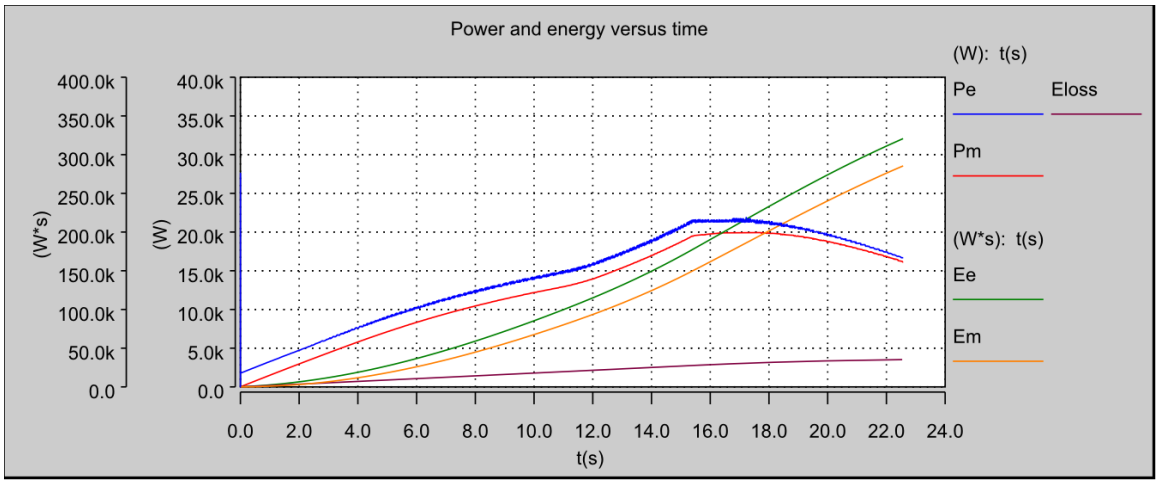

Figure 22 Power and energy as a function of time, for minimum stater torque

Table 5 Energy distribution for start-up cycle with minimum torque

Type	Energy (kJ)
Electrical	320.2
Mechanical	285.5
Loss	35.2

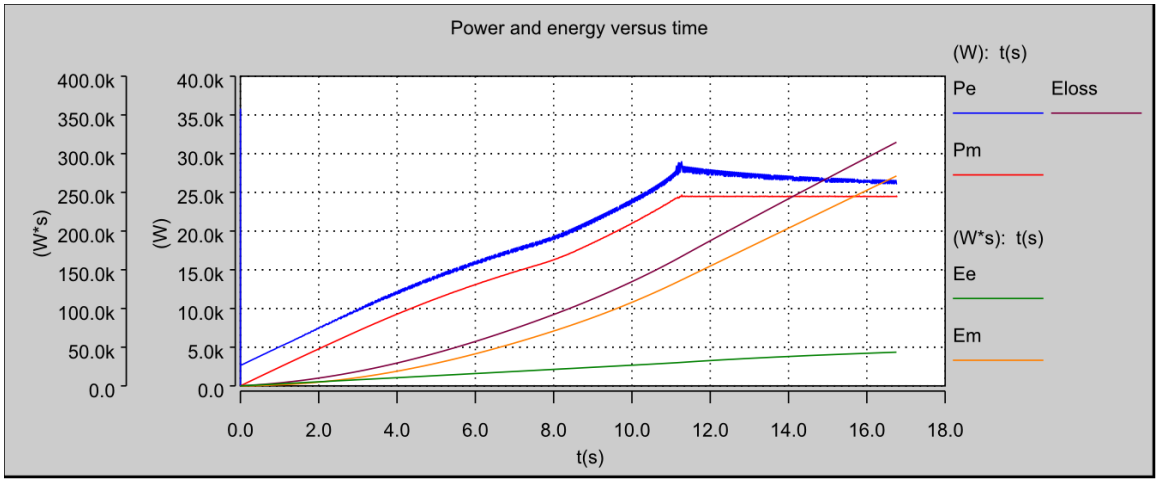

Figure 23 Power and energy as a function of time, for maximum stater torque

Table 6 Energy distribution for start-up cycle with maximum torque

Type	Energy (kJ)
Electrical	314.7
Mechanical	271.2
Loss	43.5

5.4 Torque, current and voltage trajectories

In this section the waveforms of the torque, current and voltage will be discussed for start-up with minimum and maximum torque.

5.4.1 Minimum start-up torque

Figure 24 presents the waveforms for the minimum and maximum torque in red and green, respectively. The load torque without the contribution due to inertia (i.e. the drag torque from Figure 2) and the effective torque applied to the load inertia are shown as well in orange and purple, respectively. The torque output of the electric machine should be visible in blue, but it cannot be seen. The system is able to produce exactly the minimum torque (the reference in this case) and because of this it is underneath the red line.

The static (zero speed) load torque has been implemented by a very steep torque gradient through zero speed. Because of this it can be seen that the orange line starts at zero and goes almost straight down. With increasing speed the output torque of the machine stays constant

first, but the load torque becomes more negative. The result of this is that the effective torque that is left to speed up the load inertia becomes smaller. This is the cause of the flattening of the speed curve (lower acceleration) between 8 and 14 seconds in Figure 21. When the speed increases even more, the load torque becomes less negative at first and then becomes positive. This is due to the turbine engine that has been started and which produces positive torque (torque which increases the speed). The effective torque does not vary much anymore because the torque output of the electric machine starts to decrease.

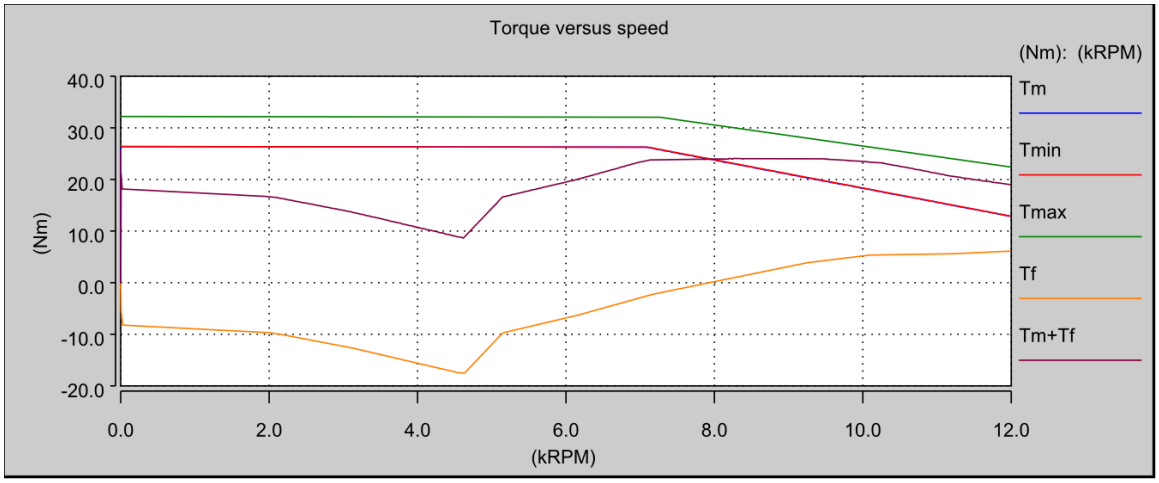

Figure 24 Torque as a function of speed, with minimum starter torque

Figure 25 shows the current through the electric machine in the rotor reference frame. The Park transform used in this thesis is amplitude invariant, thus the values in the rotor reference frame are equal to the peak values in the untransformed stator reference frame. For the largest part of the start-up no field weakening is needed. This results in a zero direct axis current (since the machine is non-salient, current in this axis cannot be used to produce torque). Only after about 17 seconds field weakening is used to be able to drive enough quadrature axis current through the machine given the voltage limit imposed by the voltage source.

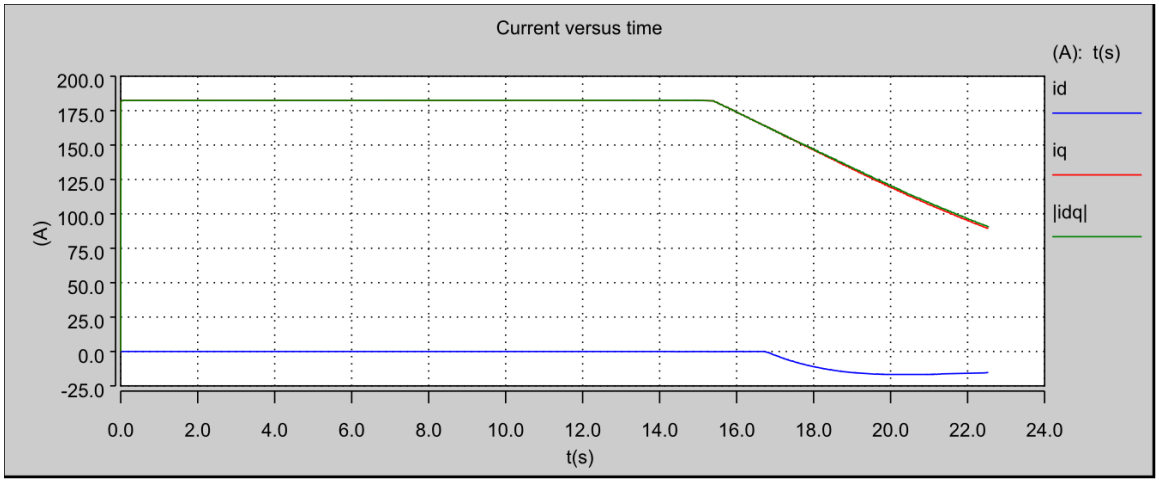

Figure 25 Current as a function of time, with minimum starter torque

The fact that field weakening is needed can also be observed in Figure 26. The voltage magnitude keeps increasing until it is almost equal (a safety margin was included as discussed in section 4.4.2) to the maximum voltage output of the inverter. The absolute maximum is given by equation 5-10.

$$\widehat{U}_{dq} = \frac{U_{dc}}{\sqrt{3}} = \frac{270}{\sqrt{3}} = 155\ V \qquad 5\text{-}10$$

In the figure it can be seen that the output voltage stays just below $150\ V$. When the voltage magnitude is this high it is not possible to increase the voltage much more. At this point there are two options, decrease the torque (and thus the current) or apply field weakening to reduce the voltage vector magnitude. Using the first option it would not be possible to deliver the wanted amount of torque. With the latter option it is possible at the cost of increasing current.

Ideally the voltage magnitude would be constant after about 18 seconds, fixed to the maximum output. However a small drop in voltage can be observed over time. This drop is caused by the reference signal generator for the two orthogonal currents, which did not take into account the voltage drop over the resistive part of the machine. The result is that voltage drop over the resistive part decreases with decreasing current and this is not compensated for by the reference signal generator. Thus the inverter could actually put out a slightly higher voltage than what it does right now (resulting in slightly lower currents).

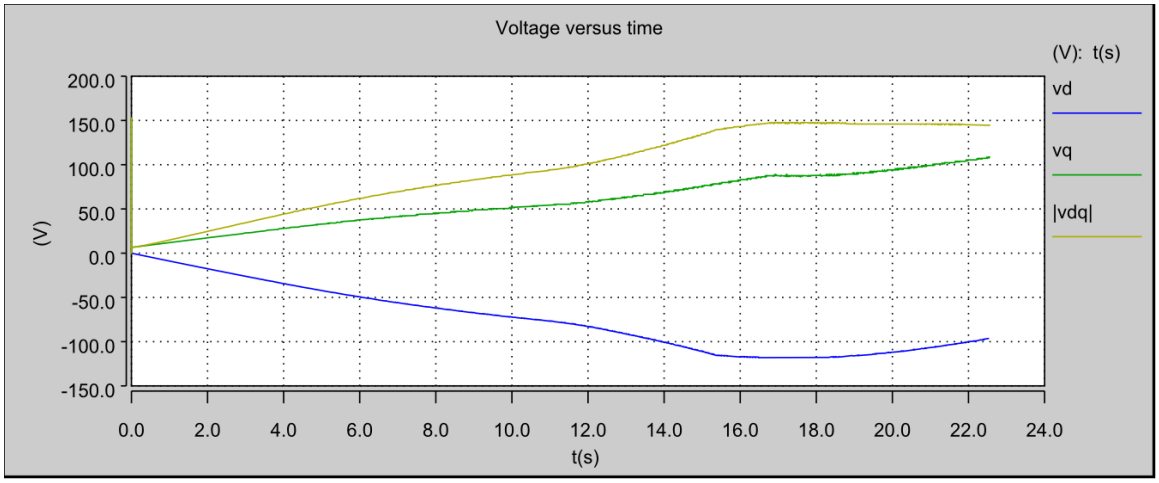

Figure 26 Voltage as a function of time, with minimum starter torque

5.4.2 Maximum start-up torque

Figure 27 shows again the torque levels as a function of speed, but this time the torque should be equal to the maximum starter torque. The colour schemes are the same as for minimum torque. This time the blue colour of the electric machine output torque waveform is visible, whilst previously it was not. At low speed the blue line is overshadowed by the maximum torque reference, but the machine is not able to produce this torque at higher speeds and because of this the green and the blue waveform start to deviate from each other. We will find out why this is when we look at the current and voltage waveforms.

In this figure it can also be seen that the impact of especially the negative peak in the load torque (again without the torque due to the inertia) is less in this case. Since the torque is now constantly higher than with the minimum torque reference the relative magnitude of the load torque is smaller.

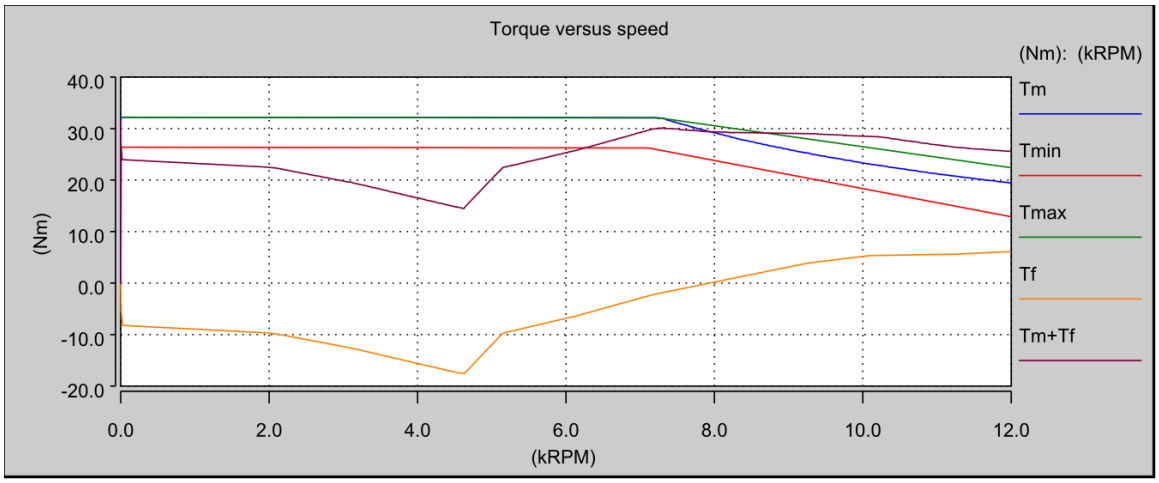

Figure 27 Torque as a function of speed, with maximum starter torque

Figure 28 gives the reason why it is not possible to follow the maximum torque reference for all speeds. This time the direct axis current reaches its maximum negative value (it could go more negative, but this would be counter-productive). Before reaching maximum field weakening it is possible to increase the torque or produce the same amount of torque at a higher speed. However, when the limit of the power supply is reached there is simply no headroom anymore and the torque has to be decreased for increasing speeds. The torque reference decreases as well, but not enough to be able to follow it.

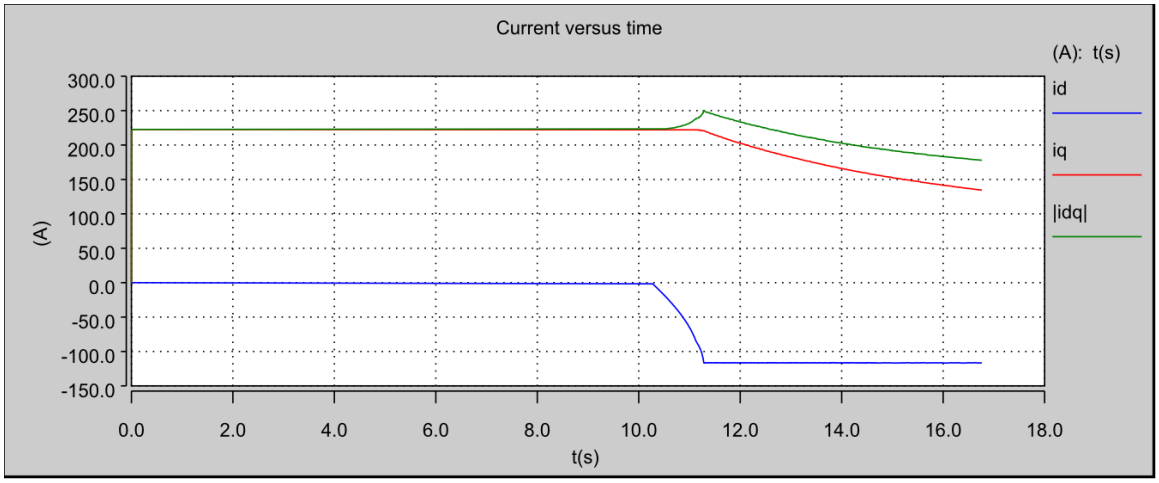

Figure 28 Current as a function of time, with maximum starter torque

The voltage waveforms in Figure 29 give an even better picture of what is happening. From the start the voltage magnitude increases in both the direct and quadrature axis. Field weakening starts when the vector magnitude reaches its maximum value (after about 10 seconds). This causes the quadrature axis (the axis of the induced EMF) voltage to rapidly decrease. It does not go down to zero completely, which is expected when keeping equation 3-7 in mind (the resistive and inductive term do not disappear).

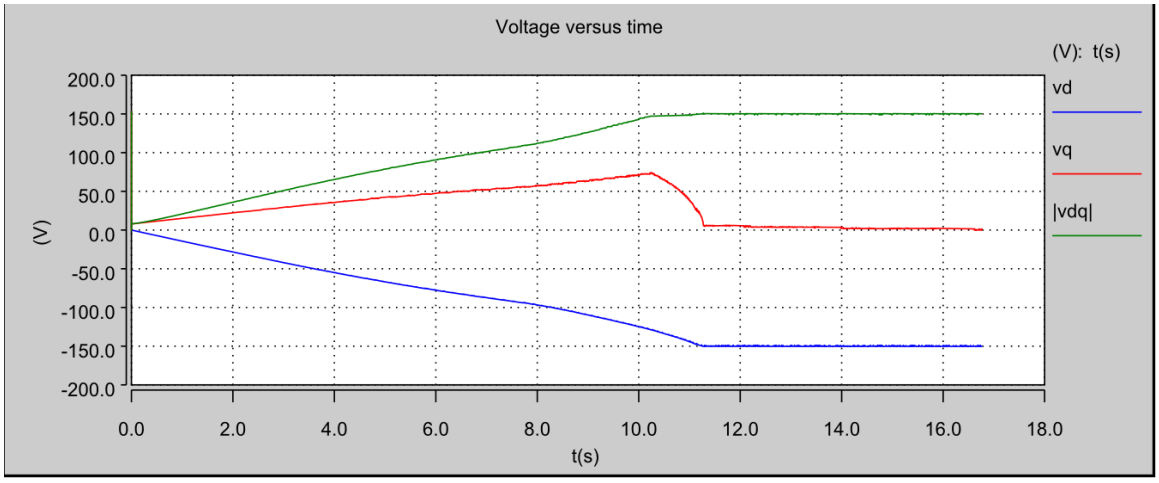

Figure 29 Voltage as a function of time, with maximum starter torque

6 System validation

In this chapter an attempt will be made to validate the system model of the starter/generator. This will be done by comparing the system model with data obtained from a real machine. The machine that will be used is the “high speed electrical machine” (HISPEM). This machine is substantially different from the starter/generator and therefore it cannot be used to validate the results for current distribution within the starter/generator. Nevertheless, it possible to compare the models for the drive consisting of the machine and its control with a real machine to find out if the system functions correctly.

6.1 HISPEM overview

The HISPEM has been designed to drive an air compressor at speeds up to 60 kRPM. This machine is also to be used in aerospace applications. With the HISPEM there is a larger emphasis on safety than for the starter/generator. Measures that have been taken to make the machine more reliable and safe are for example the presence of six phase windings and low magnetic coupling between the phases by means of unwound teeth between each of the concentrated, tooth wound, coils. The latter creates a low reluctance path for the flux generated by one phase without going through another, such that the flux linked with other nearby coils is low. This can be used to isolate a fault in one of the phases. A cutaway image of the machine is shown in Figure 30.

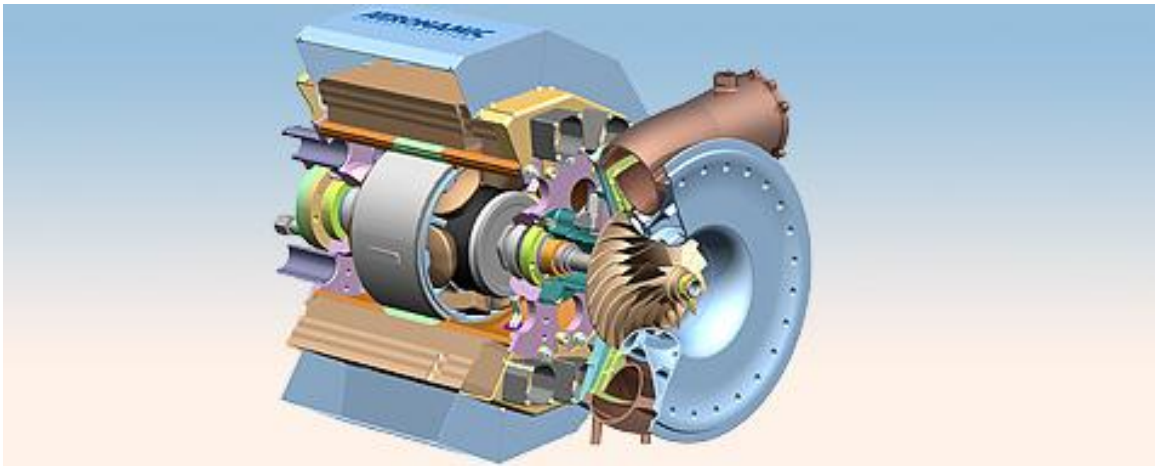

Figure 30 Cutaway image of the HISPEM [29]

The geometric spacing between phases in the HISPEM is 60°, while the electrical spacing is 120°. This means that there are two phases with the same electrical phase angle. This configuration is illustrated in Figure 31, where the geometric spacing is shown in the upper left corner. From the electrical representation can be concluded that there is no star or delta connection, instead both ends of the phase windings is brought to the outside of the machine, where each phase can be connected to a separate full bridge inverter. It has to be noted that while phases with the same phase angle are drawn next to each other in the electrical representation, there is actually no magnetic coupling between them since there is a large geometrical separation between

them. It will be shown that there is magnetic coupling between phases that are geometrically next to each other, but this coupling is low due to the empty teeth in-between phases as mentioned previously.

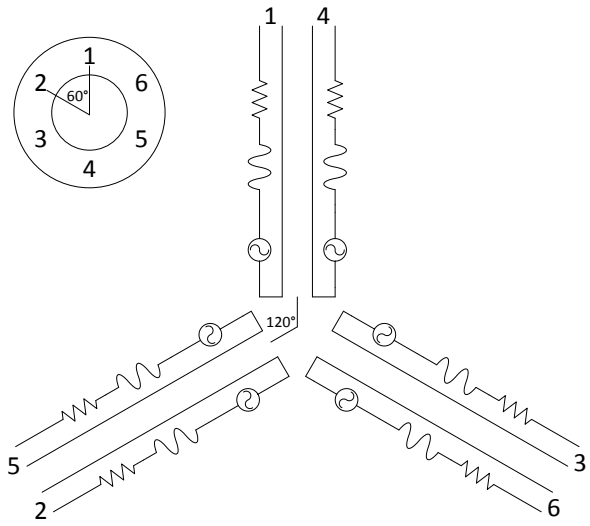

Figure 31 Geometric phase distribution and electrical representation of HISPEM

6.2 Machine properties

The machine properties of the HISPEM are needed to developed a model, which reflects the behaviour of this specific machine. Most of these properties will be determined experimentally in this section.

6.2.1 Measurement setup

A picture of the machine together with the power electronics and the control board can be seen in Figure 32. The circuit boards with the power electronics are mounted on the circumference of the machine. The electronic switches (IGBTS) cannot be seen as they are mounted on the back of the circuit boards, but the big blue capacitor banks are clearly visible. In front of the machine is the control board, which (amongst other things) controls the state of the switches. There are four BNC connectors on this control board. A digital to analogue converter (DAC) is used to turn digital signals coming from the processor on the control board into analogue signals on the BNC connectors. The signals on these connectors are used in combination with an oscilloscope to visualize signals measured or calculated by the processor like current, voltage, torque, speed, temperature, rotor angle, etc.

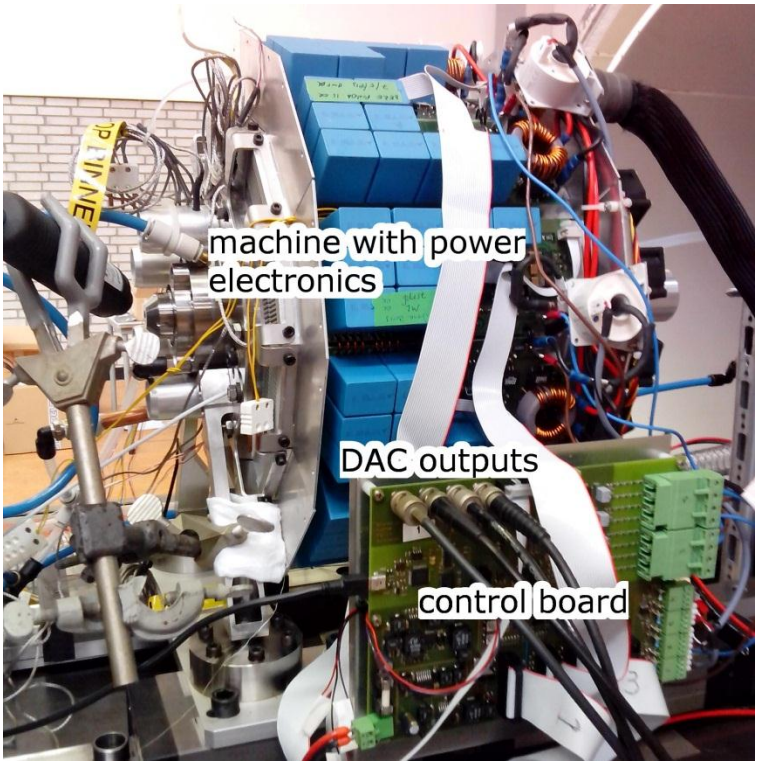

Figure 32 The machine with power electronics and control board

A graphical user interface has been made in cooperation with Dr.Ir. B. Roodenburg to be able to control what signal should be visible on which DAC channel. With this user interface it is also possible to determine the state of the controller, change control settings, and graph variables coming from the processor. A screenshot of the user interface is shown in Figure 33.

The equipment that has been used during the measurements is:
- LCR meter: Hameg HM8018
- Power supply: Delta D 030_1
- Oscilloscope: Yokogawa DLM2034
- Multimeters: 2x Fluke 189

More equipment is needed to operate the machine, but that equipment is part of the standard lab setup for this machine and has not been listed.

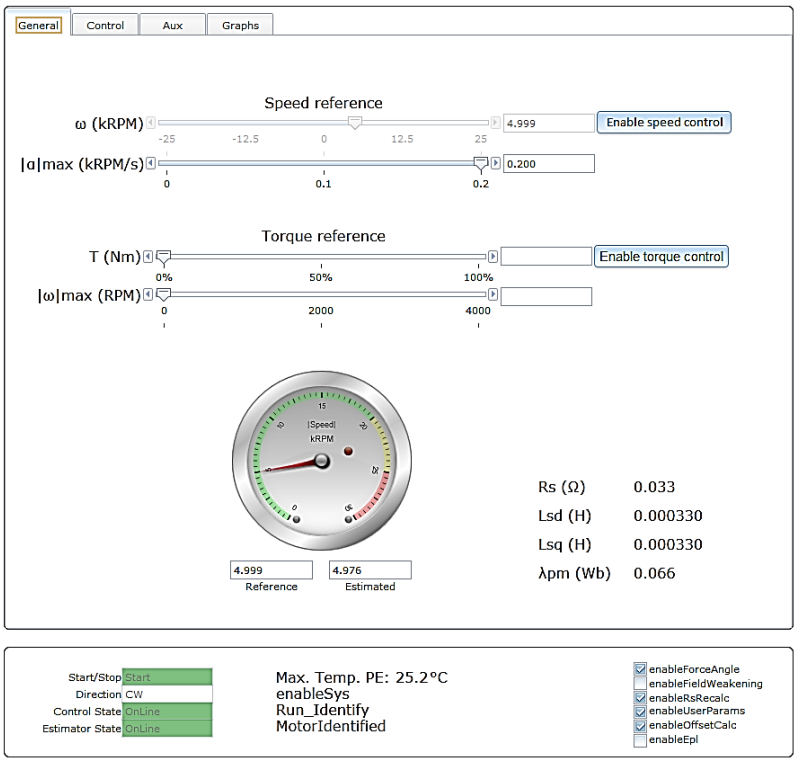

Figure 33 Graphical user interface

6.2.2 Phase resistance

The resistance of a single phase has been measured using a multimeter and two test leads for the connections. From this measurement it became clear that the resistance of the phases is low compared to the resistance of the test leads. Because of this, measuring resistance using the build-in resistance measurement function of the multimeter becomes inaccurate (since the resistance of the phase is only a small portion of the total measured resistance). To overcome this problem a so-called four-wire sensing method has been applied. Two multimeters, five test leads and a power supply were used. One multimeter has been put in series with the power supply and the phase winding (using 3 leads) to determine the current in this circuit. The power supply was adjusted to supply 1 A (with an error of less than 1%). The other multimeter has been connected parallel to the phase winding to measure the voltage drop over the winding. The connection points have to be very close to the phase winding in order not to measure a voltage drop over the current carrying test leads. Since the current was set to 1 Ampere the reading of this multimeter is the resistance in Ohms of the phase winding. The effect of the resistance of the test leads on the measurements has been eliminated, because the leads used in the voltage measurement do not carry any current and thus there is not voltage drop over these leads. This method is illustrated in Figure 34.

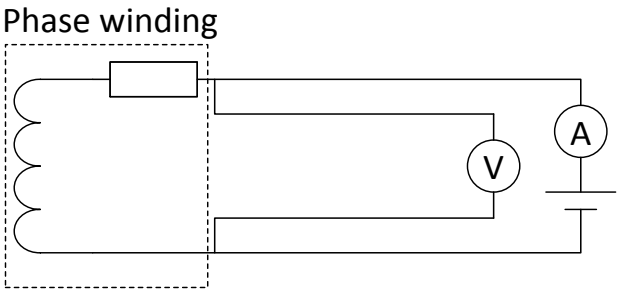

Figure 34 Four-wire sensing

The measurement results are shown in Table 7. The temperature during the measurements was approximately 25 °C. It can be seen that the phases have about the same resistance, except for phase 5. It has been reported that a breakdown has occurred between one of the phases and the machine chassis during high voltage testing. It is however not entirely certain on which phase this occurred (not even if it was on this machine or its duplicate), thus it is not clear if this is the cause of the higher resistance.

In the Saber model of this machine the average resistance will be used for all phases unless it is mentioned otherwise. This has been done because it is hard to measure with tenths of milliohms precision. It has to be taken into account that phase 5 may show different results from the other phases in reality.

Table 7 Phase resistance

phase #	R [mΩ]	difference [%]
1	72.2	-3.9
2	73.8	-1.8
3	73.0	-2.8
4	74.3	-1.1
5	83.3	10.9
6	74.1	-1.4
average	75.1	reference

6.2.3 Induced EMF

The induced EMF of three of the six phase has been determined by making the machine rotate at constant speed (by driving phases 1, 2 and 3) and then measure the voltage on the open phases (4, 5 and 6). The result can be seen in Figure 35, where the coloured waveforms represent the measurement data. There are also three black waveforms, covered by the coloured waveforms, which represent curve fittings to the measurement data. The fact that they can hardly be seen means that the fit is quite accurate.

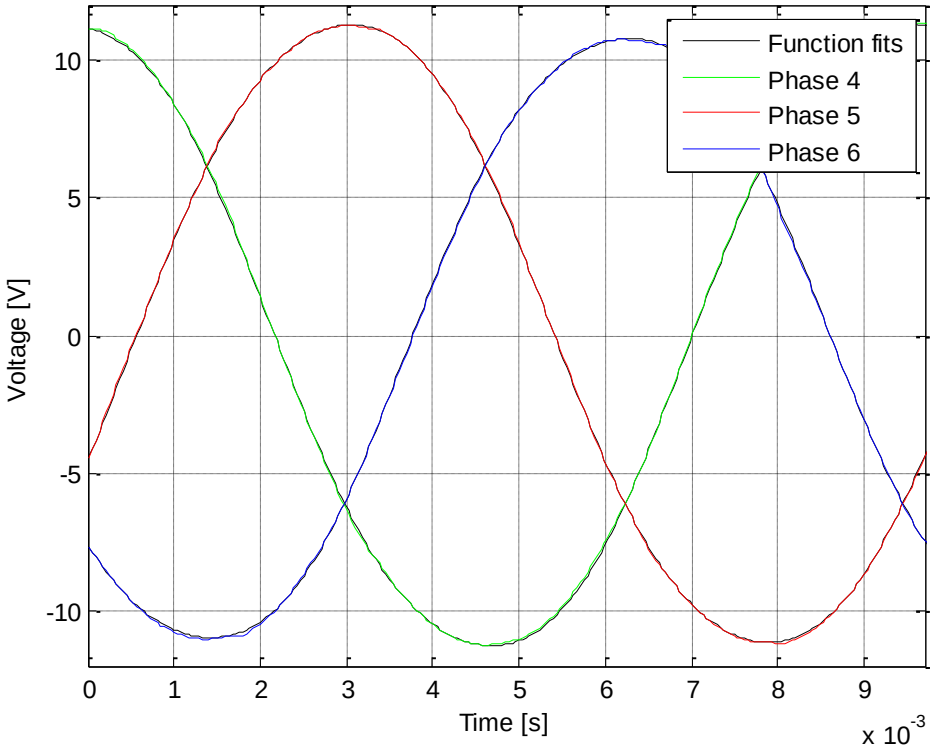

Figure 35 Induced EMF at an electrical frequency of 103 Hz

Unfortunately, only the induced EMF of three phases has been recorded. By rerouting the wiring of the machine it would have been possible to drive phases 4, 5 and 6 and to measure the induced EMF of phases 1, 2 and 3. Capturing all six phase voltage at once is difficult because the machine could not be driven mechanically.

Zooming in on the peaks of the induced voltage and at the same zooming out on the timescale gives Figure 36. This figure has been plotted to show the harmonics at and above the mechanical frequency (which is four times lower than the fundamental electrical frequency, because this is a four pole pair machine). It looks as if there is some misalignment of the magnets on the rotor, which causes the presence of harmonics at (and above) the mechanical frequency of the machine. These harmonics cause a staircase shape in the amplitude of the phases. The colour scheme in this figure has been kept the same and it can be seen that the curve fits give a good representation of the low frequency harmonics.

It can also be observed that the amplitude of the phase voltages is not entirely the same, but fortunately the differences are small. The differences might not even be due to the machine, but due to measurement errors. This could easily be the case, since the differences are only about 1%.

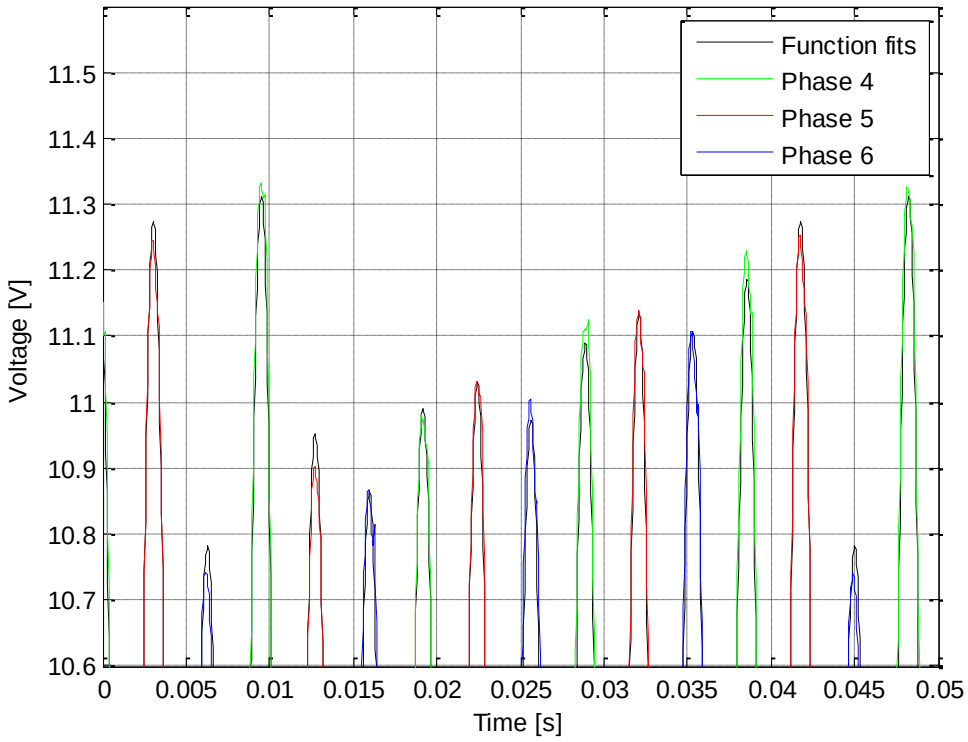

Figure 36 Harmonics of the mechanical frequency in the induced EMF

The sinusoidal functions that have been fit to the measurement data consist of four frequency components: at 1 and 3 time the fundamental electrical frequency (f_e and $3f_e$) and at 1 and 2 times the fundamental mechanical frequency ($f_e/4$ and $f_e/2$). These frequency components have been used to find the relatively size of the harmonics with respect to the fundamental wave at the electrical frequency. More frequency components could have been used, but the measurement accuracy would have to be higher and the practical value would be questionable.

Table 8 shows the amplitude of the induced EMF for the fundamental frequency and the relative size of the lower and higher harmonics. This data shows that the amplitude of the harmonics is relatively small. Even though the amplitude is small, the choice has been made to include the harmonics in the Saber model that will be developed for this machine (the average values will be used for each phase). This makes it possible to see the effect of these harmonics on for example torque ripple, an effect which has not been included in the helicopter starter/generator considered in this thesis.

Table 8 Several frequency components in the induced EMF at f_e = 103 Hz

phase #	U_{f_e} [V_p]	$U_{f_e/4}$ [%]	$U_{f_e/2}$ [%]	U_{3f_e} [%]
4	11.51	1.3	0.5	3.4
5	11.43	1.4	0.5	3.1
6	11.35	1.4	0.5	4.0
average	11.43	1.4	0.5	3.5

6.2.4 Phase inductance

The inductance of the phases has been measured using an LCR meter (inductance, capacitance and resistance meter). Measurement frequencies of 100 Hz, 1 kHz, 10 kHz and 25 kHz have been used. Since the speed of the machine has been kept low (mostly below an electrical frequency of 500 Hz) the high frequency measurements are not of direct importance. However, during initial setup of the meter it was found that at high frequency the inductance of one of the phases decreased much more rapidly than the others (a decrease is expected because of eddy currents). Because of this, one set of measurement data for a frequency of 10 kHz has been included in Table 9. This table also shows the result for a testing frequency of 100 Hz, which is in the operating range of the machine.

Phase 5 is the phase with the rapidly decreasing inductance with increasing frequency. This is also the phase with the higher resistance. It is expected that one or more turns in this phase are short-circuited. This expectation is reinforced by the fact that at very high speed (around 30 kRPM) the temperature in one of the slots rises with about 2 °C per second. One or a few short circuited turns will have a very low inductance, which causes the current through them to be very large at high speed (low impedance in combination with a relatively large induced EMF).

The inductance of one phase has been measured while the other phases were left open (i.e. no circuit). Therefore the effect of mutual inductance is not taken into account in these measurements, but mutual coupling will be discussed next. It follows from the measurement data that the inductance of the phases at a low electrical frequency is almost the same (most probably within the measurement error range). At high frequency the differences stay small, except for phase 5, as mentioned previously.

Table 9 Phase inductance

phase #	$L_{100\ Hz}$ [µH]	difference [%]	$L_{10\ kHz}$ [µH]	difference [%]
1	924	0.1	895	7.4
2	924	0.1	900	8.0
3	923	0.0	898	7.8
4	925	0.2	900	8.0
5	920	-0.4	529	-36.5
6	924	0.1	877	5.3
average	923	reference	833	reference

The mutual coupling has been determined by doing two experiments. In both experiment a sweep has been made in the machine speed while measuring the current through phase 5. In one experiment only phase 5 had been short circuited and in the other phase 4, 5 and 6 had been short circuited. The results are shown in Figure 37.

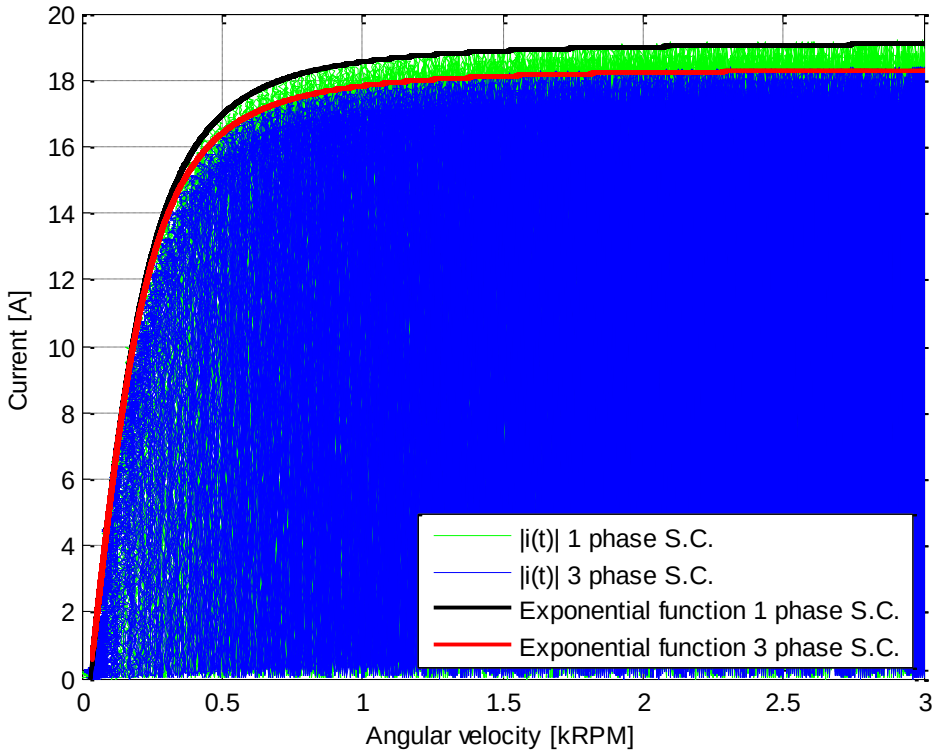

Figure 37 Short circuit current as a function of speed

The blue area in this figure represents the time dependent current through phase 5 during a short circuit of phase 4, 5 and 6. The green area, which is largely overshadowed by blue, shows the same when only phase 5 is short circuited. When the neighbouring phases of phase 5 (which are phase 4 and 6) are short circuited the current amplitude decreases due to mutual coupling.

Two exponential curves have been plotted as well, which follow the peak values of the currents. For the red curve the impedance consists of a resistance of 95 mΩ and an inductance of 960 µH, for the black curve the resistance is the same, but the inductance is 920 µH. The peak flux linkage in the curve fits was taken to be 17.6 mWb, which follows from the EMF measurements when taking only the fundamental component of the EMF into account. From this experiment (which is not very accurate) follows that the mutual coupling is approximately 40 µH and that the short circuit added to the phase has a resistance of about 12 mΩ (95 minus 83 of the phase itself).

It has to be noted that there is a slight shifting in the origin of the graphs, the fitted curves are shifted 30 RPM to the right to give a good approximation of the measurement data. It is not

exactly known why this shift is necessary, but this might have to do with the AC coupling that was used on the measurement instrument, which gives problems at low frequencies (i.e. low speed of the machine).

6.2.5 Rotor moment of inertia

For this machine it is more important to determine the moment of inertia of the rotor than it is for the starter/generator, since (except for friction) no other mechanical load is connected to the machine. The moment of inertia has been determined from a CAD model of the machine, but before this information was available the inertia had already been determined experimentally.

The approach that has been taken is to put a step input on the speed of the machine. The machine controller has built-in limits on acceleration and torque. The result of the step input on speed can be seen in Figure 38. In this case the machine runs into the maximum acceleration limit of about 200 RPM/s. Once acceleration starts there is a step (with a relatively large oscillation) visible in the torque output of the machine. This step, together with the acceleration, will be used to experimentally determine the moment of inertia of the rotor.

Equation 6-1 will be used to determine the moment of inertia.

$$T_{machine} - T_{friction} = \Delta T = J\frac{d\omega}{dt} \rightarrow J = \frac{\Delta T}{\frac{d\omega}{dt}} \approx \frac{\Delta T}{\Delta\omega}\Delta t \qquad \text{6-1}$$

The data points that are needed to perform this calculation are listed in Figure 38. Filling in the data results in equation 6-2.

$$J \approx \frac{\Delta T}{\Delta\omega}\Delta t = \frac{0.568 - 0.475}{(4.63 - 2.72)\cdot\frac{1000\cdot 2\pi}{60}}\cdot(16.4 - 6.9) = 0.044\ kg\cdot m^2 \qquad \text{6-2}$$

The moment of inertia has been experimentally determined to be 0.0044 kgm^2. From the CAD model this inertia was shown to be 0.0046 kgm^2. These results are very close together, but the accuracy of the experimental value is most probably lower than the two significant digits make believe. For the model of the machine the value obtained from CAD will be used.

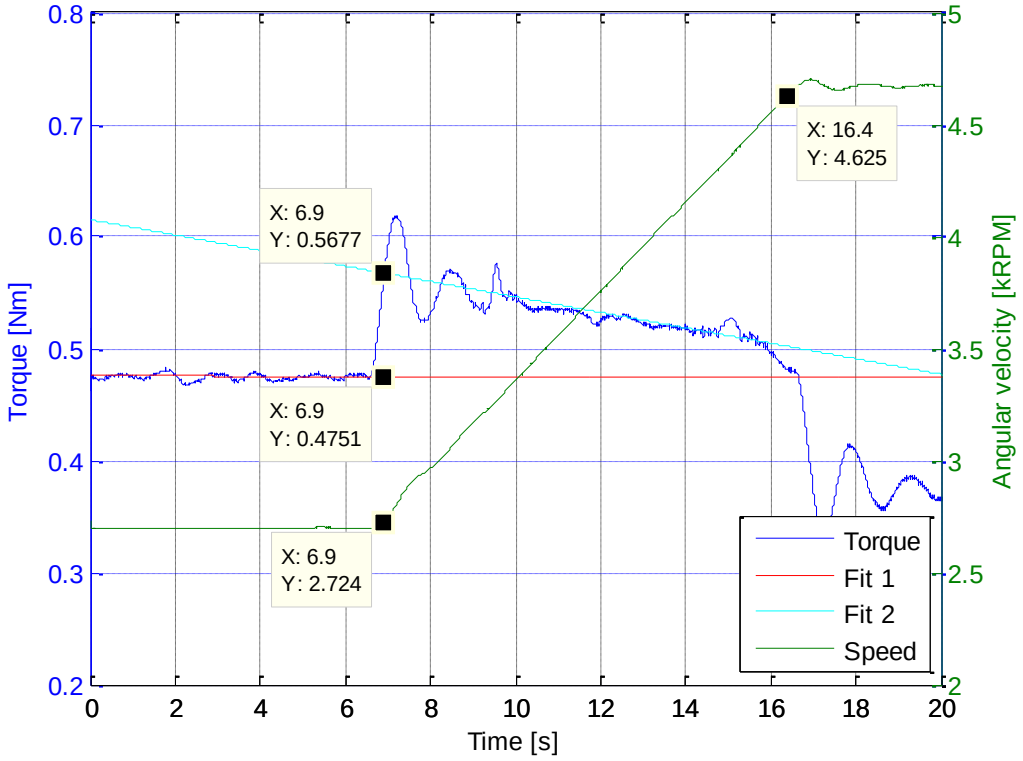

Figure 38 Torque and speed as a function of time, datapoint are added to dermine the rotor inertia

The measurement data used to plot Figure 38 has been filtered using a moving average filter. In reality there is a lot of variation in the torque, which looks like a broad noise band around the torque line in this figure.

6.2.6 Mechanical friction

The magnitude of the torque produced by the machine is not much higher than the torque due to friction, at least at low speed. The machine has only been tested at low speed during the experiments, thus friction should not be neglected. The friction will be determined as a function of speed by making the machine accelerate very slowly while recording the torque produced by the machine. The control electronics is able to give the (estimated) torque output of the machine.

The experiment has been repeated four times and the results are shown in Figure 39. During the first experiment the machine bearings had not been receiving oil flow for about halve an hour. Because of previous experiments the bearing temperature had risen to around 55 °C. The second measurement series had been made when the machine had cooled down and while oil was pumped through the bearings. This results in good lubrication (lower friction), but also in a lower temperature of the oil (higher friction). The third and fourth series of measurements have been made directly after the second. It can be seen that with low temperature and no oil flow the torque needed to overcome friction becomes much higher. Also the temperature dependence can be seen clearly in the last measurements series, where the torque curve

resembles the previous run without oil flow very well, but with a lower magnitude due to a higher temperature.

Unfortunately, no recordings of temperature have been made during any of the experiments, except for one. Because of this it becomes hard to accurately model the friction. This, in combination with the fact that the torque needed to overcome friction is relatively high, means that the accuracy of the model is severely degraded for any comparison in which the friction is of importance.

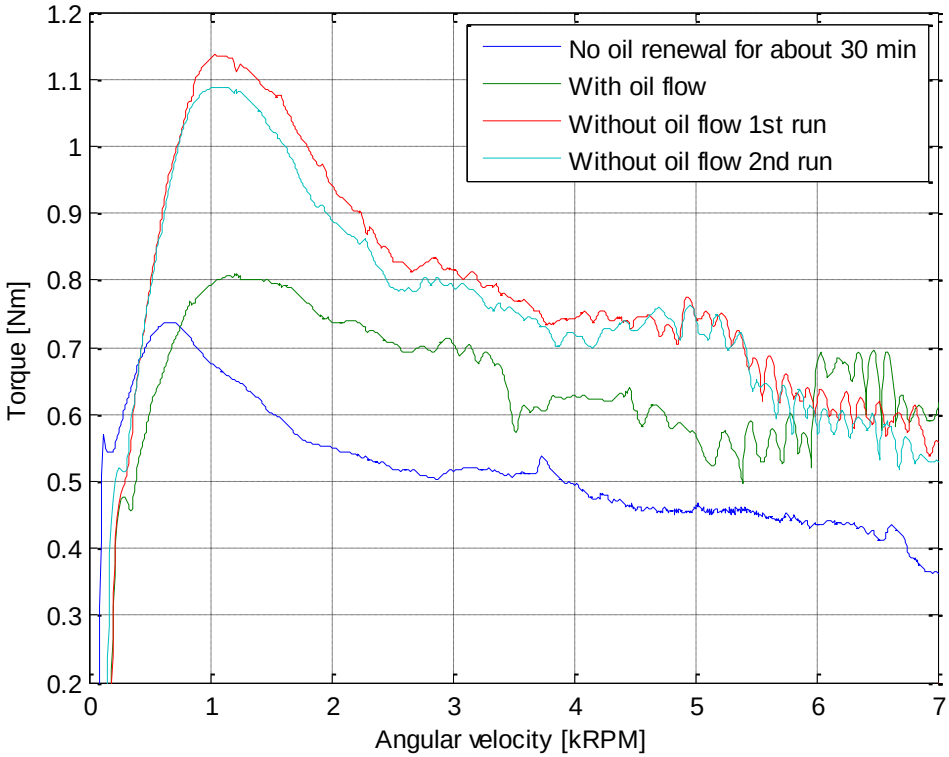

Figure 39 Friction as a function of speed with and without oil flow

It is evident that at low speed, especially around 1 kRPM, the torque (and thus the friction) is high and that it drops quite fast with increasing speed. The machine has been designed to drive an air compressor at up to 60 kRPM, which means that the operating range during the experiments is not the operating range the machine has been designed for. In practice the machine will experience negligible loading by the compressor at low speed and practically all torque can be used to overcome bearing friction and inertial loading. The low speed regime has to be traversed only to reach the required (high) operating speed. Then the question might arise why the machine has not been operated a higher speeds, the answer to this is that it is not considered to be safe to operate a machine with a rotor spinning at high speeds without proper shielding. The shielding was available, but it has not been used because it made doing the measurements more difficult and time consuming.

6.3 Current and torque scaling

Throughout this document the amplitude invariant form of the Park transform has been used. It is necessary to find out if the same form is used by the processor on the control board, since it is also very common to use the power invariant version of this transform. In order to find this out the current of a single phase has been measured using a current probe, while at the same time measuring the quadrature axis current and the torque on the DAC outputs of the control board. The results are shown in Figure 40.

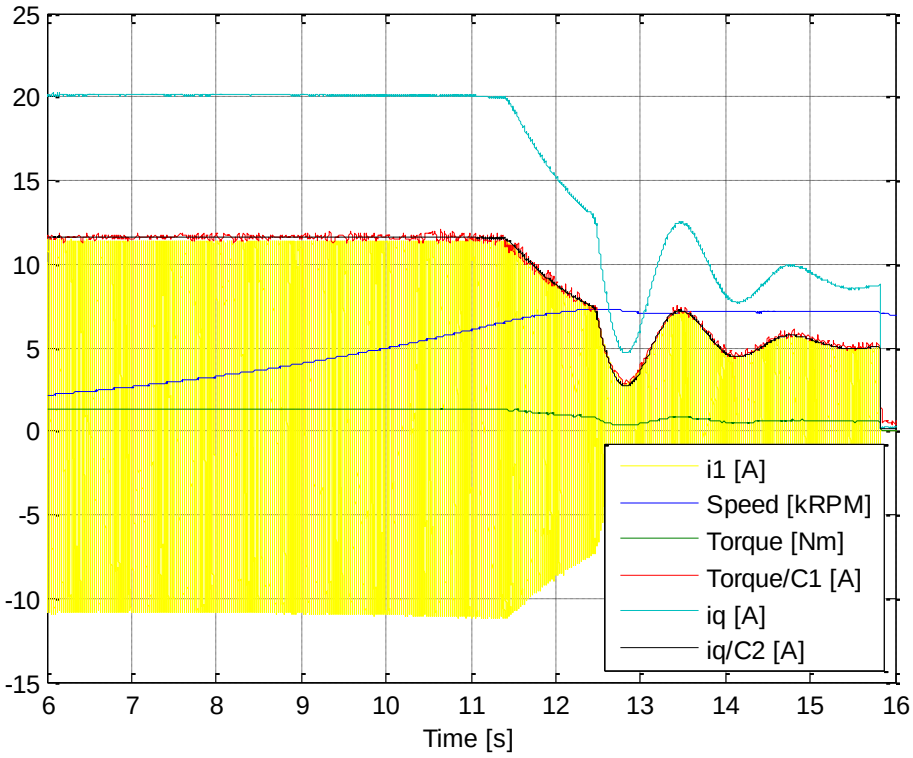

Figure 40 Current, torque and speed as a function of time

The constants C1 and C2 could be found easily, since the quadrature axis current would coincide with the peaks of the phase current if the amplitude invariant transformation had been applied. The quadrature axis current did not coincide with the peaks, but it did after dividing it by the square root of three, thus confirming that the power invariant transformation is used by the processor. Logically the same transformation has been used for the torque. The constants C1 and C2 and the relation between the currents and torque are stated in equation 6-3.

$$\hat{\imath}_1 = \frac{T}{C1} = \frac{i_q}{C2} \qquad 6\text{-}3$$

$$C1 = polepairs \cdot \hat{\lambda}_{pm} \cdot \sqrt{3} \quad C2 = \sqrt{3}$$

6.4 Machine model

The properties of the machine that have been determined in the previous experiments have been put into a model. The phases have all been taken equal, while it would be just as easy to give each phase its own set of properties (this has in fact been tested) the value of this questionable, because of measurement inaccuracies.

The model is developed in the same manner as has been done for the starter/generator. Because of this not all components will be addressed again, but an overview is given instead in Figure 41 by means of a block diagram. The electrical parameters are put in one block and is called “6 phase machine” in the diagram. The friction torque and the moment of inertia are in separate blocks, which are connected to the rotor of the machine.

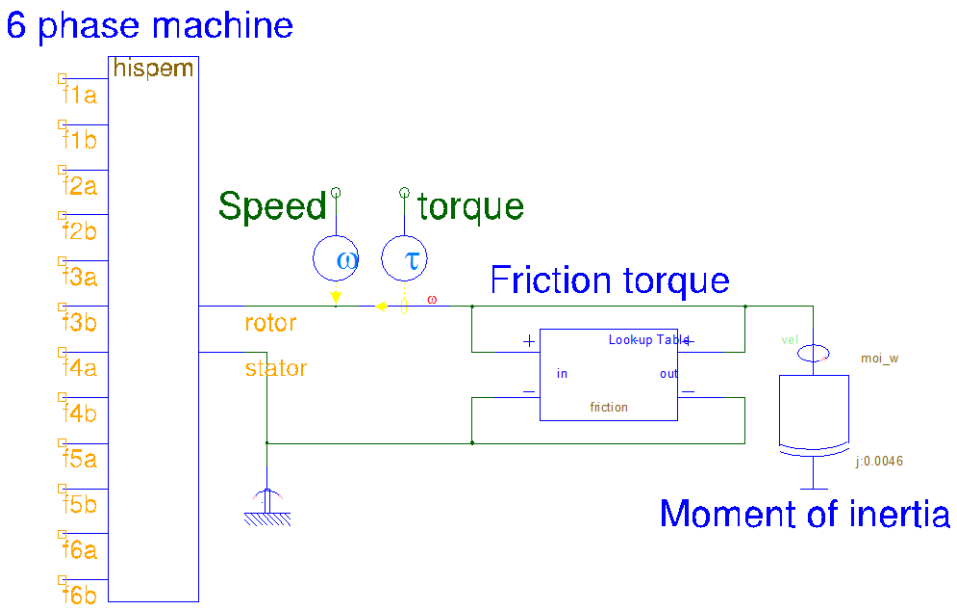

Figure 41 The machine block diagram

6.5 Comparison between measurements and simulation

Now that the machine model is complete it can be used to compare the measured data with simulated data. This should make errors in the simulation model possible and give an idea of the accuracy between physical measurement and simulation.

6.5.1 Machine impedance

The test done in section 6.2.4 has been repeated, but this time using simulation instead of experimental measurement. The resulting graph is shown in Figure 42. The function fits have been added again using the average machine parameters and by using the same flux linkage as used in Figure 37. Saber has been used to graph the peaks in the current and from this can be seen that there is a triangular shape in the peak current. These peaks are due to the lower harmonics in the induced EMF. It can also be seen that the exponential functions do not follow the highest peaks, as they did in Figure 37. This either means that the flux linkage should have

been lower, or that the phase inductance must have been higher (than the values used for the exponential functions). The measurement of the induced EMF are assumed to be fairly accurate; more accurate than the inductance measurements. The LCR meter that has been used measures using low voltage and current, whereas the actual drive uses much higher voltages and currents. This will give different values for the inductance when using an iron core, since the LCR meter will only trace small loops in the B-H characteristics, which will have different gradients than the larger loops that are used in practice.

All the lines in the graph coincide with each other very well at speeds below about 200 RPM. From this follows that the resistance seems to be at the right value. From the distance between the exponential curves and the simulation results can be concluded that the mutual inductance has been modelled properly as well.

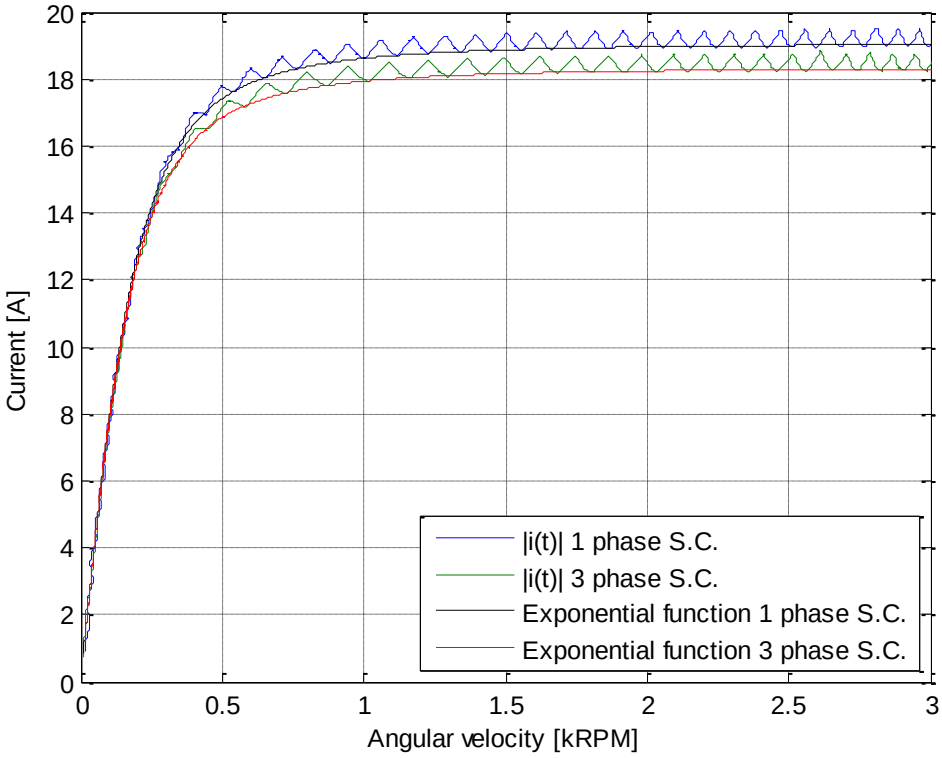

Figure 42 Simulated short circuit current as a function of speed

6.5.2 Start-up

To compare the torque and speed as a function of time during acceleration of the machine from standstill to a certain velocity, it was decided to take the torque measured during the experiment as an input to the simulation model. Thus the simulated machine would apply a certain torque as a function of time and for example the resulting speed profiles (from simulation and experiment) could be compared. However, it was experienced that the acceleration of the rotor was much faster in the simulation model than the experimental result. The reason for this can be found in Figure 39, which shows that there is quite a lot of variation in

the measured torque due to friction. This combined with the fact that the torque produced by the machine is only a little higher than the friction makes that the friction has a large influence on the outcome. The friction has been determined again in order to verify that the difference in friction could have caused the large difference between the simulation and the experiment. This time it has been determined using equation 6-4 applied to the actual experiment (the fast start-up, thus not for a very slow acceleration as for Figure 39).

$$T_{friction} = T_{mechanical} - J_{rotor}\frac{d\omega_m}{dt} \qquad 6\text{-}4$$

Figure 43 shows the result of the calculation of the torque using the above formula. Shown in this graph are the mechanical torque applied to the rotor, the calculated torque and the friction torque during the second run without oil flow from Figure 39. The reason for including the latter is that the current experiment was performed after the second run without oil (so this is the third run). It can be seen clearly that the friction during the start-up experiment is substantially higher than expected from the experiments that were specifically performed to determine the friction. The effect on the amount of torque that is left to accelerate the rotor is even larger (this torque is approximately halved just after 1 kRPM) causing a much slower acceleration.

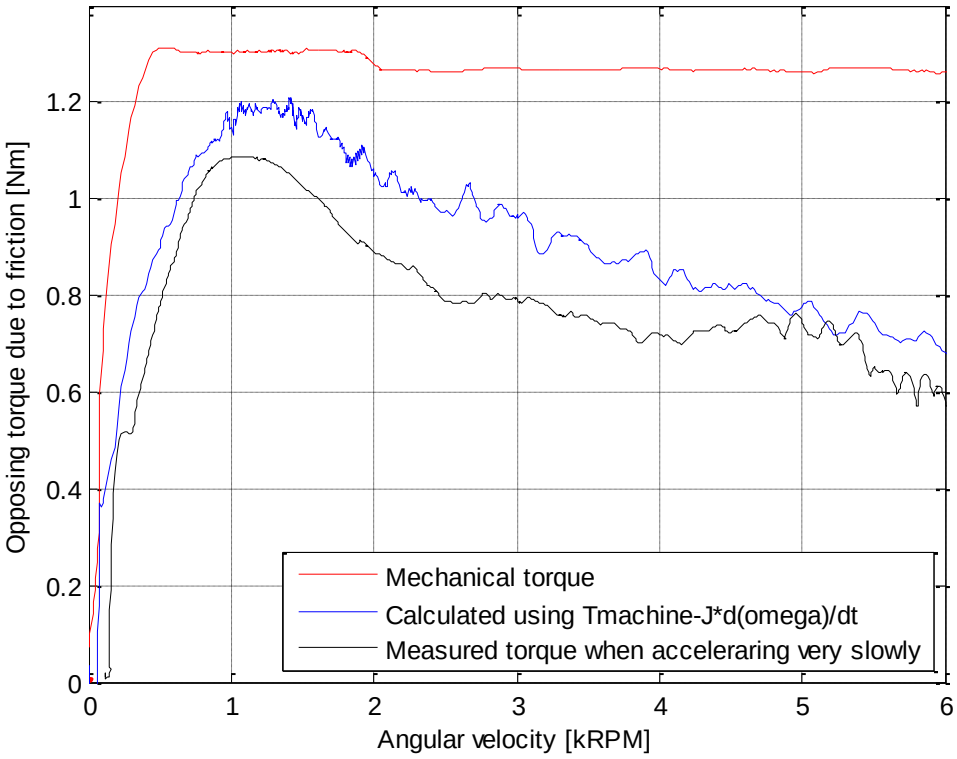

Figure 43 Torque as a function of speed

It has to be noted that a lot of smoothing (using a moving average) has been used to obtain the curves in Figure 43, especially on the torque that was determined using differentiation. The measured torque contains a lot of noise and differentiating this signal makes it even worse.

The calculated friction torque has been used in the simulation model to retry the comparison between the measurements taken from the experiment and the values following from the simulation in Saber. The results are shown in Figure 44. The upper three entries in the legend correspond to the measurements taken during the lab experiment and the lower three are related to the simulation data.

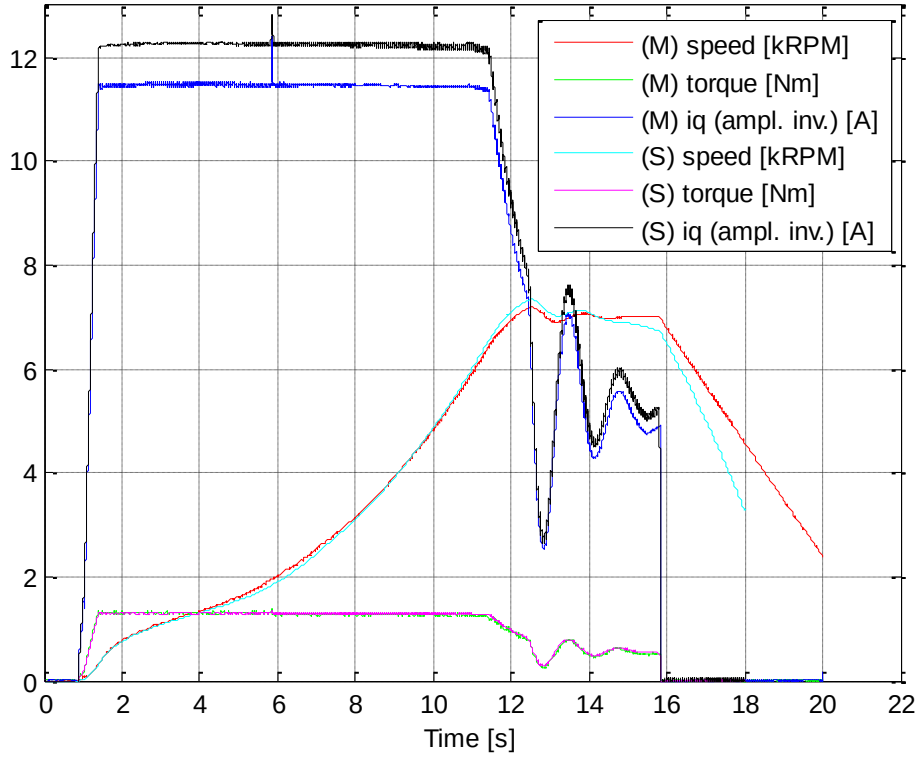

Figure 44 Comparison of start-up behaviour between measurement (M) and simulation (S)

Three values will be compared, being the torque, speed and quadrature axis current. The torque developed during the start-up is almost the same during the experiment and the simulation. This is expected, simply because the measured torque has been used as an input to the simulation. The actual speed of the machine and the simulated speed seem to agree very well for the first 14 seconds shown in the graph. The difference between the two becomes significantly larger after this time. The controller in the experimental setup has an acceleration (and deceleration) limit of 1 kRPM/s during this start-up experiment, the effect of this can clearly be seen in the straight line between 16 and 20 seconds. Only very little torque is needed to limit the deceleration, which makes it more difficult to model this effect accurately. In the simulation the deceleration happens faster, meaning that a little more torque should have been applied. The most distinctive difference between the experiment and the simulation can be

found in the quadrature axis current. The current is too large in the simulation during the entire time, even though the shape is a good representation of the experiment. The reason for this is that the peak flux linkage used in the simulation model was set to about 17.5 mWb (based on the induced EMF measurements), while the ratio between the torque and current in Figure 44 gives an effective peak flux linkage of about 18.5 mWb for the experimental data. With a lower flux linkage more current is needed to produce the same amount of torque and this effect can be seen in the graph.

It is hard to say which of the two values (or any other value) for the flux linkage is the correct one. The induced EMF has only been determined on the non-driven phases of the machine and the flux linkage has been determined using this data. However, the difference in the induced EMF over the phases that were measured are very small and based on this it is expected that the induced EMF over the driven phases is approximately the same. The flux linkage can also be determined using the ratio between the current and the torque, but unfortunately, it is hard to measure the torque and much easier to measure the induced EMF.

Figure 44 has been plotted again in Figure 45, but now with a compensated flux linkage. The flux linkage has been set to 74 mWb in the simulation model, such that it approximately equals the value deduced from the measurements. The difference between the measurement data and the simulation data has been considerably reduced. The simulation model now gives a good representation of the actual HISPEM setup.

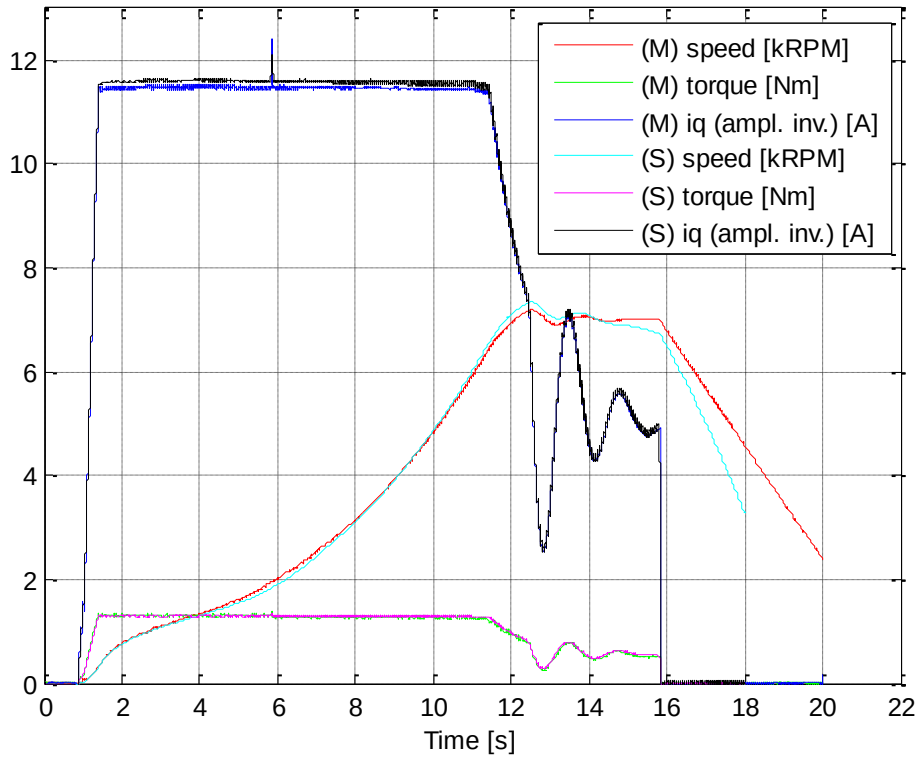

Figure 45 Comparison of start-up behaviour with a compensated flux linkage for the simulation data

6.6 Conclusion

In this chapter the simulated motor drive for the starter/generator has been validated using the HISPEM. First the properties of the HISPEM that are needed to make a relatively simple model have been determined. Subsequently this model was used to replace the starter/generator machine in the motor drive simulation. After this the impedance of the machine in the simulation was compared with the data from the actual machine. Finally a start-up of the HISPEM was simulated in order to validate the simulated motor drive.

It has been rather difficult to determine the properties of the HISPEM with a decent accuracy. This also follows from the comparison of the impedance between the actual machine and the simulation model. It was shown that the short circuit current in the simulation model was somewhat too high due to a too low inductivity. Fortunately, the errors are still small enough to make a reasonable comparison between the simulation and the experimental data.

The start-up of the HISPEM has been used to validate the motor drive simulation. Three important signals have been shown, the torque, the current and the speed. In first instance the friction had to be calculated from the measurement data, since the error in using the data from previous runs (specifically performed to determine the friction torque) gave an error that was too large. With the calculated friction torque it was possible to follow the speed profile found from the measurement data rather well. Only one problem remained, specifically a quadrature axis current that was significantly higher in the simulated motor drive than in the actual drive. The problem was found to be situated in the determination of the peak flux linkage. The simulated drive and the actual drive performed almost the same after correcting for the difference in flux linkage. From this it is concluded that the simulated drive gives a valid representation of the actual drive.

The measurements and the comparison between the experimental results and the simulations that have been performed put the data used for the starter/generator in perspective. It is hard to measure with the accuracy of the machine data presented in Appendix A and it will also be difficult to build a machine with this accuracy. Nevertheless, it was shown that also in practice phases can be wound with very similar properties.

When further research is done using data from the HISPEM, it is recommended to:

- Take a good look at the influence of the fault (probably a short circuit between turns) in one of the phases.
- Measure the inductance of the windings using a larger excitation of the core and measure the mutual inductance as well.
- Make a more accurate model for the friction. The first step could be do determine the amount of friction as a function of temperature.
- Determine the rotor inertia with a higher accuracy than presented here.

- Measure the induced EMF on all phases, to be sure that they are all approximately equal (and determine if the small differences that are present are not because of a measurement error).

Furthermore when the comparison between the starter/generator and the HISPEM would be continued, then it might be interesting to parallel phases and measure the current distribution. It can be argued whether this is very useful though, because of the large difference between coils with very good coupling (in the starter/generator) and parallel phases that have no magnetic coupling with each other (in the HISPEM).

7 Results

In this chapter the two main research objectives will be investigated. Firstly the presence of circulating currents will be discussed in case the electrical machine has open electrical terminals and is driven mechanically. Secondly a quantitative analysis of circulating currents in the electrical machine during start-up will be presented. Furthermore the case of a short circuit between one of the terminals of the machine and the neutral point will be discussed briefly. Take note that this chapter returns to the starter/generator, i.e. the coming discussion is *not* about the HISPEM anymore.

7.1 Circulating currents

Current circulation can take place when the magnitude or the phase of the voltage induced in parallel coils is not the same for every coil. To investigate if this is happening, and to what extent, the machine will be driven mechanically without anything connected to its electrical terminals.

Table 10 shows the magnitude and phase of the permanent magnet flux linked with the coils inside the machine. There are 9 entries in this table, while there are 36 coils in the machine. This is because of the three identical teeth per phase which have been combined as explained in section 3.5. The first three columns are related to the magnitude of the flux linkage. The first column shows the magnitude of the flux linkage, the second column gives the difference with respect to the first coil on the same tooth and the third column gives the resulting voltage difference at a speed of 24 kRPM. The second to last and the last column give the phase angle and the difference in phase angle, again with respect to the first coil on the same tooth.

The coils on a single tooth have an almost equal flux linkage. The differences in induced voltage are very small and because of this it is expected that circulating currents will occur, although with a very small magnitude. The phases are almost exactly 120 degrees out of phase. It is noticed that the first three rows of the fourth column, belonging to phase A, are not zero. This is because the three phases have been positioned such that the average error from the 0, 120 and 240 degree positions is as small as possible. The differences in phase are so small that it is assumed that this causes no significant circulating currents.

It has to be noted that in practice it will be hard to apply a winding as accurately as in the FEM model that was used to obtain this data, but phases with very similar properties can in fact be wound.

Table 10 Differences in flux linkage and flux angle

$\hat{\lambda}_{pm}$ [mWb]	$\Delta\hat{\lambda}_{pm}$ [μWb]	$\Delta\hat{e}$ [mV]	$\emptyset$ [rad]	$\Delta\emptyset$ [mrad]
24.09099	ref	0.00	-0.000078	ref
24.09130	0.31	3.12	-0.000078	0.00
24.09332	2.33	23.4	-0.000078	0.00
24.09193	ref	0.00	-4.188731	ref
24.09224	0.31	3.12	-4.188731	0.00
24.09426	2.33	23.4	-4.188731	0.00
24.08844	ref	0.00	-2.094376	ref
24.08875	0.31	3.12	-2.094376	0.00
24.09077	2.33	23.4	-2.094376	0.00

Figure 46 presents the waveforms for the current around a tooth in phase A. One phase was chosen to make the figure less cluttered. The other phases give a similar result because the difference in induced voltages is the same for the three phases. There is a small difference in impedance for the three phases though and because of this one graph has been added that shows the current all phases. The current in this figure and other figures is the current that would actually flow in one of the 36 coils in the machine, not in one of the 9 combined coils (unless stated otherwise for a specific case).

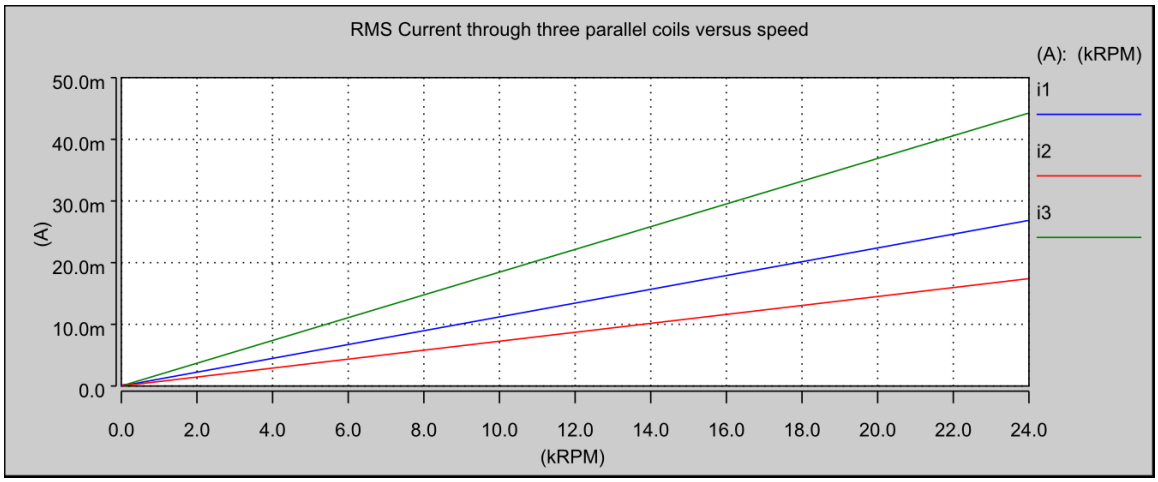

Figure 46 RMS currents as a function of speed

In Figure 19 it was shown that the current becomes almost independent of speed for the largest part of the speed range. It was limited to a nearly constant value due to the inductance of the machine. Figure 46 does not show this behaviour, in this case the current keeps increasing in a linear fashion, which is characteristic for resistive impedance. From this graph can be deduced that the inductance plays a very small role in limiting the current. This is because of the very good magnetic coupling between coils wound around the same tooth. Only the resistance and the leakage inductance will limit the current and the leakage inductance will be very small because of the very good magnetic coupling.

Figure 47 has been drawn to show why the inductance plays such a small role in limiting the current. Parallel coils wound around the same core are shown on the left (a). The current in one of the coils is in the reverse direction of the other two. The same circuit is redrawn on the right (b) which shows the current flowing from top to bottom. In this figure it can clearly be seen (using the dot convention for the coils) that the flux produced by the upper coil will be cancelled by the two lower coils (assuming the coils are the same and are perfectly coupled).

This effect of flux cancellation is also used to an advantage in the production of low inductivity wire-wound resistors (using a so-called bifilar winding). However, in the machine the circulating current should be limited and unfortunately the decreased inductivity lowers the impedance of the coils.

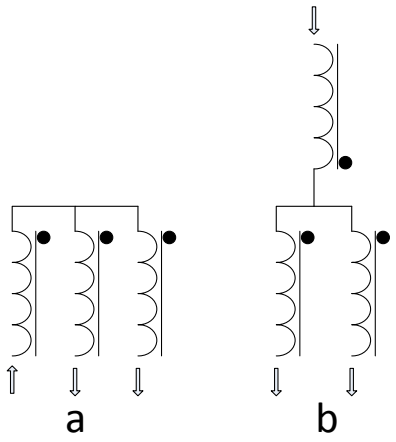

Figure 47 Three coils around the same core (a) and the same circuit redrawn (b). The arrows indicate the direction of the current through the coils at a certain point time.

According to Kirchhoff's current law the sum of the instantaneous current through the three coils should sum to zero, since they are all connected to the same node. From the third column of Table 10 follows that coil three has the highest voltage magnitude. Furthermore, in Figure 46 can be seen that the RMS value of current through coil three is as large as the sum of the RMS currents through the other two coils. From this information can be deduced that when the current through coil 3 is in the positive direction, it will be in the negative direction in the other two coils (and vice versa). Since the magnitude of the induced voltage in the first coil is the lowest (hence the largest voltage difference with the third coil), it is also expected that the current through this coil will be larger than through the second coil. The currents in three coils of phase A have been plotted in Figure 48 and this confirms the expected result.

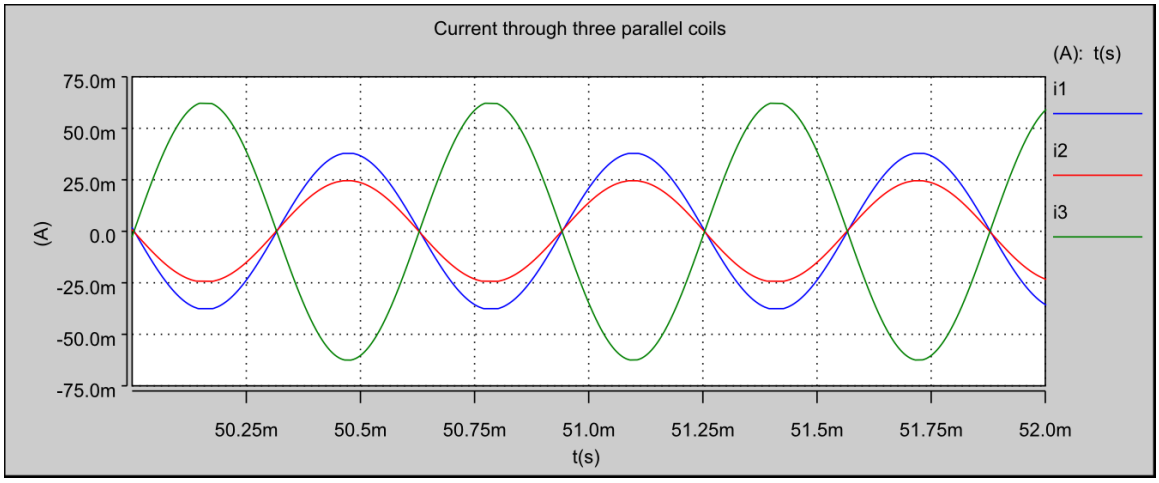

Figure 48 Current through three parallel coils at 24 kRPM

Figure 49 shows the voltage drop across the resistance (ur1, ur2 and ur3) and the inductance (ul1, ul2 and ul3) in the same three coils of phase A. The speed is set to 24 kRPM, this high speed has been chosen on purpose to show the influence of the inductivity (of which the impedance is speed dependent). Even at this speed the voltage drop over the inductance in much smaller than the voltage drop over the resistance. It is because of this that the waveforms in Figure 46 are approximately linear.

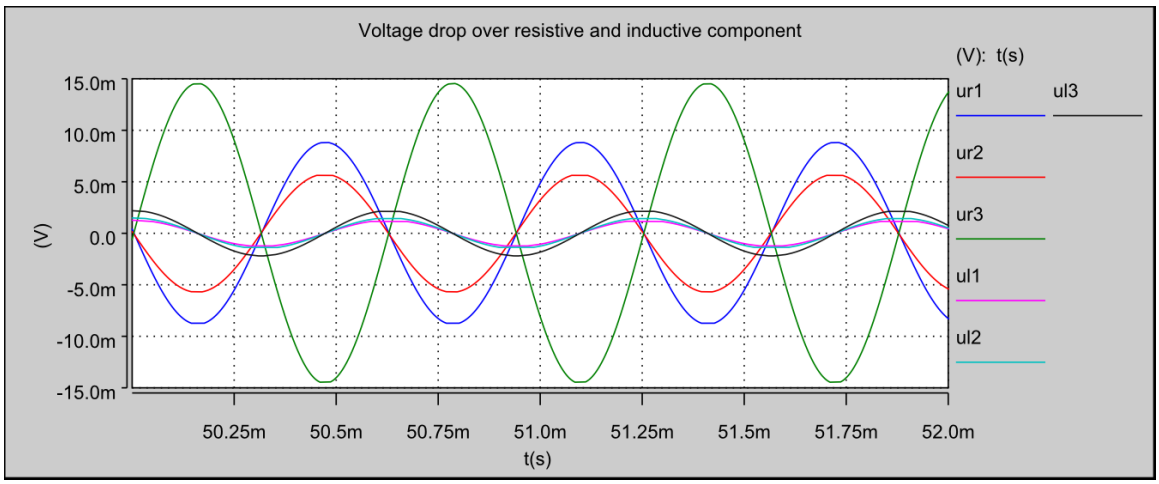

Figure 49 Voltage drop over resistive and inductive component at 24 kRPM

The RMS values of the voltage drop as shown in the figure above and the current through the coils is shown in Table 11. Now that the currents and the voltages are known it is possible to determine the impedance, the result is shown in the last column of the table. As expected the impedance is very close to the resistance of $233\ m\Omega$ of the coils.

Table 11 Voltage, current and impedance for three parallel coils

Coil	$U_R\ [mV_{RMS}]$	$U_L\ [mV_{RMS}]$	$I\ [mA_{RMS}]$	$\lvert Z\rvert\ [m\Omega]$
1	6.25	0.901	26.9	235
2	4.05	1.06	17.4	241
3	10.3	1.55	44.3	235

7.2 Current distribution

In this section distribution of current among parallel coils will be investigated. This will be done using normal operating conditions. First attention is paid to the situation in which the torque reference is set to its minimum value and after this to the situation with maximum torque.

7.2.1 Minimum start-up torque

In Figure 50 the three waveforms of the RMS currents through three parallel coils of phase A are shown. The three lines are on top of each other, because the RMS current through the three coils is almost the same. Knowing only this it seems that the current is distributed equally amongst the coils, which is a good result.

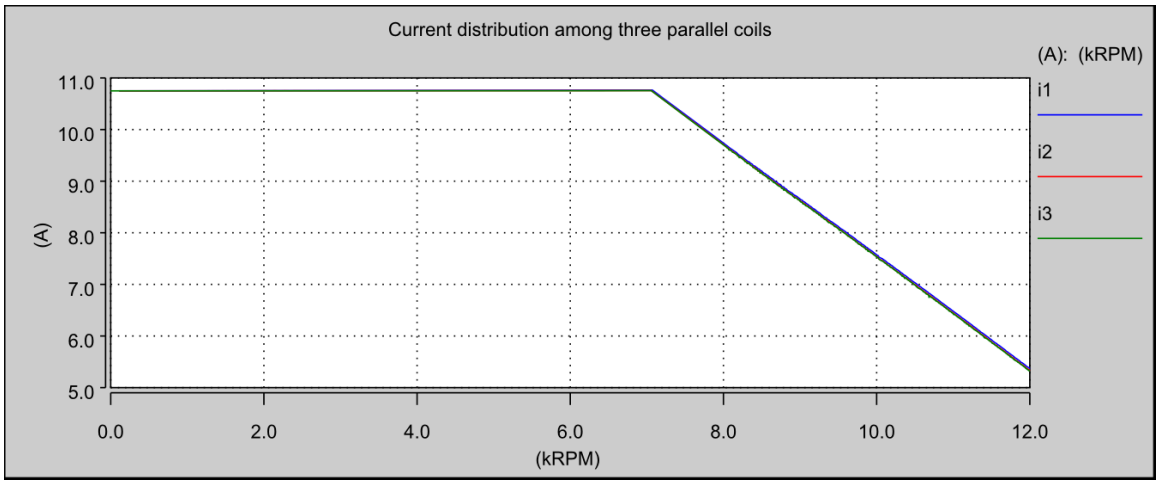

Figure 50 RMS Current through three coils of phase A as a function of speed, with minimum starter torque

Figure 51 gives a better view of the differences in current as a function of speed. Here the average of the three currents is use to normalize the waveforms. This makes it possible zoom in on the difference between the currents and still show the results for the entire speed range (for starting). With increasing speed the currents start to diverge, but the differences stay very small. The entire vertical axis covers only ±1%, and the waveforms easily fit in this range.

Two things that need to be mentioned are the vertical lines at low speed and the noise after about 8 kRPM. The vertical lines at low speed are there as a result of the RMS current measurement. The current has been determined using the peak values of the sinusoidal waves, and at very low speed it becomes difficult to properly determine the RMS value this way. Thus

this is a measurement error, not a property of the system. The noise on the waveforms has been reduced quite a lot by taking very small timesteps in the simulation, however removing the last bit of noise was found to be very hard. Because the noise that was left is only a few tenths of a percent of the total current, and it would take much more effort to remove this, no further action was taken.

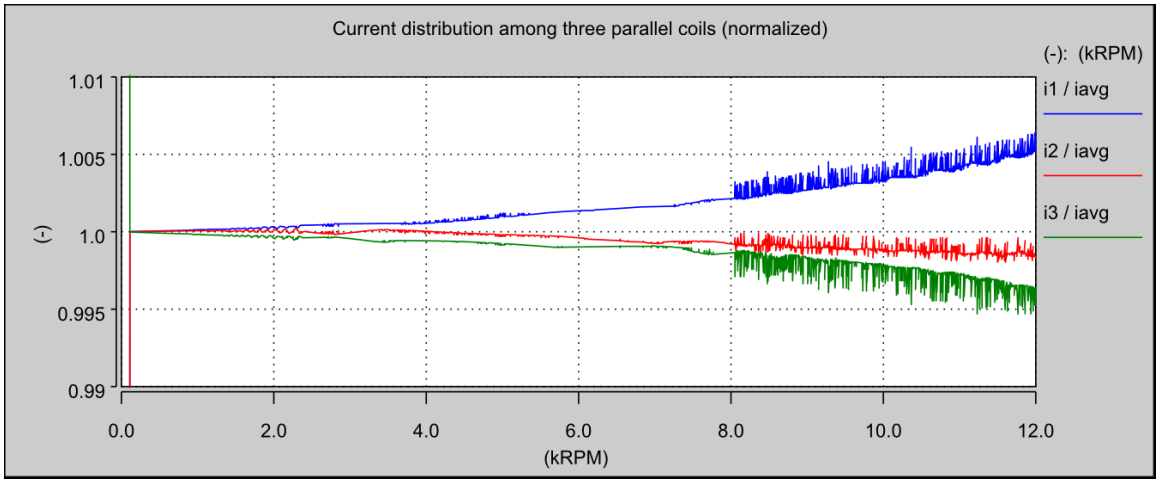

Figure 51 Current through three coils of phase A relative to the average current, with minimum starter torque

The RMS values of the currents are almost identical, but this alone does not give enough information to conclude that the current distribution among coils is satifactory. Figure 52 shows the current trough three coils in phase A, B and C as a function of time at 12 kRPM. This means that one tooth from each phase was taken; the other teeth in a phase are identical. The highest speed during starting has been taken, because at high speed the (different) values of the inductivity for the coils plays the largest role. It can clearly be seen that the amplitudes of the waveforms are about the same, but the phase shift between coil currents in the same phase is definitely not the same. This phase shift increases with increasing speed.

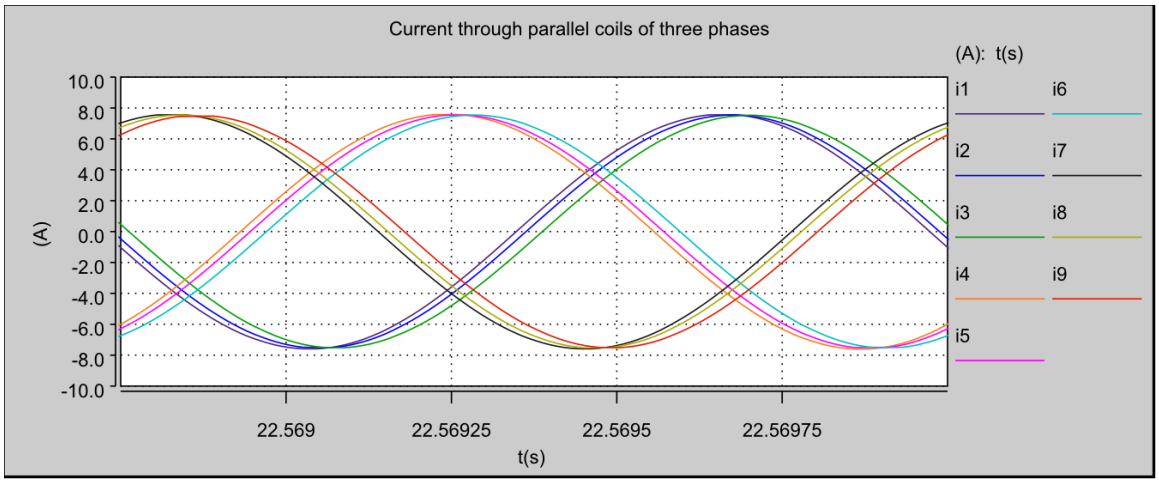

Figure 52 Current through three coils of phase A as a function of time, with minimum starter torque

Table 12 shows the current through three parallel coils and the phase shift between them at 12 kRPM. If the currents were in phase with each other and have the same value as mentioned in the table, then the resulting current (i.e. the current for one tooth) would be $16.01\ A_{RMS}$. Taking into account the phase shift the resulting current is $15.97\ A_{RMS}$, thus this difference is very small.

Table 12 Coil current and phase shift, the latter with respect to the vector sum of the currents

$\boldsymbol{Coil}$	$\boldsymbol{Current\ (A_{RMS})}$	$\boldsymbol{Phase\ (deg)}$
1	5.32	-10.4
2	5.33	-1.90
3	5.36	12.3

It is already clear from the graph that there is not much difference in amplitude between the currents, but the difference in phase shift cannot be neglected. The values in the table above confirm this observation. It would of course be interesting to find the source of this phase shift. In reference [17] measurements and calculations have been performed on the current distribution between magnetically coupled parallel coils. It was shown that a small difference in inductance has a rather large influence on the current distribution. Another simulation has been done to confirm that this is also the case in the parallel coils of the starter/generator. The circuit that has been used for this simulation is shown in Figure 53. In this circuit there are three voltage sources that represent the induced EMF, three coupled coils that represent the coils around a tooth and a current source that drives a current in-phase with the voltage sources. Coupling with other phases has not been taken into account, this has been done on purpose to separate the effects of coupling with other phases and the coupling with coils in the same phase.

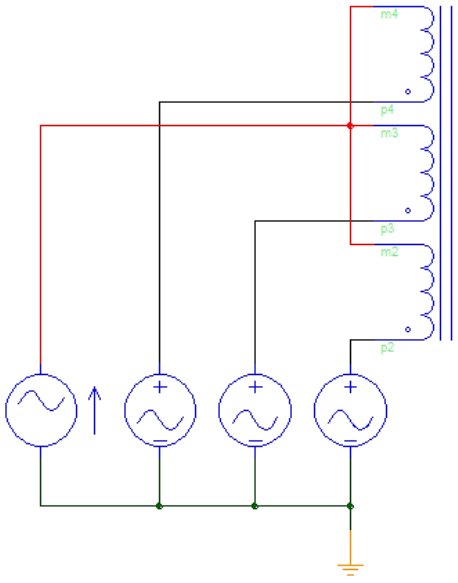

Figure 53 Simulation model for determining the influence of unequal inductance on current distribution

The simulation has been performed for four different sets of parameters. The first case is representative for the machine under investigation, which means that the inductance and magnetic coupling is the same as the data presented in Appendix A. In the second and third case the difference in self-inductance has been increased (inductances of 144, 145, 146 and 142,145,148 µH respectively), while the coupling factors stay the same. The last case has the same self-inductances as the third, but now the coupling factor has been set to zero, i.e. no magnetic coupling.

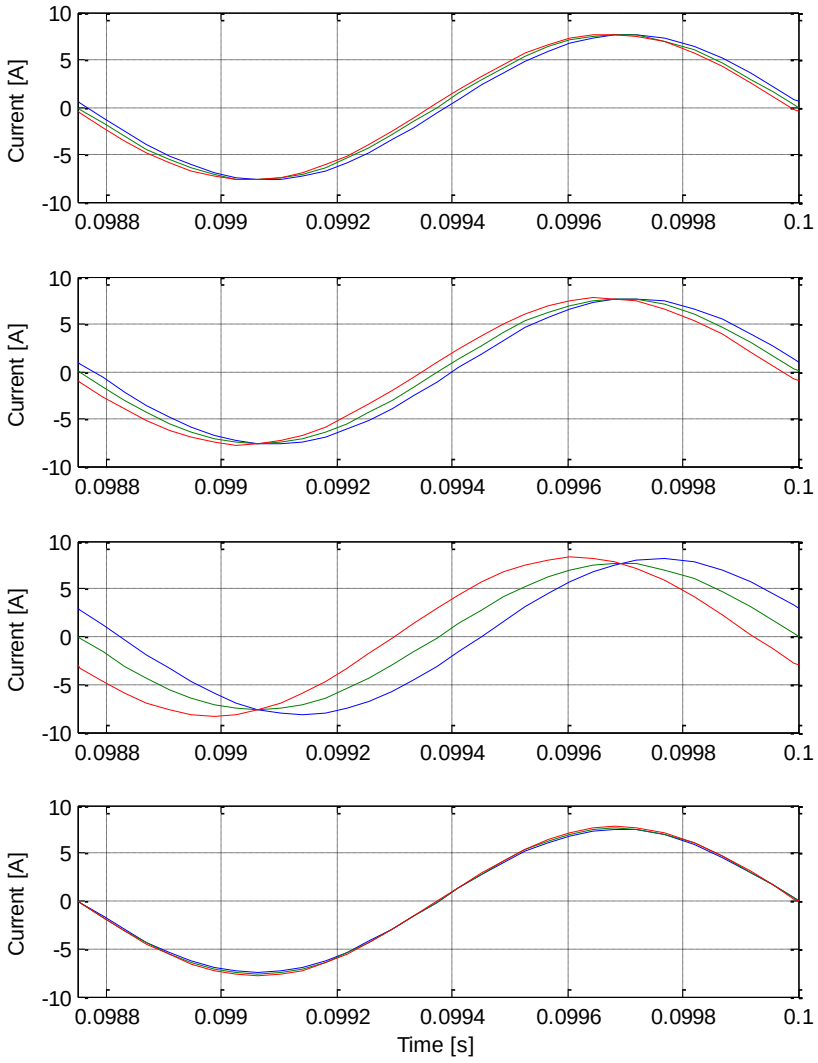

Figure 54 Current distribution for a single phase, from top to bottom: actual machine parameters, inductance variation of ±1 µH, inductance variation of ±3 µH, as previous but without mutual coupling

The phase shift between the currents in the parallel coils is not as large without the mutual coupling with the other phases, from which it can be concluded that the mutual coupling between different phase plays a significant role. Furthermore, it can be seen that increasing differences in self-inductance between parallel coils leads to increasing phase shifts. With only

minor differences of a few micro Henry the phase shift becomes quite large. This confirms the findings of reference [17], that a small difference in self-inductance has a large influence on current distribution. Fortunately, it follows from the determination of the phase inductance of the HISPEM in section 6.2.4, that it is possible to obtain almost the same inductance for different coils (although this machine did not have parallel coils and we know from reference [5] that it is much harder to make coils around the same tooth with similar inductance). In the last case, in which the difference in self-inductance is the largest and the magnetic coupling is zero, it can be seen that the currents all have about the same amplitude and phase. This means that besides the magnetic coupling with other phases, the magnetic coupling within a phase plays a large role as well. Experiments have been performed with other degrees of magnetic coupling between coils in the same phase also, from which it became apperent that also a substantial difference in the current *amplitudes* can be seen.

7.2.2 Maximum start-up torque

The same approach has been taken for the maximum start-up torque. First the RMS values of the currents through three parallel coils will be discussed and then the actual time varying currents at 12 kRPM are shown to see if there are other differences. In Figure 55 and Figure 56 there is again a vertical line at low speed. The reason for this is the same as for Figure 51 and the explanation can be found there as well.

From the overlapping lines in Figure 55 can be concluded that the RMS values for the current are very similar this time as well. At high speeds the difference between the currents seems to be relatively larger, but this is due to the different scaling.

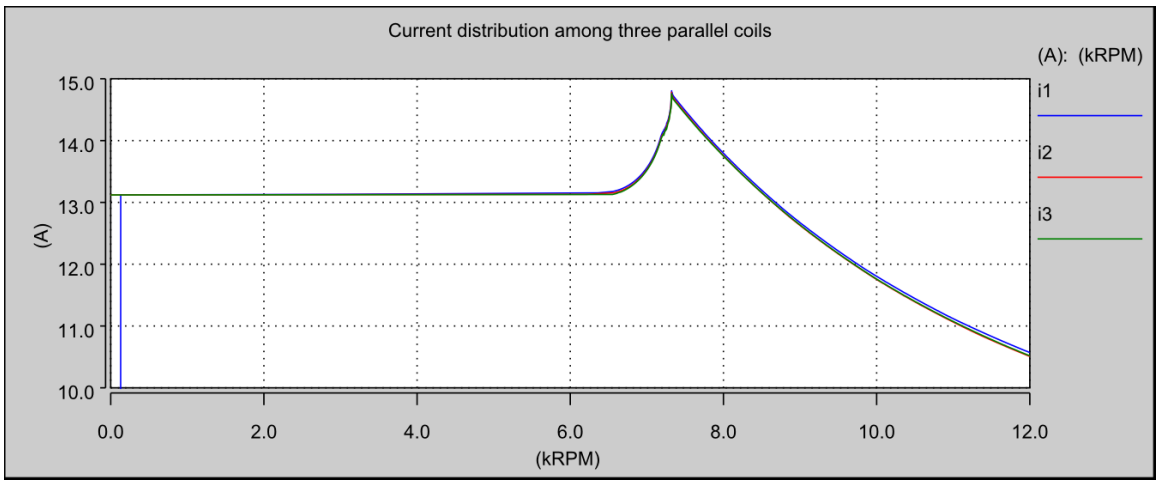

Figure 55 RMS Current through three coils of phase A as a function of speed, with maximum starter torque

Figure 56 confirms that the difference in current between the parallel coils is very small. This time the scaling of the vertical axis has been changed such that the range is ±0.5%. This means that the relative difference between the currents is even smaller with maximum torque than with minimum torque.

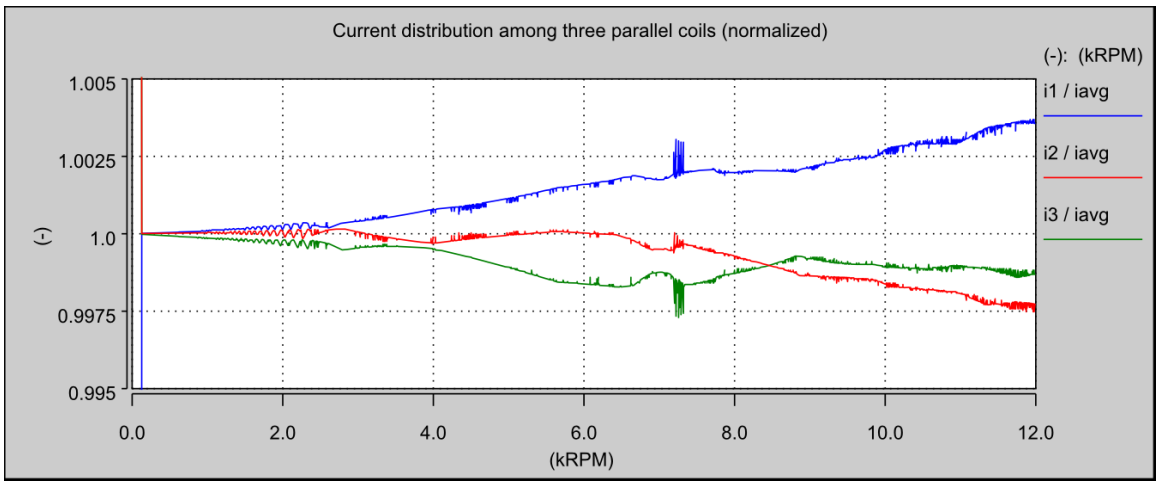

Figure 56 Current through three coils of phase A relative to the average current, with maximum starter torque

Figure 57 shows the current through three coils of phase A, B and C. The similarity with Figure 52 is striking. Of course the amplitudes of the currents are different in the two graphs (because the torque is different), but the phase shift seems to be the same.

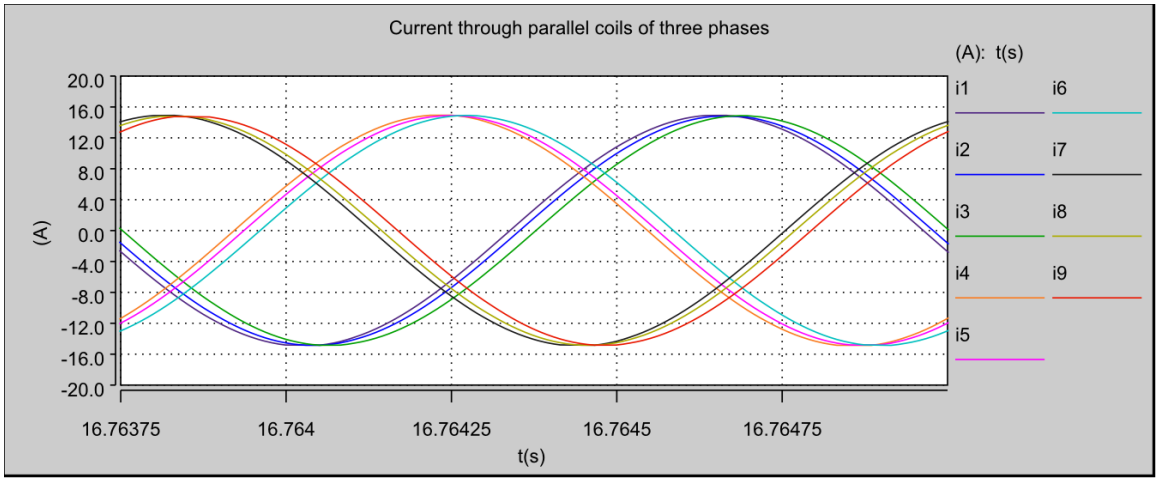

Figure 57 Current through three coils of phase a as a function of time, with maximum starter torque

Table 13 confirms the similarity in phase shift, the difference between the cases of minimum and maximum torque are very small. This is not an unexpected result, since the phase shift due to inductance is not depend on the magnitude of the current (at least not with a linear model, if saturation were present the situation would change). The resultant current in phase A is 31.5 A_{RMS}, whereas it would be 31.6 A_{RMS} if the currents were in-phase. This time the difference is very small as well (which it must be considering the phase shift between the currents is approximately the same).

Table 13 Coil current and phase shift, the latter with respect to the vector sum of the currents

$Coil$	$Current\ (A_{RMS})$	$Phase\ (deg)$
1	10.6	-10.4
2	10.5	-1.84
3	10.5	12.2

7.3 Single phase to neutral short circuit

In this section the single phase to neutral short circuit will be discussed briefly. The emphasis in this thesis is on system modelling and the distribution of current in the machine model. Up till now the system is considered to be in perfect condition. It should, however, also be possible to investigate other (fault) situations with the same system model. The only case that will be looked at is the short circuit of one of the machine phase terminals to the neutral terminal. It will be shown that this is a very severe fault and in practice continued operation with such a fault should be avoided.

The electric machine is not symmetric anymore when one (or two) of the phase terminals is short circuited to the neutral terminal. Because of this, the voltages and currents in the rotor reference frame will contain AC components with a frequency equal to the electrical frequency of the machine. This means that the measured currents that are fed back to the current controller are no longer DC values. This will make it harder for the controller to reduce the error between the reference current and the actual current through the machine.

The inverter that was used throughout this text consists of ideal voltage sources. These sources immediately supply the voltage that is requested from them, as long as it is in between the upper and lower limit of the voltage source. In practice the VSI is made by pulse width modulation of a DC voltage source. The period of this signal determines how long it takes to obtain the requested voltage. Thus there is a time delay and this delay puts an upper limit on the bandwidth of the current controllers. When a fault occurs that introduces an AC component in the currents in the rotor reference frame then this delay makes it even harder for the current controllers to deliver the requested current (the reference).

The maximum electrical frequency of the electric machine during starting is 800 Hz (12000 RPM, 8 poles). The switching frequency of the inverter is arbitrarily chosen to be 10 times higher, i.e. 8 kHz. Since the actual switching is not implemented, the delay between the input and output of the inverter is imitated by introducing a delay of one switching period (125 µs). Simulating the start-up without faults works fine with a current (torque) controller bandwidth of 800 Hz (again arbitrarily chosen to be 10 times lower than what the switching frequency would be). However, when a fault is introduced the situation changes. Figure 58 shows the inverter output voltages when phase A is short circuited to neutral at a speed of 1 kRPM. On the left in this figure are the waveforms which are characteristic for space vector modulation. When time progresses suddenly the short circuit is introduced and the current controllers are not able properly control

the current anymore, which causes the inverter output to oscillate between its upper and lower limit. Figure 59 shows the current output of the inverter (not the current through the machine) in the rotor reference frame and the torque produced by the machine. The result of the high frequency oscillations in the inverter output can clearly be seen in the two current waveforms. There is also a lower frequency oscillation at the electrical frequency of the machine which appears in all of the signals. The amplitude of the currents is very large and unless the inverter is very much over-dimensioned it will not be able to cope with this situation for a long time. Also the mechanical system will be highly stressed in this condition. There will be severe vibrations and the torque momentarily changes sign which is especially bad for gearboxes.

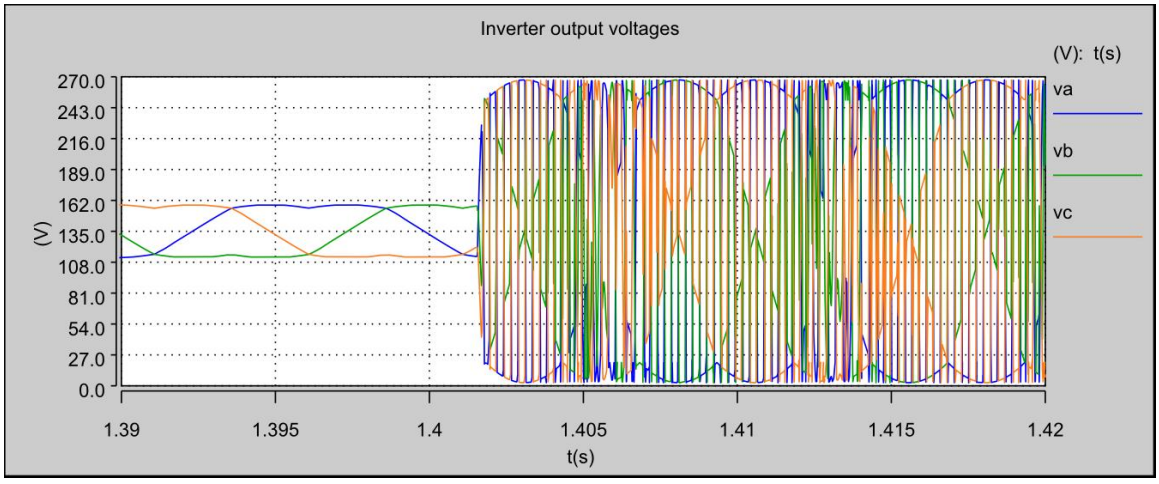

Figure 58 Inverter output voltage waveforms when using a high bandwidth controller

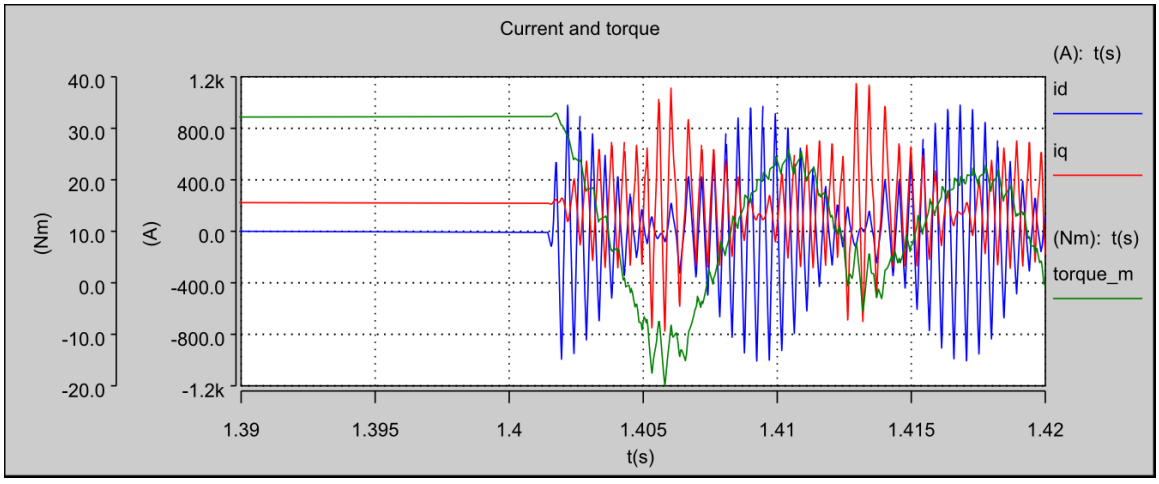

Figure 59 Current and torque waveforms when using a high bandwidth controller

It is possible to avoid the high frequency oscillations in the voltages, currents and torque by further reducing the bandwidth of the current controllers. The same fault has been simulated again, but this time the bandwidth has been reduced to 80 Hz. The results are shown in Figure 60 and Figure 61. The voltages, currents and torque do not show the high frequency oscillation

anymore, but it is still not possible to continue operation with this fault. The torque still contains a large sinusoidal component, which will cause vibration and a low resultant torque. Fortunately the stress on the inverter is much lower in this case since the amplitude of the current is much lower.

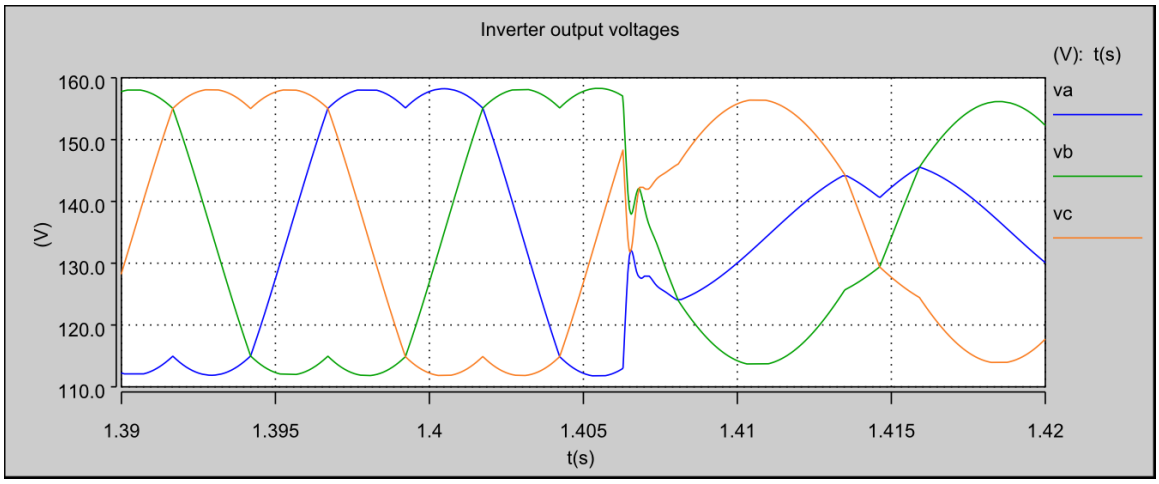

Figure 60 Inverter output voltage waveforms with reduced bandwidth of the current controller

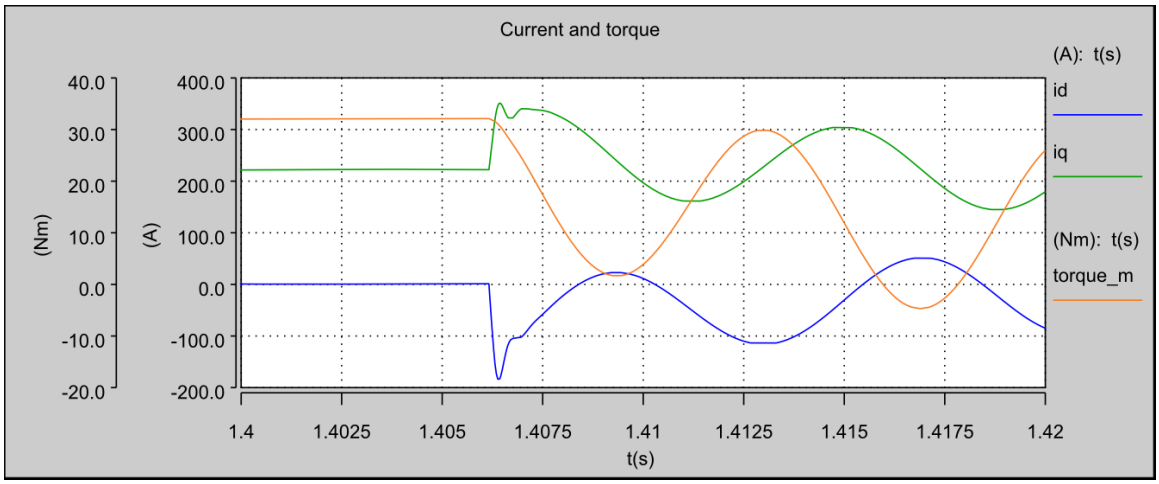

Figure 61 Current and torque waveforms with reduced bandwidth of the current controller

8 Conclusions

The aim of this research has been to develop a model for a starter/generator system using Synopsis Saber and to use this model to analyse the presence of circulating currents and current distribution in a PMSM with parallel windings. Furthermore, the case in which a phase terminal has been short circuited to the neutral terminal of the machine has been briefly discussed. The general behaviour of the system has been investigated in chapter 5. This has been done to validate the machine model and to determine the start-up time, efficiency and the waveforms of the voltage, current and torque during start-up. Further validation has been performed in chapter 6, in which the machine model has been compared with experimentally obtained data. Subsequently the results from the analyses of circulating currents, current distribution and a short circuit fault were presented in chapter 7.

To be able to develop a model for the starter/generator system it was necessary to perform a literature review. Using the knowledge obtained from literature it was possible to describe the different parts of the system and to finally implement them in Saber. The different parts of the system were connected to each other to form a representation of an actual starter/generator system. With the development of this model the first objective of this thesis has been reached. This has been a requirement for further research on circulating currents and current distribution and forms a contribution to the much larger project focused on the actual realisation of this starter/generator system.

At first, the electrical machine has been driven mechanically and stand-alone, without anything connected to its terminals. This way it is possible to determine the induced EMF at the terminals of the machine. The EMF has first been calculated from the speed and the permanent magnet flux linked with the stator coils. Then the induced EMF of the machine was measured at the terminals. It was found that the result from the calculation and the measurements were in agreement.

Secondly the machine was again driven mechanically, but this time with the three phase terminals short circuited to the neutral terminal. Using this setup it is possible to determine the short circuit current as a function of speed. At low speed the current is determined by the resistance of the coils, while at high speed the current was constant due to the inductance of the coils. The resistance and the inductance have been determined from the current and the induced voltage and these compared very well to the machine data in appendix A.

After this the start-up time and efficiency of the machine have been determined. When using the minimum allowed amount of torque the start-up took 22.6 seconds to complete, while only 16.8 seconds where needed with maximum allowed torque. The good thing about using the maximum torque was found to be the lower total energy consumption. The downside is however, that while the total energy consumption is lower, the amount of electric energy turned into heat in the cables between the inverter and the machine and in the machine itself is

higher. If the temperature of the machine is high before start-up, then it might be wise to use the minimum allowed start-up torque to avoid overheating the machine. It should be mentioned however, that the losses in the machine are determined only by the resistance of the windings and the current through them. In reality there are also losses due to eddy currents and hysteresis.

Before the results section a system validation has been performed using the “high speed electrical machine” (HISPEM) experimental setup present in the power electronics lab. The basic properties of this machine have been determined in order to build a representative model. This model has been used to replace the starter/generator in the motor drive simulation, which enables the comparison of the simulated motor drive with experimental data. It was found that the simulated motor drive gave a good representation of the actual drive.

Following the system validation is the analysis of the circulating current, in the results section. The setup used for this is the same as for determining the open circuit voltage, i.e. the stand-alone machine without connections to the phase terminals. Because of this setup, there is no current flow from inside the machine to the outside. It has been shown that there are currents inside the machine, flowing between the parallel coils around a tooth. These currents are the result of the differences in induced voltage in the coils (there is no phase shift between the induced voltages, thus there is no current flow because of this). The magnitude of these currents is very small, being less than 50 mA over the entire speed range. An important observation is that the current is primarily limited by the resistance of the copper wire. The difference in induced voltages in parallel coils is very small in this machine, but if a machine would be used in which the differences are larger and the copper resistance is also low, than the circulating currents might become much higher.

The next part of the results concerns the current distribution in the machine during start-up. The start-up has been performed with minimum and maximum allowed torque. It was shown that the difference between the RMS value of the current through a coil, relative to averaged RMS current through parallel coils, was about ±1% at high speed, at low speed the differences were even smaller. The phase difference between the currents in parallel coils seems to be substantial at 12 kRPM. The phase difference between the most lagging and leading current sums up to 22 degrees. The effective current for three parallel coils has been compared to the current that would result when there were no phase differences and from this can be concluded that the effect of the phase shift is very small.

Finally the phase to neutral short circuit has been analysed. Due to the fluctuating torque it is not realistic to continue operation with this fault. The effect of a delay in the inverter, combined with a high bandwidth of the current controller, has been investigated. It was shown that with a high bandwidth controller the amplitude of the currents became very high, enough to destroy an inverter. The amplitude of the currents became much more acceptable once the bandwidth

of the controller was reduced. Under these conditions more time will be available to safely shut down the inverter.

It should be noted that the analysis in this thesis has been performed using machine parameters obtained from 2D FEM calculations. One of the results of this is that all coils in the machine have the same resistance, since the end windings of the coils are not modelled in 2D. This also means that the inductance matrix of the machine changes. It is expected that due to the end windings the leakage inductance will increase more relative to the overall increase in inductance. It may therefore be necessary to re-evaluate the results and conclusions with machine parameters from 3D FEM calculations, to conclude if the current distribution is really good enough.

Further research on this subject is of course possible. The most interesting subject for this is the investigation of current distribution in the case of a fault in the machine. It will be interesting to find out how the current distributes in case some turns in a single coil are short circuited. A tenth equation must be added to the machine model used in this thesis in order to simulate the machine with this fault. This is a relatively easy modification which can be performed quickly, but the analysis of the results will most probably take much more time. The latter is also the reason why this analysis has not yet been performed in this thesis.

9 Bibliography

[1] B. C. Mecrow, A. G. Jack, D. J. Atkinson and J. A. Haylock, “Fault tolerant drives for safety critical applications,” *New Topologies for Permanent Magnet Machines (Digest No: 1997/090), IEE Colloquium on,* pp. 5/1-5/7, 1997.

[2] S. Khwan-on, L. d. Lillo, L. Empringham, P. Wheeler and C. Gerada, “Fault tolerant power converter topologies for PMSM drives,” *Power Electronics and Applications, 2009. EPE '09. 13th European Conference on ,* pp. 1-9, 2009.

[3] N. Leboeuf, T. Boileau, B. Nahid-Mobarakeh, G. Clerc and F. Meibody-Tabar, “Real-time detection of interturn faults in PM drives using back-EMF estimation and residual analysis,” *Industry Applications, IEEE Transactions on,* pp. 2402-2412, 2011.

[4] M. Villani, M. Tursini, G. Fabri and L. Castellini, “Fault-tolerant PM brushless DC drive for aerospace application,” *Electrical Machines (ICEM), 2010 XIX International Conference on ,* pp. 1-7, 2010.

[5] M. v. d. Geest, H. Polinder, J. A. Ferreira and D. Zeilstra, “Current sharing analysis of parallel strands in low voltage high speed machines,” *Industrial Electronics, IEEE Transactions on,* vol. PP, no. 99, p. 1, 2013.

[6] D. Birolleau, C. Chillet and L. Albert, “Internal short circuit in a tooth wound PMSM with stranded conductors,” *Power Electronics and Motion Control Conference, 2008. EPE-PEMC 2008. 13th,* pp. 2037-2042, 2008.

[7] T. Finken, M. Felden and K. Hameyer, “Comparison and design of different electrical machine types regarding their applicability in hybrid electrical vehicles,” *Electrical Machines, 2008. ICEM 2008. 18th International Conference on,* pp. 1-5, 2008.

[8] J. G. W. West, “DC, induction, reluctance and PM motors for electric vehicles,” *Power engineering journal,* vol. 8, no. 2, pp. 77-88, 1994.

[9] X. D. Xue, K. W. E. Cheng and N. C. Cheung, “Selection of Electric Motor Drives,” *Power Engineering Conference, 2008. AUPEC '08. Australasian Universities ,* pp. 1-6, 2008.

[10] M. Zeraoulia, M. Benbouzid and D. Diallo, “Electric motor drive selection issues for HEV propulsion systems: a comparative study,” *Vehicle Power and Propulsion, 2005 IEEE Conference,* pp. 280-287, 2005.

[11] T.-L. Chern, P.-L. Pan, Y.-L. Chern and D.-M. Tsay, “Sensorless speed control of BLDC motor using six step square wave and rotor position detection,” *Industrial Electronics and Applications (ICIEA), 2010 the 5th IEEE Conference on,* pp. 1358-1362, 2010.

[12] R. d. Doncker, D. W. J. Pulle and A. Veltman, “Synchronous machine modeling concepts,” in *Advanced electrical drives*, Springer, 2011, p. 169.

[13] R. d. Doncker, D. W. J. Pulle and A. Veltman, “Current control of generalized load,” in *Advanced electrical drives*, Springer, 2011, pp. 55-82.

[14] R. d. Doncker, D. W. J. Pulle and A. Veltman, “Control of synchronous machine drives,” in *Advanced electrical drives*, Springer, 2011, pp. 201-212.

[15] A. Foggia, J.-É. Torlay, C. Corenwinder, A. Audoli and J. Hérigault, “Circulating current analysis in the parallel-connected windings of synchronous generators under abnormal operating conditions,” *Electric Machines and Drives, 1999. International Conference IEMD '99,* pp. 634-636, 1999.

[16] W. Shuting, L. Heming, L. Yonggang and M. Fanchao, “Analysis of stator winding parallel-connected branches circulating current and its application in generator fault diagnosis,” *Industry Applications Conference, 2005. Fourtieth IAS Annual Meeting. Conference Record of the 2005,* vol. 1, pp. 42-45, 2005.

[17] A. Leicht, M. Albach, M. Spang and D. Kuebrich, “Current distribution in copper coils with parallel windings,” *Power Electronics and Applications (EPE 2011), Proceedings of the 2011-14th European Conference on ,* pp. 1-8, 2011.

[18] X. Roboam, B. Sareni and A. d. Andrade, “More electricity in the air: toward optimized electrical networks embedded in more-electrical aircraft,” *Industrial Electronics Magazine, IEEE,* vol. 6, no. 4, pp. 6-17, 2012.

[19] J. Liu, “Modeling, analysis and design of integrated starter generator system based on field oriented controlled induction machines,” The Ohio State University, Columbus, 2005.

[20] J. Sun, Z. Wei, S. Wang, Q. Zhan and Z. Ma, “Modeling and design of switched reluctance starter/generator system,” *PIERS Proceedings, Moscow, Russia,* pp. 1976-1982, 2009.

[21] S. Chwirka, “Using the powerful SABER simulator for simulation, modeling, and analysis of power systems, circuits, and devices,” *Computers in Power Electronics, 2000. COMPEL 2000. The 7th Workshop on,* pp. 172-176, 2000.

[22] H. Elmqvist and S. E. Mattsson, “Modelica - The next generation modeling language,” *1st World Congress on System Simulation (WCSS'97), Proceedings of the ,* 1997.

[23] M. Bengtsson and D. Isaksson, “Modelling a Distributed Power System in Saber,” Chalmers University of Technology, Göteborg, 2008.

[24] P. Liu, H.-P. Liu and J. Guo, “SABER-Based modeling and simulation of induction motor drive system for EVs,” *IPCSIT,* vol. 53, 2010.

[25] R. d. Doncker, D. W. J. Pulle and A. Veltman, “Modulation for power electronic converters,” in *Advanced electrical drives*, Springer, 2011, pp. 18-38.

[26] A. E. Fitzgerald, C. J. Kingsley and S. D. Umans, “Basic synchronous-machine relations in dq0 variables,” in *Electric machinery*, McGraw-Hill, 2003, pp. 660-663.

[27] N. Mohan, “Designing feedback controllers for motor drives,” in *Electric drives an integrative approach*, Minneapolis, MNPERE, 2000, pp. (8-1)-(8-23).

[28] J.-M. Kim and S.-K. Sul, “Speed control of interior permanent magnet synchronous motor drive for the flux weakening operating,” *Industry Applications, IEEE Transactions on,* vol. 33, no. 1, pp. 43-48, 1997.

[29] NLR, “Ultrasnelle, veelzijdige elektromotor,” 2009. [Online]. Available: http://annualreport.nlr.nl/2009/milieu/ultrasnelle-veelzijdige-elektromotor-2/. [Accessed 8 August 2013].

[30] B. Raman, “How to Write a Good Report,” 15 May 2006. [Online]. Available: http://www.cse.iitk.ac.in/users/braman/students/good-report.html. [Accessed 14 June 2013].

Appendix A Machine parameters and cable impedance.

The electric machine has 3 phases, 8 poles and 12 teeth. There are 4 identical teeth in each phase and these have been combined to one virtual tooth that has an impedance that is four times lower than the actual impedance of a tooth. Around each tooth there are 3 coils in parallel. There are nine coils in total when using the virtual tooth (i.e. the combination of four identical teeth in the same phase).

The machine parameters were obtained by the machine designer from a 2D FEM calculation. The resistance of all coils is the same, because the 2D analysis does not included the effect of the end windings. The parameters that are used in the simulation are:

$$R = \begin{matrix} 58.13743 \\ 58.13743 \\ 58.13743 \\ 58.13743 \\ 58.13743 \\ 58.13743 \\ 58.13743 \\ 58.13743 \\ 58.13743 \end{matrix} [m\Omega] \quad \hat{\lambda}_{pm} = \begin{matrix} 24.09099 \\ 24.09130 \\ 24.09332 \\ 24.09193 \\ 24.09224 \\ 24.09426 \\ 24.08844 \\ 24.08875 \\ 24.09177 \end{matrix} [\mu Wb] \quad \emptyset = \begin{matrix} -0.000078 \\ -0.000078 \\ -0.000078 \\ -4.188731 \\ -4.188731 \\ -4.188731 \\ -2.094376 \\ -2.094376 \\ -2.094376 \end{matrix} [rad]$$

$$L =$$

$$\begin{matrix}
144.7267 & 144.7085 & 145.0082 & -62.37832 & -62.46427 & -62.62943 & -62.35701 & -62.44295 & -62.60811 \\
144.7085 & 145.1032 & 145.2380 & -62.46426 & -62.55140 & -62.71733 & -62.44295 & -62.53008 & -62.69601 \\
145.0082 & 145.2380 & 145.7493 & -62.62941 & -62.71732 & -62.88520 & -62.60809 & -62.69600 & -62.86388 \\
-62.37832 & -62.46426 & -62.62941 & 143.9679 & 143.9497 & 144.2493 & -61.59840 & -61.68434 & -61.84944 \\
-62.46427 & -62.55140 & -62.71732 & 143.9497 & 144.3444 & 144.4791 & -61.68433 & -61.77146 & -61.93733 \\
-62.62943 & -62.71733 & -62.88520 & 144.2493 & 144.4791 & 144.9904 & -61.84940 & -61.93731 & -62.10513 \\
-62.35701 & -62.44295 & -62.60809 & -61.59840 & -61.68433 & -61.84940 & 143.9453 & 143.9271 & 144.2268 \\
-62.44295 & -62.53008 & -62.69600 & -61.68434 & -61.77146 & -61.93731 & 143.9271 & 144.3218 & 144.4565 \\
-62.60811 & -62.69601 & -62.86388 & -61.84944 & -61.93733 & -62.10513 & 144.2268 & 144.4565 & 144.9678
\end{matrix}$$

$$[\mu H]$$

Clarification: *The resistance of four identical coils in parallel is 58.14 mΩ (the arrangement used in the virtual tooth). This means that the resistance of a single coil in the actual machine is four times higher, i.e. 232.5 mΩ. The impedance of a complete phase is 232.5 mΩ (resistance per coil) divided by 3 (parallel coils per tooth) divided by 4 (parallel teeth per phase) = 19.38 mΩ.*

The three cables running from the inverter to the machine have each been modelled as a series connection of a 16 mΩ resistor and a 7 µH inductor.